7.3 1 2542

1. หัวหน้าโครงการทำหน้าที่เป็น member ของ International Organizing Committee ในการประชุมนานาชาติ Asian-European International Conference on Plasma Surface Engineering, Beijing, 15 – 19 September 1999.

7.4 ผลงานด้านการพัฒนาอุปกรณ์วิทยาศาสตร์

- 1. ได้พัฒนาและปรับปรุงอุปกรณ์การวิจัยหลัก ได้แก่ เครื่องยิงไอออนมวลหนักและ เครื่องกำเนิดนิวตรอนความถี่สูง ที่มีอยู่ทั้ง 3 เครื่อง ให้มีสมรรถนะในการทำงาน เทียบเคียงกับที่มีใช้อยู่ในต่างประเทศ ทำให้ประหยัดเงินของประเทศชาติได้ไม่ต่ำ กว่า 40 ล้านบาท และทำให้มหาวิทยาลัยเชียงใหม่มีอุปกรณ์การวิจัยระดับสูง สำหรับสร้างนักวิจัยและผลิตนักศึกษาระดับโท-เอกได้
- 2. ได้ออกแบบสร้างต้นแบบเครื่อง Multiparameter Thermoluminescence Spectrometer โดยมีรายละเอียดดังเอกสารแนบ ซึ่งสามารถนำไปเป็นขยายผลใน เชิงพาณิชย์ได้

รายชื่อผู้ทำงาหในโครงการ

ชื่อ - นามสกูล	ตำแหน่งวิชาการ	วิชาการ		ด้นสังก็ค		ตำแหน่งในโครงการ	สถานภาพปัจจบัน
•	เมื่อเข้าร่วมโครงการ	ปัจจุบัน	ภาควิชา	คณะ	มหาวิทยาลัย/สถาบัน	tugi 1 gi	(เอกสารหมายเลข 1-1)*
1. ดร.ถิรพัฒน์ วิลัยทอง	รองศาสตราจารย์	รองศาสตราจารย์	พิสิกส์	วิทยาศาสตร์	เชียงใหม่	หัวหน้าโครงการ	อยู่ในโครงการ
2. Dr. H. Wiedermann	Professor	Professor	Applied Physics	r	Stanford	ที่ปรึกษาโครงการ	อยู่ในโครงการ
3. Dr. K. N. Leung	Senior Researcher	Senior Researcher	lon Beam Technology Program	nology Program	Lawrence Berkeley National Laboratory	ที่ปรึกษาโครงการ	ไม่อยู่ในโครงการ
4. Dr. A. S. Schlachter	Senior Researcher	Senior Researcher	Advanced Light Source	ight Source	Lawrence Berkeley National Laboratory	ที่ปรึกษาโครงการ	อยู่ในโครงการ
5. Dr. B. Larsson	Professor		Institute of Medical Radiobiology	al Radiobiology	Zurich	ที่ปรึกษาโครงการ	เสียชีวิตแล้ว
6. Dr. J. Crawford	Senior Researcher	Senior Researcher	Paul Sherer Institute	er Institute	Zurich	ที่ปรึกษาโครงการ	อยู่ในโครงการ
7. Dr. W. Hoffmann	Professor	Professor	Physics	Science	Wuppertal	ที่ปรึกษาโครงการ	อยู่ในโครงการ
8. Dr. A. Takahashi	Professor	Professor	Nuclear Engineering	ngineering	Osaka	ที่ปรึกษาโครงการ	อยู่ในโครงการ
9. Dr. H. Maekawa	Senior Researcher	Deputy Director	Reactor Engineering	ngineering	Japan Atomic Energy Research Institute	ที่ปรึกษาโครงการ	อยู่ในโครงการ
10. Dr. G. Grosshoeg	Associate Professor		Reactor Physics	Chalmer Univ	Chalmer University of Technology	ที่ปรึกษาโครงการ	ะเบลิยนอายุราชการ
11. Dr. P. E. Hodgson	Group Leader	Group Leader	Nuclear Physics		Oxford	ที่ปรึกษาโครงการ	อยู่ในโครงการ
12. ดร. สมศร สิงขรัดน์	รองศาสตราจารย์	รองศาสตราจารย์	พิสิกส์	วิทยาศาสตร์	เชียงใหม่	นักวิจัย	อยู่ในโครงการ
13. ดร.นรา จิรภัทรพิมล	รองศาสตราจารย์	รองศาสตราจารย์	พิสิกส์	วิทยาศาสตร์	เชียงใหม่	นักวิจัย	อยู่ในโครงการ
14. ดร.บรรจบ ยศสมบัติ	ผู้ช่วยศาสตราจารย์	ผู้ช่วยศาสตราจารย์	พิสิกส์	วิทยาศาสตร์	เชียงใหม่	นักวิจัย	อยู่ในโครงการ

รายชื่อผู้ทำงานในโครงการ

เมื่อเข้าร่วมโครงการ ปัจจุบัน ภาควิชา เมื่อเข้าร่วมโครงการ ผู้ช่วยศาสตราจารย์ ผู้ช่วยศาสตราจารย์ ผู้ช่วยศาสตราจารย์ ผู้ช่วยศาสตราจารย์ ผู้ช่วยศาสตราจารย์ หีสิกส์ กาโภชัย รองศาสตราจารย์ ผู้ช่วยศาสตราจารย์ หีสิกส์ กาโภชัย รองศาสตราจารย์ ผู้ช่วยศาสตราจารย์ หีสิกส์ กาโภชัย รองศาสตราจารย์ ผู้ช่วยศาสตราจารย์ หีสิกส์ กาโภชัย อาจารย์ อาจารย์ อาจารย์ หีสิกส์ ล อาจารย์ อาจารย์ อาจารย์ หีสิกส์ ล อาจารย์ อาจารย์ สถาบันวิจัย Researcher Senior Research es Research Engineer Senior Research แ	ชื่อ - นามสกูล	ตำแหน่งวิชาการ		ด้นสังกัด		ตำแหน่งในโครงการ	สถานภาพปัจจุบัน
น์ท์ ผู้ช่วยตาลตราจารย์ ผู้ช่วยตาลตราจารย์ พิสิทส์ ผู้ช่วยตาลตราจารย์ ผู้ช่วยตาลตราจารย์ พิสิทส์ รับ รองศาสตราจารย์ ผู้ช่วยศาสตราจารย์ พิสิทส์ อาจารย์ อาจารย์ อาจารย์ พิสิทส์ อาจารย์ อาจารย์ อาจารย์ พิสิทส์	เมื่อเข้าร่วมโคร		ภาควิชา	ansu	มหาวิทยาลัย/สถาบัน		(เอกสารหมายเลข 1-1)*
นั้ช่วยตาสตราจารย์ นั้ช่วยตาสตราจารย์ พิลิทส์ รองศาสตราจารย์ นั้ช่วยตาสตราจารย์ พิลิทส์ อาจารย์ มั่ช่วยศาสตราจารย์ พิลิทส์ อาจารย์ มั่ช่วยศาสตราจารย์ พิลิทส์ อาจารย์ อาจารย์ มั่ช่วยศาสตราจารย์ พิลิทส์ อาจารย์ อาจารย์ มีสาส์ อาจารย์ อาจารย์ พิลิทส์ อาจารย์ อาจารย์ พิลิทส์ Postdoctoral Fellow Researcher สถาบันวิจัย Research Engineer Senior Research	 		พิสิกส์	วิทยาศาสตร์	เชียงใหม่	นักวิจัย	อยู่ในโครงการ
รับ รองศาสตราจารย์ เม้ช่วยศาสตราจารย์ พืชสวน อาจารย์ เม้ช่วยศาสตราจารย์ พืสิกส์ อาจารย์ อาจารย์ พิสิกส์ อาจารย์ อาจารย์ พิสิกส์ อาจารย์ อาจารย์ พิสิกส์ อาจารย์ อาจารย์ พิสิกส์ อาจารย์ อาจารย์ พิสิกส์ อาจารย์ อาจารย์ พิสิกส์ Postdoctoral Fellow Researcher สถาบันวิจัย Research Engineer Senior Research			พิลิกส์	วิทยาศาสตร์	เชียงใหม่	นักวิจัย	อยู่ในโครงการ
นัช่วยตาสตราจารย์ ผู้ช่วยตาสตราจารย์ พืชสวน อาจารย์ อาจารย์ พิสิทส์ อาจารย์ อาจารย์ พิสิทส์ อาจารย์ อาจารย์ พิสิทส์ อาจารย์ อาจารย์ พิสิทส์ อาจารย์ อาจารย์ พิสิทส์ Postdoctoral Fellow Researcher สถาบันวิจัย Research Engineer Senior Research สถาบันวิจัย			ชีววิทยา	วิทยาศาสตร์	เชียงใหม่	นักวิจัย	อยู่ในโครงการ
มะ อาจารย์ มะท่วยศาสทราจารย์ พิสิทส์ อาจารย์ อาจารย์ พิสิทส์ อาจารย์ อาจารย์ พิสิทส์ อาจารย์ อาจารย์ พิสิทส์ Researcher Senior สถาบันวิจัย Postdoctoral Fellow Researcher สถาบันวิจัย Research Engineer Senior Research สถาบันวิจัย			พีซสวน	เกษตรศาสตร์	เชียงใหม่	นักวิจัย	อยู่ในโครงการ
น อาจารย์ ผู้ช่วยตาสตราจารย์ ฟิสิกส์ อาจารย์ อาจารย์ ฟิสิกส์ อาจารย์ อาจารย์ ฟิสิกส์ Researcher Senior สถาบันวิจัย Research Engineer Senior Research สถาบันวิจัย		อาจารย์	พิสิกส์	วิทยาศาสตร์	เชียงใหม่	นักวิจัย	อยู่ในโครงการ*
ยาจารย์ อาจารย์ ฟิสิทส์ อาจารย์ ฟิสิทส์ อาจารย์ ฟิสิทส์ สาจารย์ ฟิสิทส์ สิทธารย์ หิสิทส์ หิสิทส์ Researcher Researcher สถาบันวิจัย Research Engineer Engineer แน		นู้ช่วยศาสตราจารย์	พิสกส์	วิทยาศาสตร์	เชียงใหม่	นักวิจัย	อยู่ในโครงการ*
อาจารย์ อาจารย์ พิสิทส์ อาจารย์ พิสิทส์ พิสิทส์ อาจารย์ พิสิทส์ พิสิทส์ Researcher Researcher ลถาบันวิจัย เ		อาจารย์	พิลิกส์	วิทยาศาสตร์	เชียงใหม่	นักวิจัย	อยู่ในโครงการ
ลาจารย์มาจารย์พิสิทส์ResearcherSeniorสถาบันวิจัยResearcherLagineerSenior ResearchssResearch EngineerEngineer		ยาจารย์	พิสิกส์	วิทยาศาสตร์	เชียงใหม่	นักวิจัย	อยู่ในโครงการ
Researcher Senior สถาบันวิจัย แ Researcher Research Engineer Senior Research สถาบันวิจัย Engineer แ		ยาจารย์	พิลิกส์	วิทยาศาสตร์	เชียงใหม่	นักวิจัย	อยู่ในโครงการ
Researcher Researcher Research Fellow Research Senior Research สถาบันวิจัย Engineer แ		Senior	สถาบันวิจัยและ	พัฒนาวิทยาศาสตร์	เชียงใหม่	นักวิจัย	อยู่ในโครงการ
Postdoctoral Fellow Researcher สถาบันวิจัย Research Engineer Senior Research สถาบันวิจัย		Researcher	และเห	เคโนโลยี			
Research Engineer Senior Research Engineer			ศูหญิ	ศูนย์เทคโนโลยีโลหะและวัสดุแห่งชาติ	สดุแห่งชาติ	นักวิจัย	อยู่ในโดรงการ
\(\frac{1}{2}\)			สถาบันวิจัยและ และเท	พัฒนาวิทยาศาสตร์ เคโนโลยี	เชียงใหม่	วิศวกรวิจัย	อยู่ในโครงการ
อาจารย์ ฟัสิกส์	et Hoyes อาจารย์	ยาจารย์	พิลิกส์	วิทยาศาสตร์	เชียงใหม่	วิศวกรวิจัย	ไม่อยู่ในโครงการ*
28. นายเสวต อินทรศิริ นักวิจัย นักวิจัยอาวุโส สถาบันวิจัยและพัฒนาวิทยาศาสตร์ และเทคโนโลยี		นักวิจัยอาวุโส	สถาบันวิจัยและ	พัฒนาวิทยาศาสตร์ เคโนโลยี	เชียงใหม่	นักวิจัย	อยู่ในโครงการ

รายชื่อผู้ทำงานในโครงการ

¥e - ମନ୍ନ	ตำแหน่งวิชาการ	วิชาการ	100	ด้นสังก็ค		ตำแหน่งในโครงการ	สถานภาพปัจจุบัน
	เมื่อเข้าร่วมโครงการ	ปัจจุบัน	ภาควิชา	คณะ	มหาวิทยาลัย/สถาบัน		(เอกสารหมายเลง 1-1)*
29. นายบุญรักษ์ พันธ์ใชยครึ	นักวิจัย	นักวิจัย	สถาบันวิจัยและพ	สถาบันวิจัยและพัฒนาวิทยาศาสตร์ และเทคโนโลยี	เชียงใหม่	นักวิจัย	อยู่ในโครงการ
30.น.ส.ช่ออัญชัน ประพันธ์ศรี	นักวิจัย	นักวิจัย	สถาบันวิจัยและพิ	สถาบันวิจัยและพัฒนาวิทยาศาสตร์ และเทคโนโลยี	เชียงใหม่	นักวิจัย	ไม่อยู่ในโครงการ*
31. นายชาญชัย เคชธรรมรงค์	นักวิจัย	อาจารย์	ศูนย์วิจัยนิวตร	ศูนย์วิจัยนิวตรอนพลังงานสูง	เชียงใหม่	นักวิจัย	อยู่ในโครงการ*
32. น.ส.รพีพรรณ อำหนพันธุ์	นักวิจัย	อาจารย์	ศูนย์วิจัยนิวตร	ศูนย์วิจัยนิวตรอนพลังงานสูง	เชียงใหม่	นักวิจัย	ไม่อยู่ในโครงการ*
33. นายราเชนทร์ เจริญนุกูล	นายช่างเทคนิด	นายช่างเทคนิค อาวูโส	สถาบันวิจัยและพั	สถาบันวิจัยและพัฒนาวิทยาตาสตร์ และเทคโนโลยี	เชียงใหม่	ผู้ช่วยวิจัย	อยู่ในโครงการ
34. นายสมศักด์ วรรณชัย	ครูปฏิบัติการ	อาจารย์	พิลิกส์	วิทยาศาสตร์	เชียงใหม่	ผู้ช่วยวิจัย	ไม่อยู่ในโครงการ*
35. นายศักดิ์ชัย อำแก้ว	นายช่างอิเล็กทรอ- นิกส์	นายช่างอิเล็ก- ทรอนิกส์อาวุโส	สถาบันวิจัยและพั	สถาบันวิจัยและพัฒนาวิทยาศาสตร์ และเทคโนโลยี	เชียงใหม่	น้ำรบวิจับ	อยู่ในโครงการ
36. นายปถม วิชัยศิริมงคล	นายช่างอิเล็กทรอ- นิกส์	นายช่างอิเล็ก- ทรอนิกส์อาวุโส	สถาบันวิจัยและพั และเทศ	สถาบันวิจัยและพัฒนาวิทยาศาสตร์ และเทคโนโลยี	เชียงใหม่	นู้ช่วยวิจัย	อยู่ในโครงการ
37. นายใพโรจน์ การคนซ็อ	นายช่างอิเล็กทรอ- นิกส์	หัวหน้างาน	สถาบันวิจัยและพั	สถาบันวิจัยและพัฒนาวิทยาศาสตร์ และเทคโนโลยี	เชียงใหม่	นั้ช่วยวิจัย	ไม่อยู่ในโครงการ*
38. นายโฉม ทองเหลือม	นายช่างใฟฟ้า	นายช่างใฟฟ้า อาวูโส	สถาบันวิจัยและพั	สถาบันวิจัยและพัฒนาวิทยาศาสตร์ และเทคโนโลยี	เสียงใหม่	ผู้ช่วยวิจัย	อยู่ในโครงการ

รายชื่อผู้ทำงานในโครงการ

ชื่อ – นามสกูล	นหมเต	ตำแหน่งวิชาคาร		ต้นสั่งกัด		ตำแหน่งในโครงการ	สถานภาพปัจจุบัน
	เมื่อเข้าร่วมโครงการ	ปัจจุบัน	ภาควิชา	PRICE	มหาวิทยาลัย/สถาบัน		*(1-1 หมายเสมระยา)
39. นายสุวิชา รัตนรินทร์	พนักงานปฏิบัติการ	พนักงานปฏิบัติการ	พิลิกส์	วิทยาศาสตร์	เชียงใหม่	ผู้ช่วยวิจัย	อยู่ในโครงการ
40. นายวิทูร อะโน	นายช่างใฟฟ้า	นายชางใฟฟ้า	ศูนย์วิจัยนิว	ศูนย์วิจัยนิวตรอนพลังงานสูง	เชียงใหม่	ผู้ช่วยวิจัย	อยู่ในโครงการ
41. นายระเบียบ สุวรรณโกสุม	นายช่างใฟฟ้า	นายช่างไฟฟ้า	ศูนย์วิจัยนิว	ศูนย์วิจัยนิวตรอนพลังงานสูง	เชียงใหม่	ผู้ช่วยวิจัย	อยู่ในโครงการ
42. นายวิทูรย์ จินะมูล	ชางอิเล็กทรอนิกส์	ช่างอิเล็กทรอนิกส์	หูนย์วิจัยนิว	ศูนย์วิจัยนิวตรอนพลังงานสูง	เชียงใหม่	ผู้ช่วยวิจัย	อยู่ในโครงการ
43. นายทองสุข กลัคภิรมย์	ช่างเทคนิค	ช่างเทคนิค	ศูนย์วิจัยนิว	ศูนย์วิจัยนิวตรอนพลังงานสูง	เชียงใหม่	ผู้ช่วยวิจัย	อยู่ในโครงการ
44. นางสุมัทนา ธารารักษ์	เจ้าหน้าที่บริหาร เจานทั่วไป	เจ้าหน้าที่บริหาร งานทั่วไป	สถาบันวิจัยและ และเ	สถาบันวิจัยและพัฒนาวิทยาศาสตร์ และเทคโนโลยี	เชียงใหม่	เจ้าหน้าที่บริหารงาน ทั่วไป(การเงิน-บัญชี)	อยู่ในโครงการ
45. นางปรียาพร อินทะวัน	เจ้าหน้าที่บริหาร งานทั่วไป	เจ้าหน้าที่บริหาร งานทั่วไป	প্র মূল মূল মূল মূল মূল মূল মূল মূল মূল মূল	วิทยาศาสตร์	เชียงใหม่	เจ้าหน้าที่บริหารงาน ทั่วไป(พัสดุ-ธุรการ)	ใม่อยู่ในโครงการ*
46. น.ส.กุสุมาลย์ อุตตมะเวทิน	เจ้าหน้าที่บริหาร งานทั่วไป	เจ้าหน้าที่บริหาร งานทั่วไป	ศูนย์วิจัยนิว	หูนย์วิจัยนิวตรอนพลังงานสูง	เชียงใหม่	เจ้าหน้าที่บริหารงาน ทั่วไป(พัสตุ-ธุรการ)	อยู่ในโดรงการ
21. นายประดูง สวนพุฒ	อาจารย์	อาจารย์	พิลิกส์	วิทยาศาสตร์	เชียงใหม่	นักศึกษาปริญญาโท	จบการศึกษา*
47. นายทองลุน วิโลทอง	อาจารย์	ยาจารย์	พิลักส์	วิทยาศาสตร์	University of Laos	นักศึกษาปริญญาโท	จบการศึกษา
48. นายนิติศักดิ์ ปาสาจะ	นักศึกษาบัณฑิต	นักศึกษาปริญญาโท	พิลักส์	วิทยาศาสตร์	เชียงใหม่	นักศึกษาปริญญาโท	จบการศึกษา*
49. น.ส.ศุภรพรรณ ชูถิน	นักศึกษาบัณฑิต	นักศึกษาปริญญาโท	พิสิกส์	วิทยาศาสตร์	เชียงใหม่	นักศึกษาปริญญาโท	กำลังเขียนวิทยานิพนธ์
50. นายปิยะ ผ่านศึก	นักศึกษาบัณฑิต	นักศึกษาบริญญาโท	พิสาส	วิทยาศาสตร์	เชียงใหม่	นักศึกษาปริญญาโท	กำลังเขียนวิทยานิพนธ์

รายชื่อผู้ทำงานในโครงการ

เมื่อเข้าร่วมโครงการ 51. น.ส.ขนงค์ บุตย์เมือง นักศึกษาบัณฑิต 52. น.ส.ทิมพ์พร จันทร์ผง นักศึกษาบัณฑิต 53. น.ส.ทิรนันท์ สอนแก้ว นักศึกษาบัณฑิต 54. นายเอกซัย เติมสุขนิรันตร์ นักศึกษาบัณฑิต 55. น.ส.นงลักษณ์ ทนตี นักศึกษาบัณฑิต 57. นายจตุพร สายสุต นักศึกษาบัณฑิต	ร ปัจจุบัน นักศึกษาปริญญาโท นักศึกษาปริญญาโท นักศึกษาปริญญาโท นักศึกษาปริญญาโท นักศึกษาปริญญาโท นักศึกษาปริญญาโท	มาควิชา พลาส์ พลาส์ พลาส์ พลาส์	คณะ วิทยาศาสตร์ วิทยาศาสตร์ วิทยาศาสตร์ วิทยาศาสตร์	มหาวิทยาลัย/สถาบัน เชียงใหม่ เชียงใหม่	นักศึกษาปริญญาโท นักศึกษาปริญญาโท	(เอกสารหมายเลข 1-1)* กำลังเขียนวิทยานิพนธ์
7 1 2 1 2 1 2 1 2 2 2 2 2 2 2 2 2 2 2 2	นักศึกษาปริญญาโท นักศึกษาปริญญาโท นักศึกษาปริญญาโท นักศึกษาปริญญาโท นักศึกษาปริญญาโท นักศึกษาปริญญาโท		วิทยาศาสตร์ วิทยาศาสตร์ วิทยาศาสตร์ วิทยาศาสตร์	เชียงใหม่	นักศึกษาปริญญาโท นักศึกษาปริญญาโท	กำลังเขียนวิทยานิพนธ์
17.3 17.3 18.0 18.0 18.0 18.0 18.0 18.0 18.0 18.0	นักศึกษาบริญญาโท นักศึกษาบริญญาโท นักศึกษาบริญญาโท นักศึกษาบริญญาโท นักศึกษาปริญญาโท	स्त्र अर्थ अर्थ अर्थ अर्थ अर्थ अर्थ अर्थ अर	วิทยาศาสตร์ วิทยาศาสตร์ วิทยาศาสตร์	เชียงใหม่	นักศึกษาปริญญาโท	
กัว รันตร์	นักศึกษาบริญญาโท นักศึกษาบริญญาโท นักศึกษาบริญญาโท นักศึกษาบริญญาโท นักศึกษาปริญญาโท	भूक्षेत्रक भूक्षेत्रक भूक्षेत्रक भूक्षेत्रक	วิทยาศาสตร์ วิทยาศาสตร์ วิทยาศาสตร์			กำลังเขียนวิทยานิพนธ์
รันตร์	นักศึกษาบริญญาโท นักศึกษาบริญญาโท นักศึกษาบริญญาโท นักศึกษาบริญญาโท	स्त्र स्	วิทยาตาสตร์ วิทยาตาสตร์	เชยงใหม	นักศึกษาปริญญาโท	ทำลังทำวิจัย
No.	นักศึกษาปริญญาโท นักศึกษาปริญญาโท นักศึกษาปริญญาโท	भूक भूक भूक भूक भूक भूक भूक भूक भूक भूक	ริทยาศาสตร์	เชียงใหม่	นักศึกษาปริญญาโท	กำลังทำวิจัย
3	นักศึกษาปริญญาโท นักศึกษาปริญญาโท	स्त्र स्त्र स्त्र		เชียงใหม่	นักศึกษาปริญญาโท	กำลังทำวิจัย
	นักศึกษาปริญญาโท	\$ 000 G	วิทยาศาสตร์	เชียงใหม่	นักศึกษาปริญญาโท	กำลังทำวิจัย
		Merie	วิทยาศาสตร์	เชียงใหม่	นักศึกษาปริญญาโท	กำลังทำวิจัย
58. นายนิรุต ผุสดี	นักศึกษาปริญญาโท	พิลิกส์	วิทยาศาสตร์	เชียงใหม่	นักศึกษาปริญญาโท	กำลังทำวิจัย
The company of the last of the	SOM PARTY					
59.นายสมคักคี้ วรรณวิไลรัตน์ อาจารย์	อาจารย์	รังสีวิทยา	แพทย์ศาสตร์	เชียงใหม่	นักศึกษาปริญญาเอก	กำลังเขียนวิทยานิพนธ์
20. นายชีวรรณ บุญญารรรณ ผู้ช่วยศาสตราจารย์	ผู้ชวยตาสตราจารย์	พิลิกล์	วิทยาศาสตร์	เชียงใหม่	นักศึกษาปริญญาเอก	กำลังทำวิจัย
21. นายอุดมรัตน์ ที่พารรณ	อาจารย์	พิลิกล์	วิทยาศาสตร์	เชียงใหม่	นักศึกษาปริญญาเอก	กำลังทำวิจัย
23. นายมิญช์ เมรีสุวกุล	อาจารย์	भिन्नान्न	วิทยาศาสตร์	เชียงใหม่	นักศึกษาปริญญาเอก	กำลังเริ่มทำวิจัย*
60. น.ส.สาคร ริมแจ่ม นักศึกษาบัณฑิต	นักศึกษาบริญญา เอก	भ भ भ भ भ	วิทยาศาสตร์	เชียงใหม่	นักศึกษาปริญญาเอก	กำลังเริ่มทำวิจัย*

* รายชื่อผู้ที่ทำงานในโครงการ

		•	
19. น.ส.คุษฏี	16	สุวรรณขจร	ศึกษาปริญญาเอก ที่มหาวิทยาลัย Zurich ประเทศสวิสเซอร์แลนด์
20. นายธีรวรรณ	รรรรณ	م	ศึกษาปริญญาเอก ที่มหาวิทยาลัยเชียงใหม่ จ.เชียงใหม่
21. นายอุดมรัตน์	าดมรัตน์	ที่พวรรณ	ศึกษาปริญญาเอก ที่มหาวิทยาลัยเชียงใหม่ / Uppsala ภายใต้โครงการ Joint Ph. D. Program
22. นายประดุง	15293	สวนพุฒ	ศึกษาปริญญาเอกที่มหาวิทยาลัย Kyushu ประเทศญี่ปุ่น
23. นายมิญชั้	ำญช้	เมรีลุวกุล	ศึกษาปริญญาเอก ที่มหาวิทยาลัยเชียงใหม่ ทุนกาญจนาภิเษก รุ่น 2541
27. Mr.Garnet	arnet	Hoyes	ย้ายไปประจำตำแหน่งวิศวกรของคณะวิทยาศาสตร์ มหาวิทยาลัยเชียงใหม่
30. n.R.B	ออัญชัน	30. น.ส.ช่ออัญชัน ประพันธ์ศรี	ศึกษาปริญญาเอกที่มหาวิทยาลัย Technical University of Vienna ประเทศออสเศรีย
31. นายชาญชัย	ราญชัย	เดชธรรมรงค์	ดำรงตำแหน่งอาจารย์ ประจำภาควิชาวิศวกรรมไฟฟ้า สถาบันเทคโนโลยีราชมงคล วิทยาเขตภาคพายัพ
32. H.A.S	น.ส.รพีพรรณ	อำพนพันธุ์	คำรงตำแหน่งอาจารย์ มหาวิทยาลัยเอกชน กรุงเทพมหานคร
34. นายส	นายสมศักดิ์	วรรณชัย	คำรงตำแหน่งอาจารย์ ประจำภาควิชาวิศวกรรมไฟฟ้า สถาบันเทคโนโลยีราชมงคล เชียงราย
37. นายไพโรจน์	พโรจน์	การคนซื้อ	ย้ายไปทำงานบริษัทเอกชน ในตำแหน่งหัวหน้างานอิเล็คโทรนิกส์
40. น.ส.สาคร	สาคร	รมแจ่ม	ศึกษาปริญญาเอก ที่มหาวิทยาลัยเชียงใหม่ ทุนกาญจนาภิเษก รุ่น 2541
45. นางปรียาพร	เรียาพร	อินทะวัน	ลาออกไปประกอบธุรกิจส่วนตัว
48. นายนิติศักย์	เดิศักย์	ปาสาจะ	นักวิจัย ศูนย์วิจัยนิวตรอนพลังงานสูง มหาวิทยาลัยเชียงใหม่

ภาคผนวก ก.

ภาคผนวก ก1

A High Resolution Measurement of Double Differential Neutron Emission Cross Sections of ²⁰⁹Bi at 14.1 MeV Incident Energy

T. Vilaithong, U. Tippawan, and S. Singkarat

Fast Neutron Research Facility, Department of Physics, Faculty of Science,
Chiang Mai University, Chiang Mai 50200, Thailand.

Published in:

Conference Proceedings Vol. 59

Nuclear Data for Science and Technology

G. Reffo, A. Ventura and C. Grandi (Eds.)

SIF, Bologna, 1997.

ITALIAN PHYSICAL SOCIETY

CONFERENCE PROCEEDINGS

VOLUME 59

Part I

International Conference on Nuclear Data for Science and Technology

edited by G. Reffo. A. Ventura and C. Grandi Trieste, 19-24 May 1997

Centenary 1897-1997



Italian Physical Society Bologna - Italy Conference Proceedings Vol. 59

-Nuclear Data for Science and TechnologyG. Reffo, A. Ventura and C. Grandi (Eds.)
SIF. Bologna, 1997

A HIGH RESOLUTION MEASUREMENT OF DOUBLE DIFFERENTIAL NEUTRON EMISSION CROSS SECTIONS OF 209 Bi AT 14.1 MeV INCIDENT ENERGY

T. Vilaithong, U. Tippawan, and S. Singkarat

Fast Neutron Research Facility, Department of Physics, Faculty of Science, Chiang Mai University, Chiang Mai 50200, Thailand.

ABSTRACT

A high resolution time-of-flight (TOF) facility has been constructed at Chiang Mai University to measure the neutron emission cross sections at 14.1 MeV incident energy. The neutron TOF spectra could be taken at an angle ranging from 20 to 160 degrees with a 12 meters flight path. The double differential neutron emission cross sections at 14.1 MeV were measured for ²⁰⁹Bi using a 10 in diam and 4 in thick liquid scintillator. The corresponding energy resolution at 14.1 MeV was about 415 keV FWHM. The measured spectra are presented and discussed in comparison with other recent measurements and results of calculation based on pre-equilibrium and collective reactions.

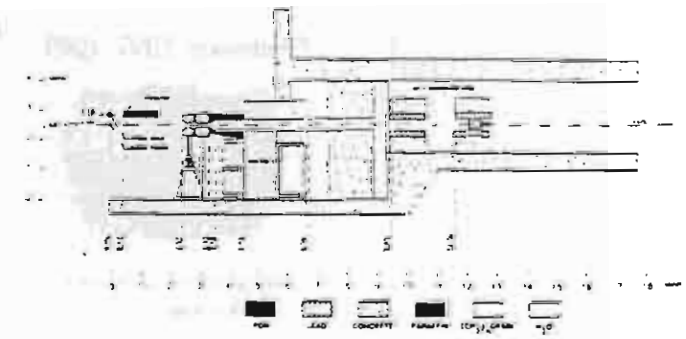
I. INTRODUCTION

Analysis of neutron emission cross sections for vibrational nuclei in terms of quantum-mechanical, statistical multistep reaction mechanisms have been complicated because of interference from neutrons resulting from collective excitations. Attempts have been made to include these contributions. Kalka et al.[1] considered only those collective excitations to the lowest 2' and 3' states. Marcinkowski et at.[2] and Demetriou et al.[3] include the direct reactions that excite isoscalar, low-energy vibrations as well as the giant resonances in the continuum in their analysis. They compared their calculated results with the high resolution measurements of Takahashi et al.[4] which show difference in the spectral region of interest. We report here an important independent determination of these spectra.

II. EXPERIMENTAL METHOD

The production of nsec pulsed neutron beam has been described elsewhere. Briefly, neutrons with kinetic energy of 14.1 MeV were produced from a high stability Cockeroft-Walton type accelerator by the $T(d,n)^4$ He reaction. The 140 keV analyzed deuteron beam was chopped by a double-plate deflecting system and then bunched to pulses with widths of 1.5 to 2.0 ns at the neutron production target by a double-gap klystron buncher. This work utilized an average beam current of about 15 μ A with a neutron pulse width of about 1.8 ns at 1 MHz repetition rate.



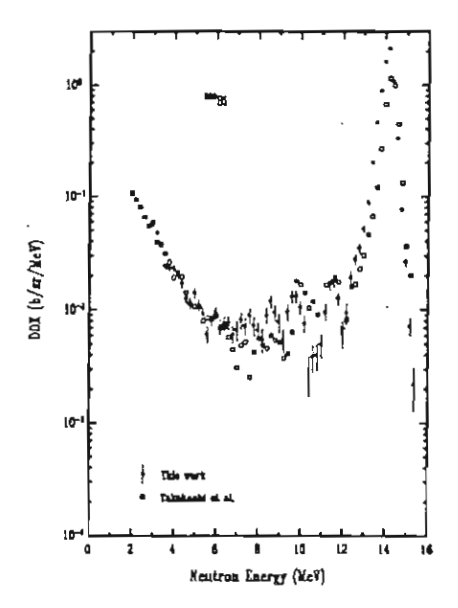


A detailed description of measurement and data reduction has been described recently [5]. A cylindrical sample of ²⁰⁹Bi, 3 cm in diameter and 5 cm long, was positioned at 90° relative to the incident deuteron beam with its axis along the axis of the beam line as shown in fig.1.

Neutrons were detected in a BC-501A liquid scintillating detector of diameter 25 cm and thickness 10 cm. The detector was coupled to a Hamamatsu R1250 photomultiplier tube via a partially coated taper light pipe. It was located at an extended flight path of 12 m inside a well shielded tunnel. Monte Carlo calculation indicates that scattering effect is less than 1% for this collimating system[6]. Time-of-flight measurements were made at angles 30°, 25° and from 20° to 150° in step of 10°. The corresponding energy resolution at 14.1 MeV was about 415 keV FWHM.

The neutron spectrum was determined from the measured TOF spectra in separate energy regions. The γ - rejection was observed for each of the TOF regions because the γ - rejection technique was pulse-height dependent. Because of the large size of the neutron detector, neutron and gamma events in the pulse shape spectrum were not completely separated and some neutrons were lost. This loss was estimated to be less than 1%.

Several corrections were made to the number of detected neutrons. The most significant one was due to multiple scattering. Correction due to this effect and the correction due to contamination of low energy neutrons in the incident neutron spectrum were carried out with the SYNTHIA Monte Carlo computer code developed by Tohoku University [7]. The overall systematic error for the value of the DDX is estimated to be about 11%. The statistical uncertainties varies from less than 1% to about 39% in the discrete region of the spectra of neutrons emitted in backward angles.



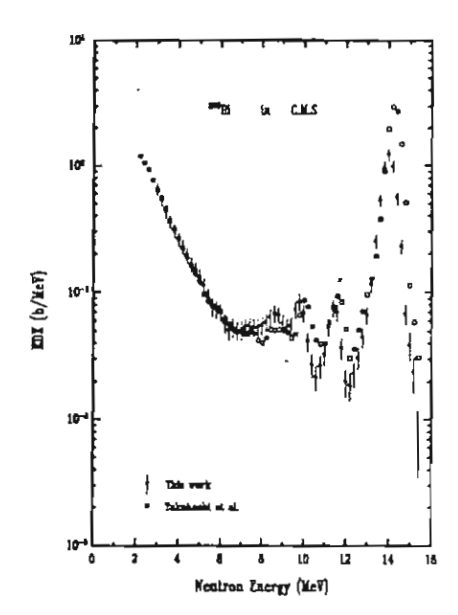
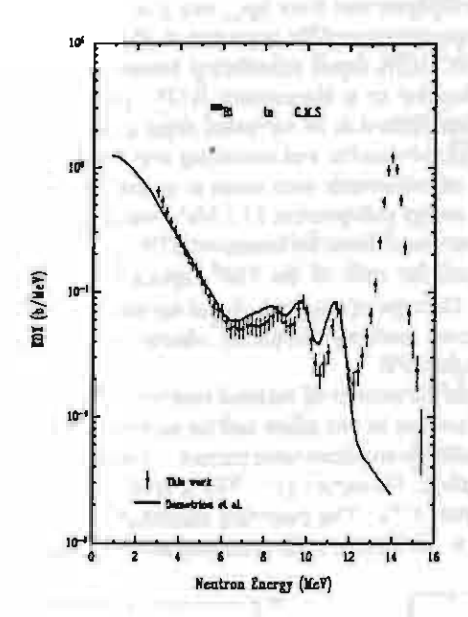


Fig. 2 Double differential cross section of ³⁰⁹Bi at 20°. The data of Takahashi et al.[4] is shown for comparison.

Fig. 3 Angle integrated spectra of ²⁰⁹Bi in the CM system.

III. RESULTS AND DISCUSSION

In fig.2. we compare our measurement at 20° with the result of Takahashi et al.[4]. The angle-integrated spectra are compared in fig.3. The two different sets of measurement are in reasonable agreement. Because of better energy resolution, our data reveal more detailed structure in the region between 6 to 12 MeV



We compare our angle integrated spectrum in fig.4. with the calculated results of Demetriou et al.[3]. based on the Feshbach-Kerman-Kooning theory. In their calculation, Demetiou et al. also include contribution from direct reactions that excite low energy vibrations as well as the giant resonances in the continuum, in addition to the incoherent multistep direct reaction, multistep compound and compound nucleus reaction.

The calculated spectrum reproduces the experimental data very well in the regions between 3 to 6 MeV and 9 to 12 MeV. In the region between 6 and 9 MeV where preequilibrium reaction dominates, the two spectra do not agree. The calculated spectrum slightly overestimates the number of emitted neutrons

Fig. 4 Comparison of angle-integrated spectrum of ³⁰⁹Bi in the CM system with the calculated spectrum of Demetriou et al.[3].

IV. CONCLUSION

We measured the double differential neutron emission cross sections above 3 MeV from bismuth at 14.1 MeV from 20° to 150° with an energy resolution of about 415 keV FWHM. The measurements are in general agreement with those of Takahashi et al.[4].

In the preequilibrium reaction region between 6 and 9 MeV where there are contributions from the collective excitations, our measurements are slightly lower than the calculated spectrum of Demetriou et al.[3].

ACKNOWLEDGEMENT

We thank A.Takahashi for providing a bismuth sample and M.Baba for the SYNTHIA code. This work was supported in part by the Thai Research Fund.

REFERENCES

- 1. H.Kalka, M. Torjman and D. Seelinger, Phy Rev. C40,1619 (1989)
- 2. A.Marcinkowski, B.Marianski, P.Demetriou and P.E.Hodgson, Phys.Rev.C52, 2021 (1995)
- 3. P.Demetriou, A.Marcinkowski and P.E.Hodgson, Nucl. Phys. A596, 67 (1996)
- A.Takahashi, M.Gotoh, Y.Sasaki and H.Sugimoto, OKTAVIAN Report A-92-01. Osaka University, 1992.
- 5. T.Vilailthong, D.Boonyawan, S.Konklong, W.Pairsuwan and S.Singkarat, Nucl.Instr. and Meth. A332, 561 (1993)
- 6 H.Kobus, T.Vilaithong, W.Pairsuwan and S.Singkarat, "Monte Carlo Simulation on the Neutron Transport of the Chiang Mai TOF-Facility," Proc.Int.Conf. on Nuclear Data for Science and Tchnology, J.K.Dickens(Ed.) Gatlinburg., 9-13 May 1994, pp 111-114.
- M.Baba, S.Matsuyama, M.Ishikawa, S.Chiba, T.Sakase and N.Hirakawa, Nucl. Instr.and Meth. A366, 354 (1995)

ภาคผนวก ก2

Double-Differential Neutron Emission Cross Sections on ²⁰⁹Bi at 14.1 MeV Incident Energy

T. Vilaithong, U. Tippawan, S. Singkarat and S. Wiboolsake

Fast Neutron Research Facility, Department of Physics, Faculty of Science,
Chiang Mai University, Chiang Mai 50200, Thailand.

Published in:

ScienceAsia 25 (1999) 43-50.

Double-Differential Neutron Emission Cross Sections on ²⁰⁹Bi at 14.1 MeV Incident Energy

I Vilaithong, U Tippawan, S Singkarat and S Wiboolsake Fast Neutron Research Facility, Department of Physics, Faculty of Science, Chiang Mai University, Chiang Mai 50200, Thailand.

Received 6 Feb 1999

ABSTRACT The energy and angular distributions of neutrons above 3 MeV emitted from collisions of 14.1 MeV neutrons with bismuth target were measured using the high resolution time-of-flight (TOF) facility at Chiang Mai University. The results are compared with the most recent measurements and with the calculated spectra based on the statistical multistep model code EXIFON. The angular distributions of the secondary neutrons were analyzed by the Kalbach-Mann systematics using the more recent coefficients of Kumabe et al. In the case of bismuth, the measured and calculated spectra only agree in the limited energy region between 6 and 12 MeV.

KEYWORDS: nuclear reaction, 209Bi (n,xn'), E=14.1 MeV, statistical multistep theory analysis.

NTRODUCTION

Analysis of neutron emission cross sections for vibrational nuclei in terms of quantum mechanical, statistical multistep reaction mechanisms have been complicated because of interference from neutrons resulting from collective excitations. Attempts have been made to include these contributions. Kalka et all considered only those collective excitations to the lowest 2° and 3° states. Marcinkowski et al2 and Demetriou et al3 include the direct reactions that excite isoscalar, low-energy vibrations as well as the giant resonance in the continuum in their analysis. They compared their calculated results with the high resolution measurements of Takahashi et al.4 The calculated and measured spectra do not agree over the entire energy region. We report here the measurements and analysis of these spectra for bismuth. The closed shell nucleus 109Bi has been one of the few elements proposed as a candidate for a neutron multiplier in the conceptual design of fusion reactor.5 Therefore, accurate measurements of its double-differential cross sections (DDX) and angle integrated cross sections are also needed for the practical application. Apart from the experiment of Takahashi et alt, there have been very few high resolution measurements of the neutron emission spectra of bismuth in the last decade. Wang et al6 measured the neutron emission spectra and angular distributions at 7 MeV neutron bombarding energies with 5.1 m flight path and 2 ns time resolution corresponding to 400 keV resolution for the elastically scattered neutrons. Marcinkowski et al7 carried out similar measurement at 20 MeV with an energy resolution of about 600 keV. The most recent DDX measurement of bismuth was performed by Baba et al⁸ for incident neutrons of 14.1 and 18.0 MeV. The overall timing resolution of their spectrometer was 2.0 to 2.5 ns and the flight path was around 6 m for 14 MeV measurement. Therefore, only one high resolution experiment has been performed at 14 MeV for bismuth, the measurements reported here provide an important separate determination of these spectra.

MATERIALS AND METHODS

Experimental Procedure

The experiment was performed at the high resolution time-of-flight (TOF) facility of the Fast Neutron Research Facility of Chiang Mai University. The production of a ns pulsed neutron beam was described in an earlier publication. Briefly, neutrons with energy of 14.1 MeV were produced from a high stability Cockcroft-Walton-type accelerator by the T(d,n) He reaction. The 140 keV analysed deuteron beam was chopped by a double-plate deflecting system and then bunched by a double-gap klystron buncher to produce beam pulses with widths of 1.5 to 2.0 ns at the neutron production target. This work utilized an average beam of about 15 mA with a neutron pulsed width of about 1.8 ns at 1 MHz repetition rate.

The experimental arrangement and data reduction procedure used in the present measurement were similar to those described previously. A schematic diagram of the experimental set up is shown in Fig 1. A cylindrical sample of ²⁰⁹Bi, 3 cm in diameter and 7 cm long, was positioned at 90° relative to the incident deuteron beam with its axis along the axis

ScienceAsia 25 (1999)

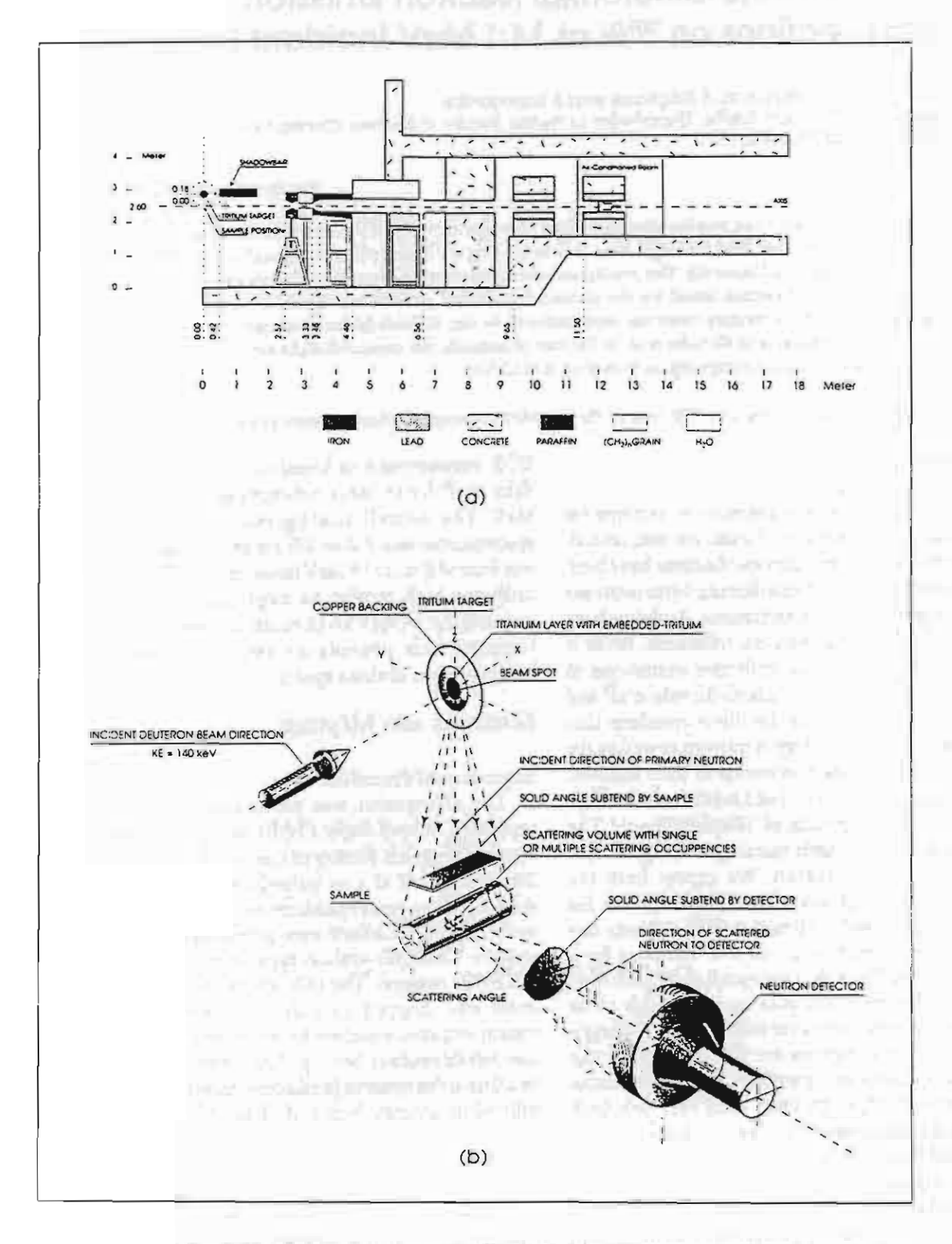


Fig 1. Experimental arrangement for the TOF measurement (a) collimating and shielding arrangement (b) target arrangement.

of the beam line. The target was cooled by forced air. A sample rotation technique provides the capability of measuring scattered neutrons over an angular range of 20° to 160°.

The scattered neutrons were detected with a 25.0 cm diam and 10.0 cm thick BC-501A liquid scintillator. The detector was coupled to a Hamamatsu R1250 photomultiplier tube via a partially coated taper light pipe. It was located at an extended flight path of 12 m inside a well shielded tunnel as shown in Fig 1. Monte Carlo calculation indicates that effect due to in-scattered neutrons is less than 1%. The neutron detector was housed in a temperature controlled room to minimize photomultipher tube gain drift. Neutron fluxes were monitored by three 5 cm diam by 5 cm thick NE-102A and NE-213 scintillators. This flux monitoring system is accurate to better than 1%.

The electronic system used in this measurement has been described in details elsewhere. Only a brief description will be given here. A pulse-shape discrimination system (PSD) based on a zero-cross over method was incorporated into the main electronic system to reduce the gamma-ray background. The data acquisition system is controlled by a 16MB MicroVAXII computer through a multiparameter-buffer system (MBS) unit. Each reaction event detected by the main detector is recorded sequentially in list mode on disk. Each event contains (i) the pulse height, (ii) the time-of-flight, and (iii) the n-gamma pulse shape discrimination data. The off line analysis software allows dynamic selection for each correlated parameter.

Calibration of the pulse height response of the main detector was performed in about 8 h intervals before and after each scattering angle with 137Cs and ²²Na gamma sources. The pulse height threshold was set at about 1.5 MeV proton energy. At this bias setting, the corresponding energy resolution of our neutron spectrometer at 14.1 MeV was about 420 keV FWHM. Time-of-flight spectra were obtained at 14 angles between 20° to 150° in 10° increment. For each set of measurement, a "sample-in" spectrum was taken followed by a "sample-out" spectrum. A polyethylene sample of the same dimension as that of the bismuth sample was used as standard and positioned at 25° relative to the incident neutron beam. Each run took about 3-4 h, therefore, the measurement at one angle including the "out target" run lasted about 7-8 h. During this period the stability of the electronic system was better than 1%

A typical TOF spectrum of bismuth at 20° is shown in Fig 2. The sample-out spectrum is also shown for comparison. The background spectrum is clean and no structure was observed in the region of interest. The prompt gamma ray peak was used as reference to convert TOF spectrum to energy spectrum.

Data reduction

Neutron energy spectra were obtained from the measured TOF spectra using the known flight path and a calibration of time-to-amplitude converter. The DDX in units of b per sr per MeV were determined using the detector efficiency, monitor counts, and ¹H(n, n) cross section as standard. The neutron detecting efficiencies were calculated with the Monte

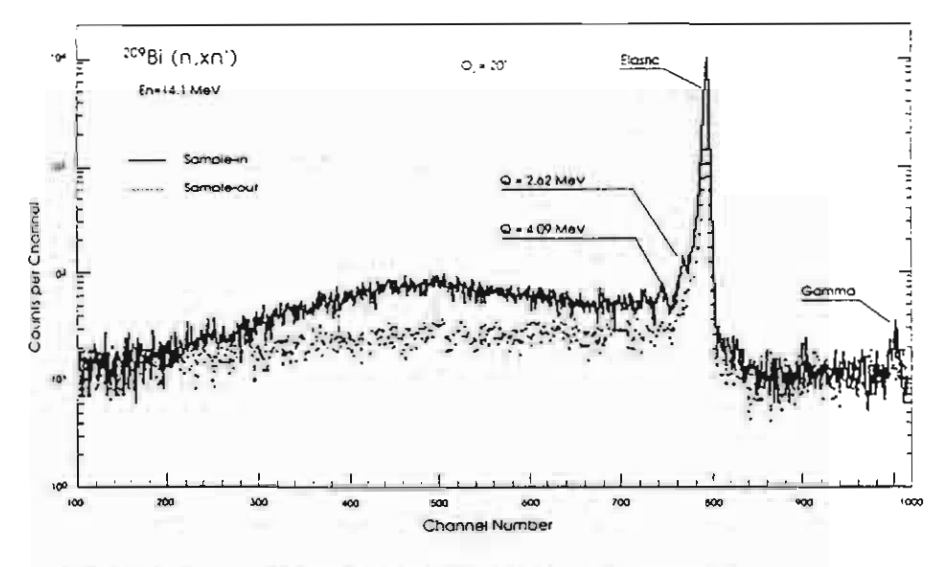


Fig 2. A typical TOF spectrum of bismuth at 20'. The sample-out run is shown for comparison.

Carlo computer code. 12 The differential cross sections were averaged over 0.2 MeV energy bin which corresponded to the energy resolution of the TOF spectrometer. The experimental procedure and data reduction is similar to that described in details elsewhere. 10 The correction for multiple scattering, flux attenuation and contamination of low energy neutrons in the incident neutron spectrum was performed using a Monte Carlo computer code SYNTHIA developed by Baba et al. 13 at Tohoku University.

The DDX data were converted from the laboratory system to the center-of-mass system (CM), by assuming the kinematics of two body reaction. ¹⁴ The angle-integrated neutr on spectrum (EDX) in the CM system was obtained by weighted the angular distribution for each energy bin with experimental uncertainties and fitted with Legendre polynomials. The EDX in the CM system is used for comparison with other measurements and calculated cross sections.

The overall systematic error for the DDX is estimated to be \pm 11%. This number was obtained from the quadratic sum of the following uncertainties: (1) \pm 3% for the neutron detecting efficiency; (2) \pm 2% for the variation of the incident neutron yield; (3) \pm 1% for H cross section: (4) \pm 1% for the monitor; (5) \pm 2% for estimating hydrogen scattering yield; (6) \pm 10% for the flux attenuation and multiple scattering corrections of polyethelene and bismuth samples. The experimental uncertainties were estimated by combining the statistical and systematic uncertainties in quadrature.

Model calculations

Nuclear model calculations of 14.1 MeV neutron inelastic scattering on ²⁰⁹Bi have been performed with the statistical multistep model code EXIFON. ¹⁵ This code is based on an analytical model for statistical multistep direct and multistep compound reaction (SMD/SMC). EXIFON predicts the secondary particle angular distributions in addition to their emission spectra (EDX). In this section we summarize these calculations and describe the parameters used in our calculations.

The code EXIFON calculates the overall energy differential cross section on the basis of pure quantum mechanical concept by summing up the contributions from the SMD, SMC and multiparticle emission (MPE) processes. This idea constitutes a very strong place in nuclear reaction theory as being supported by its counterpart in many body theory. The residual interactions are replaced by random matrices and after performing the energy ensemble

averaging, the analytical expressions for the energy differential cross section; (EDX) becomes¹⁵

$$\frac{d\sigma_{sb}(E_s)}{dE_s} = \frac{d\sigma_{sb}^{sko}(E_s)}{dE_s} + \frac{d\sigma_{sb}^{sko}(E_s)}{dE_s} + \frac{d\sigma_{sb}^{sko}(E_s)}{dE_s}$$
(1)

where the direct reaction to collective phonon and single particle states are accounted for as a part of the SMD process, and the MPE are calculated in the pure SMC concept. For our nuclide of interest, 209Bi, the optical model potentials of Wilmore and Hodgson¹⁶ are adopted. The only adjustable parameter is the pairing shift ($\Delta = 12.8 \text{ A}^{-1/2}$) which goes to zero near closed shell. The shell correction for the state density are also taken into account for the process. The present calculations are performed with a Breit-Wigner function of width 0.9 MeV instead of the built in value of 1.4 MeV to simulate the higher energy resolution in our experiments. Other parameters are left unadjusted. The effect of angular momentum and nuclear spin are not considered to make the calculation as simple as possible without any significant effects.

The ADXs are calculated using the Kalbach-Mann systematics.¹⁷ These systematics give the DDX for particle emission reaction by superposing the forward peaked distribution for SMD on the 90° symmetric distribution of SMC process taking into account the weight of the SMD:

$$\frac{d^{2}\sigma}{d\Omega dE} = a_{o}(SMD) \sum_{i=0}^{low} b_{i} P_{i}(\cos\theta) + a_{o}(SMC) \sum_{i=0}^{low} b_{i} P_{i}(\cos\theta)$$
(2)

where
$$b_{i}(E) = \frac{21+1}{1+\exp[A_{i}(B_{i}-E)]}$$

We have used the more recent coefficients of Kumabe et al¹⁸

$$A_1 = 0.0561 + 0.03771 \text{ MeV}^{-1}$$

 $B_1 = 47.9 - 27.11^{-1/2} \text{ MeV}$

The coefficients a in (2) satisfy the relation

$$a_o(total) = a_o(SMD) + a_o(SMC)$$
 (3)

a_o(SMD) and a_o(SMC) are obtained from EXIFON taking account of direct (DR) and MPE components in multistep direct (SMD) and multistep compound (SMC) respectively.

RESULTS AND DISCUSSION

Comparison with other measurements

The double-differential cross sections obtained in our measurement for bismuth are shown in Fig. 3 and they are available in tabular form upon request. The angle-integrated cross sections (EDX) are presented in Table 1. In Fig 4, we compare our measurements at 30° and 120° with those of Takahashi et alt and Baba et al8 The error bars shown on our data are statistical only. The three different sets of measurements are in general agreement to within 10 to 20%. Nevertheless, our data reveals more detailed structures in the region between 6 to 12 MeV which is due to direct excitation of lowlying vibrational levels. It should be noted that Takahashi et al4 used 8.3 m flight path for his TOF measurement so his energy resolution is almost comparable to ours whereas Baba et al8 measured their neutron spectra with poorer energy resolution. Fig 5 illustrates the angle-integrated cross sections of Bi from three different experiments. The effect due to difference in the energy resolution of the TOF

spectrometer can be clearly observed in the spectral regions where broad peaks are located. The enhancement of these structures in ²⁰⁰Bi is to be expected because it is next to the double-closed-shell ²⁰⁰Pb.

Theoretical analysis

Angle-integrated neutron emission cross section (EDX)

The nuclear model calculations described under the heading model calculations have been performed and the results compared to the experimental data. The calculated spectrum is presented together with

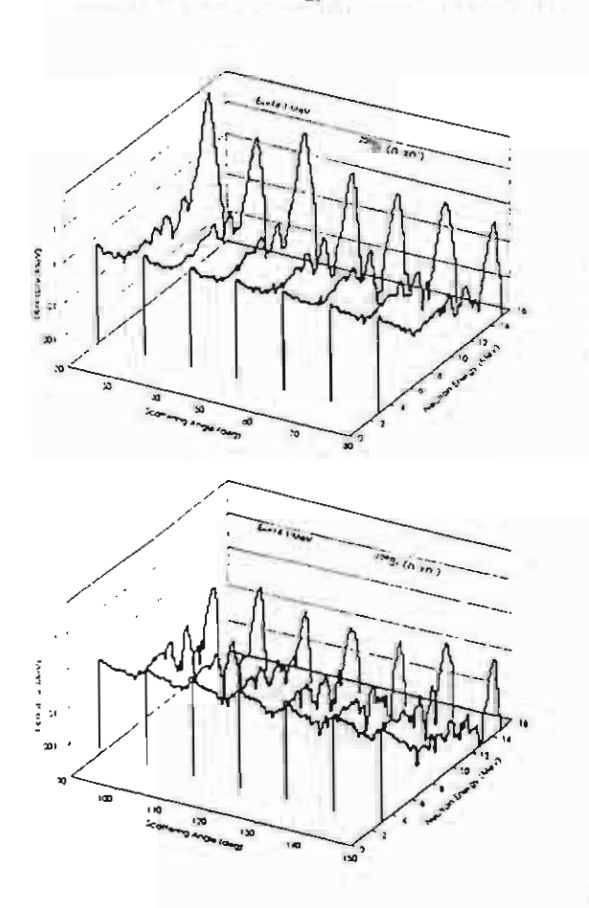


Fig 3. Double-differential cross sections of 100 Bi from 20' to 150' in step of 10' at 1+.1 MeV in the laboratory system.

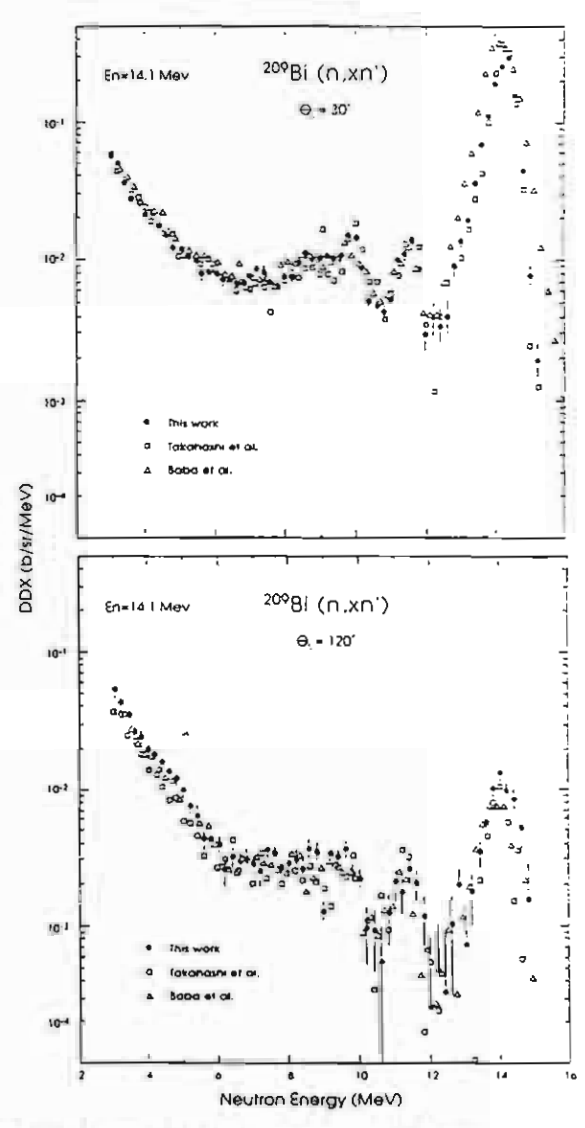


Fig 4. Double-differential cross sections of 20°Bi at (a) 30° and (b) 120°. The data of Takahashi et al* and Baba et al* are shown for comparison.

Table 1. Angle-integrated cross-sections of ²⁰⁰Bi in the CM system. The errors shown are experimental uncertainties.

Energy (MeV)	EDX (b/MeV)	Energy (MeV)	EDX(b/MeV)
3.0	6.45±0.74E-1	9.2	5.31±0.89E-2
3.2	5.35±0.62E-1	9.4	5.49±0.90E-2
3.4	4.32±0.51E-1	9.6	7.30±1.12E-2
3.6	3.59±0.43E-1	9.8	8.38±1.26E-2
3.8	3.03±0.37E-1	10.0	6.89±1.09E-2
4.0	2.60±0.32E-1	10.2	4.11±0.75E-2
4.2	2.26±0.28E-1	10.4	2.67±0.56E-2
4.4	1.94±0.25E-1	10.6	2.14±0.48E-2
4.6	1.66±0.22E-1	10.8	2.62±0.56E-2
4.8	1.51±0.20E-1	11.0	3.25±0.63E-2
5.0	1.32±0.18E-1	11.2	5.30±0.88E-2
5.2	1.14±0.16E-1	11.4	7.49±1.14E-2
5.4	9.24±1.36E-2	11.6	6.97±1.09E-2
5.6	7.61±1.17E-2	11.8	3.65±0.70E-2
5.8	7.24±1.12E-2	12.0	1.99±0.50E-2
6.0	6.93±1.09E-2	12.2	1.84±0.47E-2
6.2	5.71±0.94E-2	12.4	2.29±0.52E-2
6.4	5.05±0.86E-2	12.6	3.05±0.60E-2
6.6	5.28±0.89E-2	12.8	4.41±0.77E-2
6.8	4.99±0.85E-2	13.0	6.60±1.01E-2
7.0	5.04±0.85E-2	13.2	1.15±0.16E-1
7.2	5.40±0.90E-2	13.4	2.51±0.30E-1
7.4	5.43±0.90E-2	13.6	5.32±0.61E-1
7.6	5.28±0.89E-2	13.8	9.58±1.07E-1
7.8	5.28±0.89E-2	14.0	1.22±0.14E-0
8.0	5.54±0.94E-2	14.2	9.81±1.10E-1
8.2	5.81±0.96E-2	14.4	5.53±0.65E-1
8.4	6.36±1.02E-2	14.6	2.29±0.29E-1
8.6	6.79±1.07E-2	14.8	6.74±1.19E-2
8.8	6.63±1.06E-2	15.0	3.87±0.96€-2
9.0	5.64±0.94E-2	15.2	2.35±0.73E-2

Science Asia 25 (1999) 49

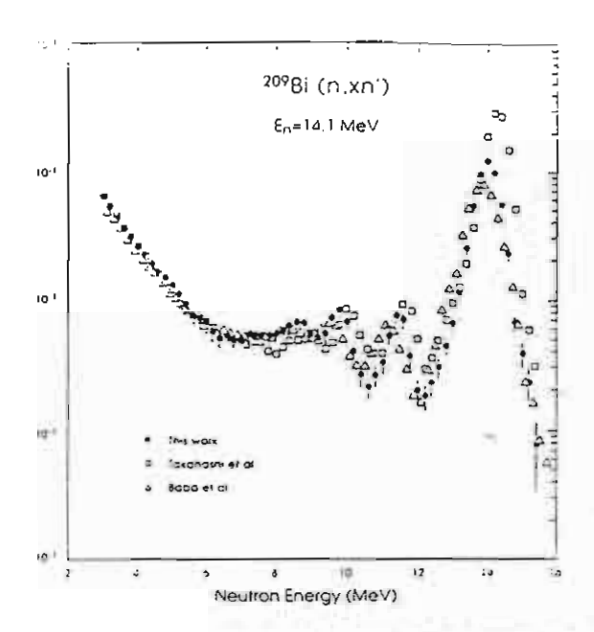


Fig 5. Angle-integrated spectra of ²⁰⁰Bi in the CM system. The error bars are derived from experimental uncertainties.

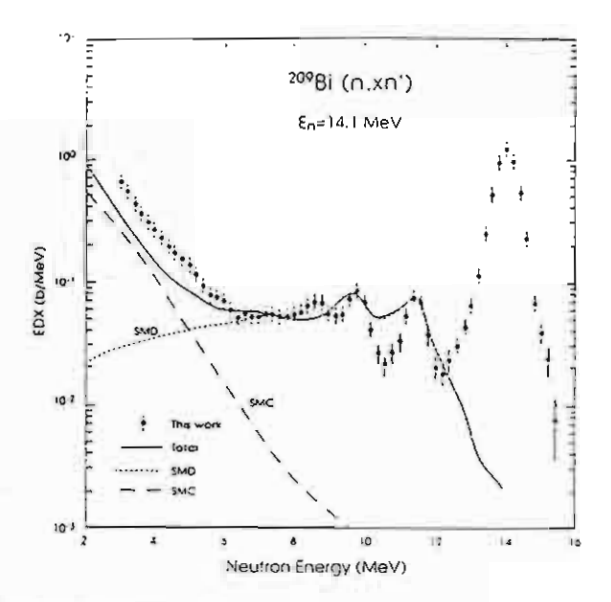


Fig 6. Comparison of the angle-integrated spectrum with the calculation by ENIFON.

the measured spectrum in Fig 6. For the sake of comparison, the separate contributions from SMD and SMC are also shown in the figure. On the whole, the neutron production spectrum in the continuum between 3 - 5 MeV (low emission energy region, or high excitation energies of the residual nucleus) is underestimated by the model calculation by about 30%. As the measurement has relatively small uncertainties, some deviation between calculations and experiments are clearly noticed. At about 5 - 8 MeV, the calculations reproduce the data very well. In the energy region between 8 to 11 MeV when only two excited levels 2* and 3* are considered, the shapes and structures of the measured spectrum are poorly reproduced by the calculation. But when all nine excited levels (2°, 3°, 4°, 5°, 6°, 7°, 8°, 9°, 10°) are incorporated, the calculated result reproduces the experimental data fairly well apart from the bump at 10 MeV, which is to be expected as the calculated spectrum is smeared out using a Gaussian resolution function normalized to the gamma width. The values of the deformation parameter, β1, and the energies. E,, of the collective excited low-lying states are taken from those of 208 Pb. 3 The result confirms that in this energy region, the collective excitations to low-lying states play important role. However, the code also takes only the lowest energy state of each level as an input for calculations. This may as well be the cause of the remaining discrepancy between the calculated and measured spectra in this energy region. Changing the values of model parameters does not significantly improve the calculated results. Since all the energy levels are taken from those of ²⁰⁸Pb, the double magic nuclei, the difficulty discussed by Marcinkowski *et al*⁷ may be relevant here.

In summary, our calculation largely underestimates the present measured EDX data for ²⁰⁹Bi in the continuum region. The shape and structures of the measured spectrum are fairly reproduced in the region where collective excitation of low-lying states are important. The discrepancies in the yield and structure reproduction, as a result of taking only the 2* and 3' levels into consideration, are also reported by Baba *et al.*¹³

Angular distribution (ADX)

Fig 7 a) to d) compare the measured ADX at fixed energy of 3-4, 5-6, 6-7 and 8-9 MeV with the calculated ADXs obtained from Kalbach-Mann systematics¹⁷ with the new coefficient of Kumabe et al.¹⁸ The shape of the calculated angular distributions are in good agreement with those of the measured ones, although the magnitudes are slightly underestimated. The DR and MPE components have been included into SMD and SMC, respectively.

To summarize, Kalbach-Mann systematics with the new coefficients from Kumabe et al¹⁸ reproduce quite satisfactorily the neutron ADX for ²⁰⁹Bi using the SMD and SMC spectra for a (SMD) and a (SMC).

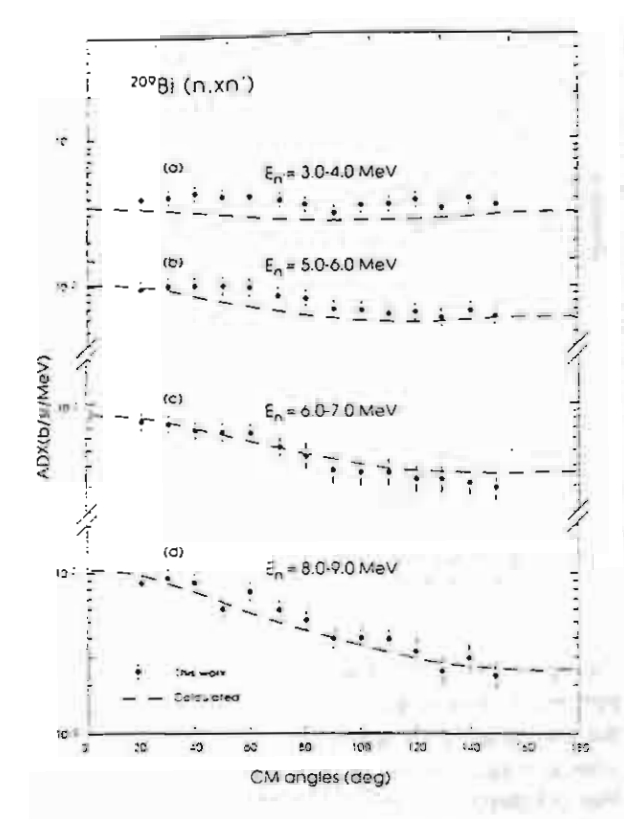


Fig 7. Comparison of the ADXs with the calculated distributions using Kalbach-Mann systematics.

CONCLUSIONS

We measured the double differential neutron emission cross sections of 209Bi induced by 14.1 MeV neutrons with a high resolution time-of-flight spectrometer. The measured spectra are in reasonable agreement with the other high resolution measurements and reveals structures in the region between 8 to 12 MeV. The calculated spectrum based on the statistical multistep model code EXIFON reproduces the experimental data fairly well in the limited energy range between 6 and 12 MeV. The code underestimates the neutron vield in the compound nucleus region by as much as 30%. The shape of the angular distribution is reproduced reasonably well by the systematics of Kalbach Mann using coefficients of Kumabe et al. For better reproduction of neutron yields and structures in the measured spectra further theoretical studies are required.

ACKNOWLEDGEMENTS

We are grateful to A Takahashi for providing the bismuth sample and M Baba for the SYNTHIA computer code. We thank F Maekawa for the latest version of the Japanese evaluated nuclear data library and helpful discussions. The technical support of S Rattanarin in running the pulsed neutron generator and M Rhode in maintaining the data acquisition system are gratefully acknowledged. This work was supported in part by the Thailand Research Fund.

REFERENCES

- H Kalka, M Torjman and D Seclinger (1989) Phys Rev C+0, 1619.
- A Marcinkowski, B Marianski, P Demetriou and PE Hodgson. (1995) Phys Rev C52, 2021.
- P Demetriou, A Marcinkowski and PE Hodgson (1996) Nucl Phys A529, 67.
- A Takahashi, M Gotoh, Y Sasaki and H Sugimoto (1992). OKTAVIAN Report A-92-01, Osaka University.
- ET Cheng (1986) Proc IAEA Advisory Group Meeting on Nuclear Data for Fusion Reactor Technology, Dresden.
- X Wang, Y Wang, D Wang and J Rapaport, (1987) Nucl Phys A465, 483
- A Marcinkowski, J Rapaport, R Finlay and X Aslanoglou. (1991) Nucl Phys A530, 75.
- M Baba, S Matsuyama, T Ito, T Ohkubo and N Hirakawa (1994) J Nucl Sci Technol 31, 757.
- T Vilanhong, S Singkarat, W Pairsuwan, JF Kral, D Boonyawan, D Suwannakachorn, S Konklong, P Kanjanarat and GG Hoyes (1991) A Pulsed Neutron TOF Facility at Chiang Mai. In: Proc Int Com Nuclear Data for Science and Technology, Juelich, 1991. SM Qaim (Ed) Springer-Verlag, pp 482-6.
- T. Vilanthong, D. Boonyawan, S. Konklong, W. Pairsuwan and S. Singkarai (1993) Nucl. Instr. and Meth. A332, 561.
- 11. H Kobus, T Vilanthong, W Pairsuwan and S Singkarat (1994) Monte Carlo Simulation on the Neutron Transport of the Chiang Mai TOF-Facility. In: Proc Int Conf on Nuclear Data for Science and Technology. Gatlinburg. 1994. JK Dickens (Ed) pp111-4
- 12 R Cecil, BD Anderson and R Madey (1979) Nucl Instrument Meth 161, +39.
- M Baba, S Maisuyama, M Ishikawa, S Chiba, T Sakase, H Hirakawa (1995) Nucl Instr and Meth A306, 354.
- 14 A Takahashi, Y Sasaki and H Sugmoto (1988) Report JAERI-M-88-065, p 279.
- 15.H Kalka (1991) Code EXIFON (version 2.0).
- 16. D Wilmore and PE Hodgson (1964) Nacl Phys 55, 673.
- 17. C Kalbach and FM Mann (1981) Phys Rev C23, 112.
- 18.1 Kumabe, Y Watanabe, Y Nohtomi, M Hanada (1990) Nucl Sci Eng 104, 280.

ภาคผนวก ก3

Utilization of a Pulsed D-T Neutron Generator

T. Vilaithong, S. Singkarat and U. Tippawan

Fast Neutron Research Facility, Department of Physics, Faculty of Science,
Chiang Mai University, Chiang Mai 50200, Thailand.

Presented at:

The Advisory Group Meeting on the Optimal Use of Accelerator

Based Neutron Generators,

13-16 October 1998,

IAEA, Vienna, Austria.

UTILIZATION OF A PULSED D-T NEUTRON GENERATOR T. VILAITHONG, S. SINGKARAT AND U. TIPPAWAN.

Fast Neutron Research Facility, Department of Physics, Faculty of Science Chiang Mai University, Chiang Mai 50200, Thailand.

ABSTRACT

The Fast Neutron Research Facility at Chiang Mai University is equipped with a nano-second pulsed 14 MeV neutron generator, a multiparameters data acquisition and analysis system and various radiation detectors. Fast neutrons from the low energy ion accelerator are used in the field of radiation dosimetry, neutron induced nuclear cross sections measurement and elemental analysis. With minor modification, the accelerator can also be used as a gaseous heavy ion implanter.

I. INTRODUCTION

In the past two decades the International Atomic Energy Agency (IAEA) has supported the establishment of neutron laboratories in many developing countries by providing small D-T neutron generators. The neutron generator is basically a low energy (100-400 keV) ion accelerator capable of producing a continuous beam of deuterons with a current in the range between 1-2.5 mA. These neutron generators are primarily intended to be used for fast neutron activation analysis.

The neutron generator is not necessarily limited to continuous beam operation. If properly modified, it can also be utilized for pulsed beam operation. The scope of utilizing such a neutron generator in analytical applications as well as in the studies of fast neutron reactions is extended considerably by pulsed beam operation. For example, the measurements of double differential neutron emission spectra at 14 MeV incident neutron energy for several materials in the interest to the fusion reactor development program are best carried out by pulsed neutron time-of-flight (TOF) technique [1]. The feasibility of using a pulsed neutron generator for the measurement of light elements such as carbon, oxygen, and nitrogen has been successfully investigated [2-3]. The main field of application of pulsed neutrons in geology is well logging analysis where a pulsed accelerator is used to produce 14 MeV neutrons. During the neutron burst, prompt y-rays resulting from neutron inelastic scattering and from reactions induced by high energy neutrons are detected. This method is a well-established technique and has been adapted for down-hole logging in both the coal and oil industries [4,5]. Miscellaneous applications of pulsed neutron generator has been reviewed by Csikai [5].

This paper describes the utilization of a 14 MeV neutron generator in continuous and pulsed beam modes in applied neutron physics program at Chiang Mai University.

IL EXPERIMENTAL FACILITY

The Fast Neutron Research Facility (FNRF) operates a 200 kV, 5 mA high stability Cockcroft-Walton type accelerator producing 14-MeV neutrons for applications in fast neutron activation analysis and the study of neutron-induced reactions. An associated alpha-particle time-of-flight (TOF) spectrometer was established [6] with moderate energy resolution (1.2 MeV at 14 MeV neutron energy) and a well-behaved time-independent background. The nano-second pulsed neutron

Presented at the Advisory Group Meeting on The Optimal Use of Accelerator Based Neutron Generators, 13-16 October 1998, IAEA, Vienna, Austria.

facility was installed in 1991 by modifying an existing continuous beam accelerator to

incooperate beam chopping and bunching devices [7].

Neutron are produced from an AID J25 accelerator by the T(d,n) He reaction. Continuous deuterium ions (D1+) from a radio frequency plasma ion source are accelerated to 140-kV by a 9-kHz switching-frequency Cockcroft-Walton type d.c. high-voltage power supply. The deuteron beam which comprises 75% atomic deuterons (D1+) and 25% molecular deuterons (D2+) is analysed by an analysing magnet. The D1ions are bent 90° to a pulsed beam channel while the D2+ ions are excluded by momentum discrimination. Beyond the analysing magnet, the beam is transported through series of collimating slits and quadrupole focussing magnets. The beam is chopped by a double-plate deflection system and then bunched to pulses with widths of 1.5 to 2.0 ns at the neutron production target by a double-gap klystron buncher. Beam sizes both in horizontal and vertical axes were monitored by means of a crossed-wire beam profile monitor. The schematic diagram shown in Fig. 1 is a layout of the beam line components from the ion source to the target. A data acquisition system is controlled by a 16 MB MicroVAX II computer through a multiparameter-buffer system (MBS) unit. Each reaction event detected by the main detector is recorded sequentially in list mode on disk. Our offline analysis software allows dynamic selections for each correlated parameter in contrast to a conventional hardware-resolution routine.

III. DOUBLE DIFFERENTIAL CROSS SECTION MEASUREMENT

Studies of fast neutron induced reactions are of significance for an under standing of nuclear reaction theory as well as for practical applications. For example, the secondary neutron energy and angular distribution from the (n, xn') reaction on certain materials are of importance for the development of fission and fusion reactor systems and other accelerator based applications. The spectrum of the emitted neutrons are usually measured using TOF technique.

In Chiang Mai, we have set up a high precision neutron TOF spectrometer system with flight path up to 12 m [8, 9]. A detailed description of measurement and data reduction has been described recently [8]. A cylindrical sample about 3 cm in diameter and 5 cm long, was positioned at 90° relative to the incident deuteron beam with its axis along the axis of the beam line as shown in Fig.2.

Neutrons were detected in a BC-501A liquid scintillating detector of diameter 25 cm and thickness 10 cm. The detector was coupled to a Hamamatsu R1250 photomultiplier tube via a partially coated taper light pipe. It was located at an extended flight path of 12 m inside a well-shielded tunnel. Monte Carlo calculation indicates that scattering effect is less than 1% for this collimating system. Time-of-flight measurements were made at angles from 20° to 150° in step of 10°. The corresponding energy resolution at 14.1 MeV was about 415 keV FWHM.

The neutron spectrum was determined from the measured TOF spectra in separate energy regions. The γ - rejection was observed for each of the TOF regions because the γ - rejection technique was pulse-height dependent. Because of the large size of the neutron detector, neutron and gamma events in the pulse shape spectrum were not completely separated and some neutrons were lost. This loss was estimated to be less than 1%.

Several corrections were made to the number of detected neutrons. The most significant one was due to multiple scattering. The overall systematic error for the value of the DDX of ²⁰⁹Bi for example is estimated to be about 11%. The statistical uncertainties varies from less than 1% to about 39% in the discrete region of the spectra of neutrons emitted in backward angles.

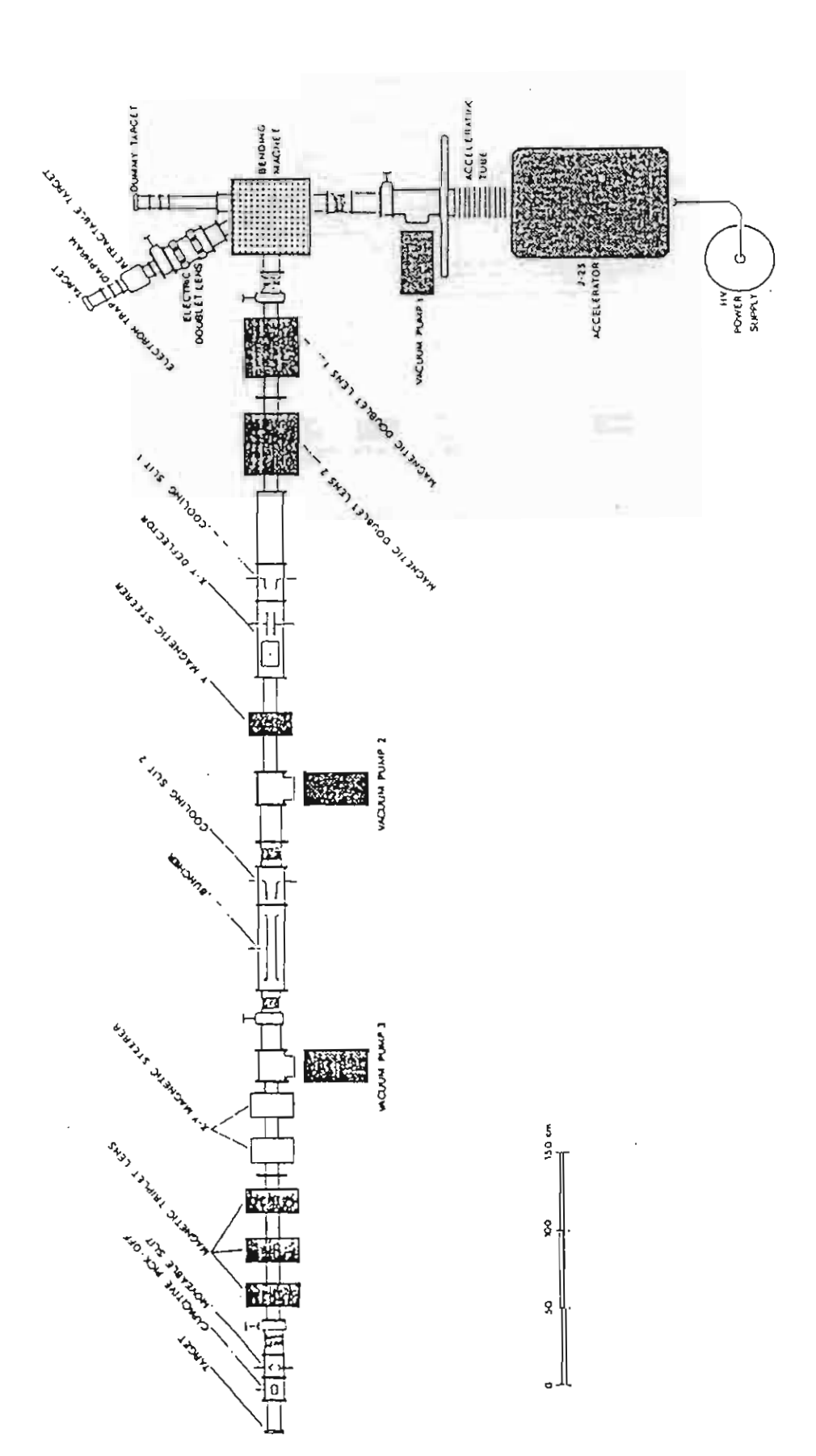


Fig. 1 Schematic diagram showing all pulsed beam line components and their geometrical arrangements

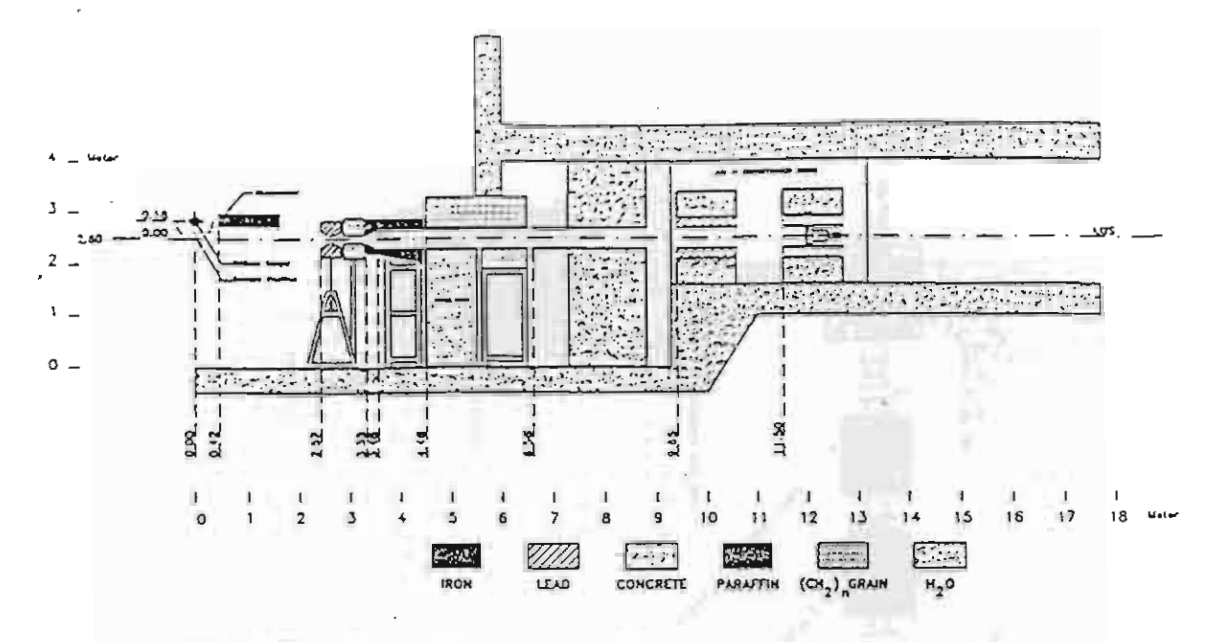


Fig. 2 Experimental arrangement for the DDX measurement [9]

In Fig. 3 we show our recent measurement at 20° in comparison with the result of Takahashi et al. [10]. The two different sets of measurement are in reasonable agreement. Because of better energy resolution, our data reveal more detailed structure in the region between 6 to 12 MeV.

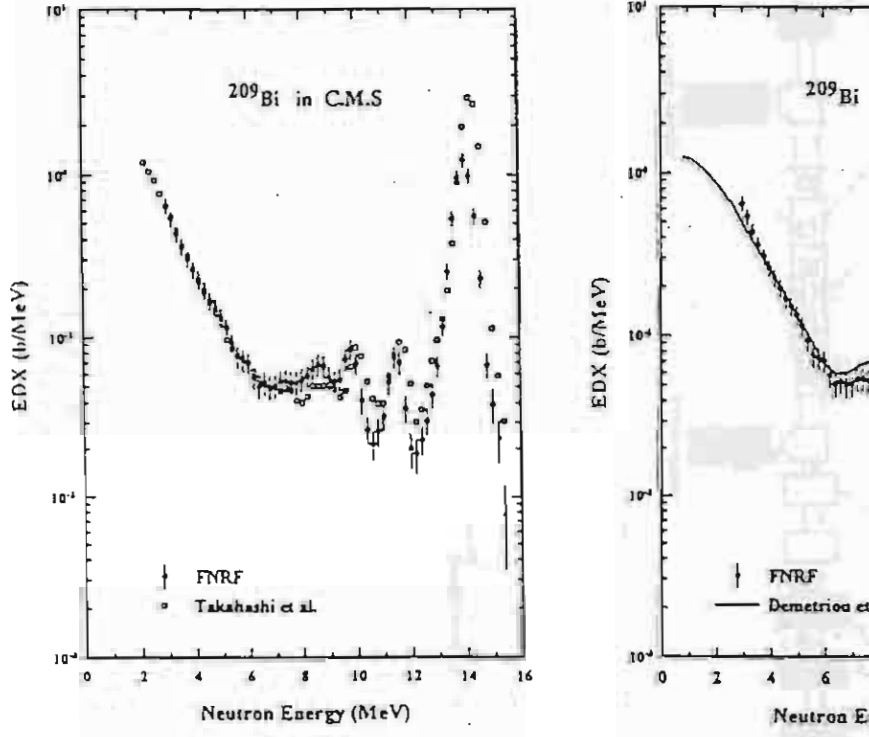


Fig. 3 Double differential cross section of ²⁰⁹Bi at 20°. The data of Takahashi et al. [10] is shown for comparison.

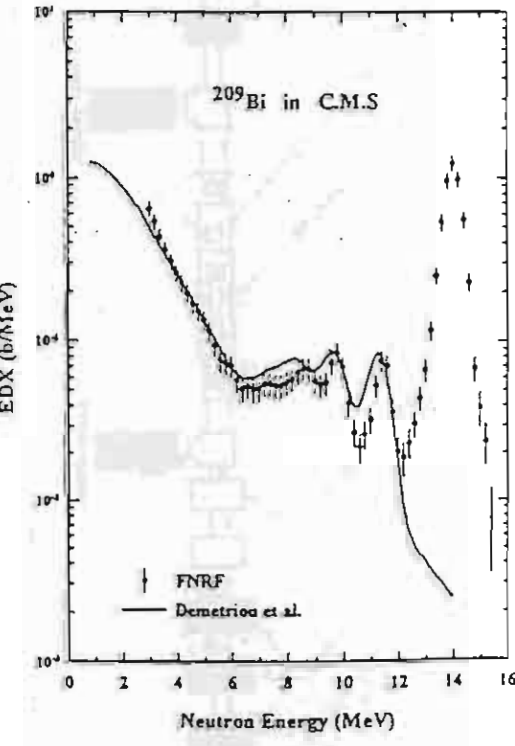


Fig. 4 Comparison of angle-integrated Spectrum of ²⁰⁹ Bi in the CM system With the calculated spectrum of Demetriou et al. [11].

We compare our angle integrated spectrum in Fig.4 with the calculated results of Demetriou et al.[11] based on the Feshbach-Kerman-Kooning theory. In their calculation, Demetiou et al. also include contribution from direct reactions that excite low energy vibrations as well as the giant resonances in the continuum, in addition to the incoherent multistep direct reaction, multistep compound and compound nucleus reaction

The calculated spectrum reproduces the experimental data very well in the regions between 3 to 6 MeV and 9 to 12 MeV. In the region between 6 and 9 MeV where preequilibrium reaction dominates, the two spectra do not agree. The calculated spectrum slightly overestimates the number of emitted neutrons.

IV. PULSED TIME-OF-FLIGHT PROMPT GAMMA-RAY ANALYSIS.

A D-T neutron generator is now routinely used in a variety of analytical applications, including nonintrusive inspection by means of prompt gamma-ray analysis (PGA). Obtaining satisfactory results from this kind of measurement requires an associated trigger signal from either the alpha particle of the D-T reaction when utilizing a continuous deuteron beam [12] or the induced signal from a capacitive pick-off when using a pulsed deuteron beam [3]. As is well known, the pulsed neutron time-of-flight (TOF) technique generally provides better signal to noise ratio than the associated-alpha particle technique. We thus choose to work with the pulsed beam technique. Also, a pulsed neutron generator is not necessarily a large machine any more [13]. However, the production of wider neutron pulse is normally simpler and cheaper than a narrow one. The aim of this work was to investigate the quality and characteristics of the results obtained using both wide and narrow pulses.

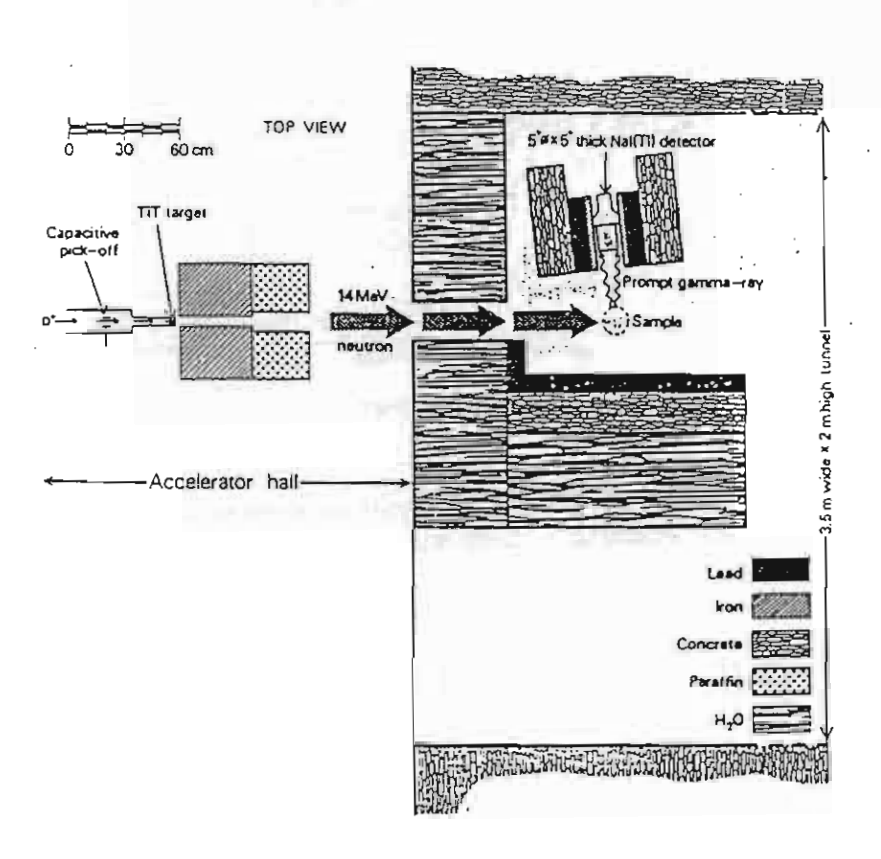


Fig. 5 Experimental arrangement for the pulsed TOF prompt gamma-ray analysis [14].

The experimental arrangement is shown in Fig. 5. The gamma-ray detector was a 5 in diameter by 5 in thick NaI(T1) scintillator. The detector was placed inside a heavy shielding about 2.4 m away from the TiT target and 37 cm from the sample position, as shown in Fig.5. The two parameter (energy-time) data acquisition and analysis system is similar to the one that has been described elsewhere [8]. The threshold detecting was fixed at around 0.5 MeV gamma-ray energy.

Our data acquisition system allows energy or pulsed height data of the gammaray signals that are associated with any interval of the peak of the time spectrum to be selected off-line. Fig. 6 shows pulse height spectrum from sample of liquid nitrogen using 2 nsec pulsed neutrons. Each spectrum belongs to different time gating as indicated in the insets. Our experiment indicates that the best signal-to-noise ratio was obtained with narrow neutron pulse (< 5 nsec).

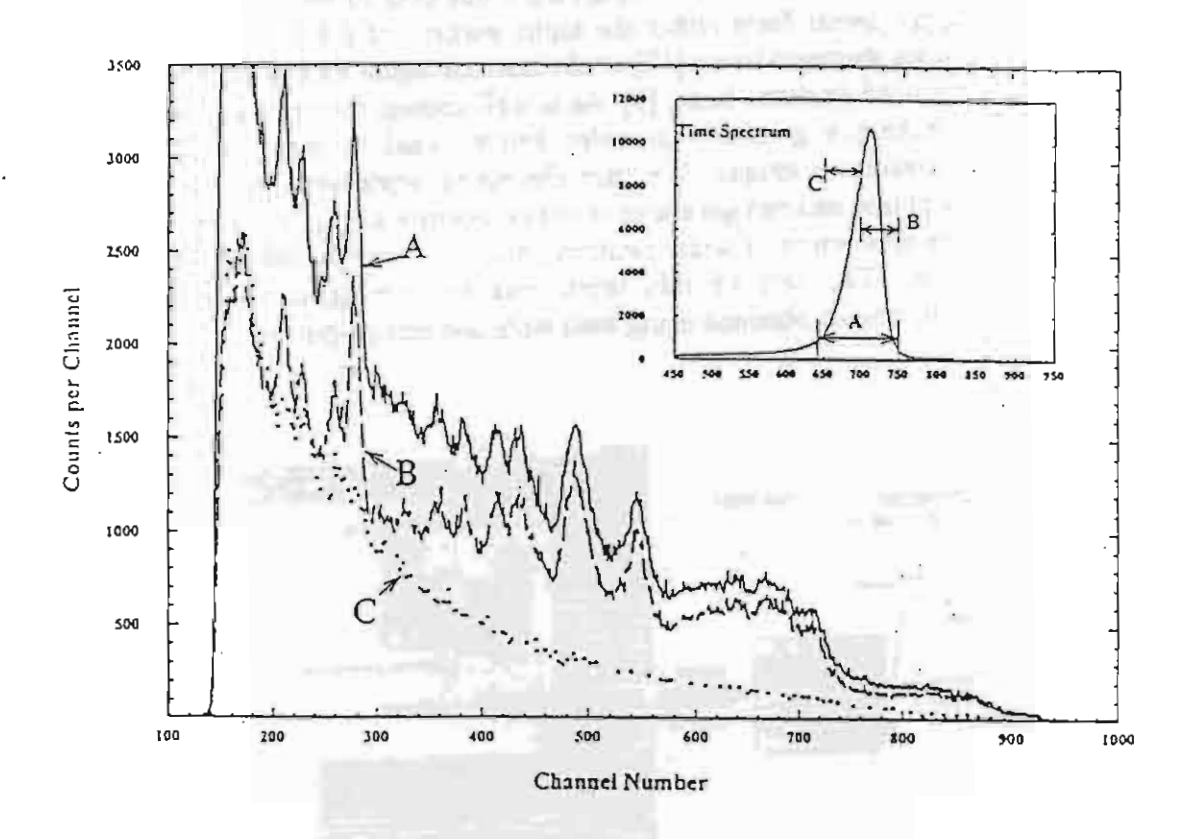


Fig 6 Gamma-ray energy spectrum of 20 kg liquid nitrogen using a 2 nsec width of neutron pulse [14]. Inset: selection of time-window on the associated time spectrum (a = 90 nsec, b = 50 nsec, c = 40 nsec).

Gamma-ray spectroscopy performed using 1.4 kg of C-3 explosive with 2 nsec pulse reveals all expected photopeoks at 1.6, 2.3, 2.8, 3.7, 4.4, 5.1 and 6.1 MeV as shown in Fig. 7.

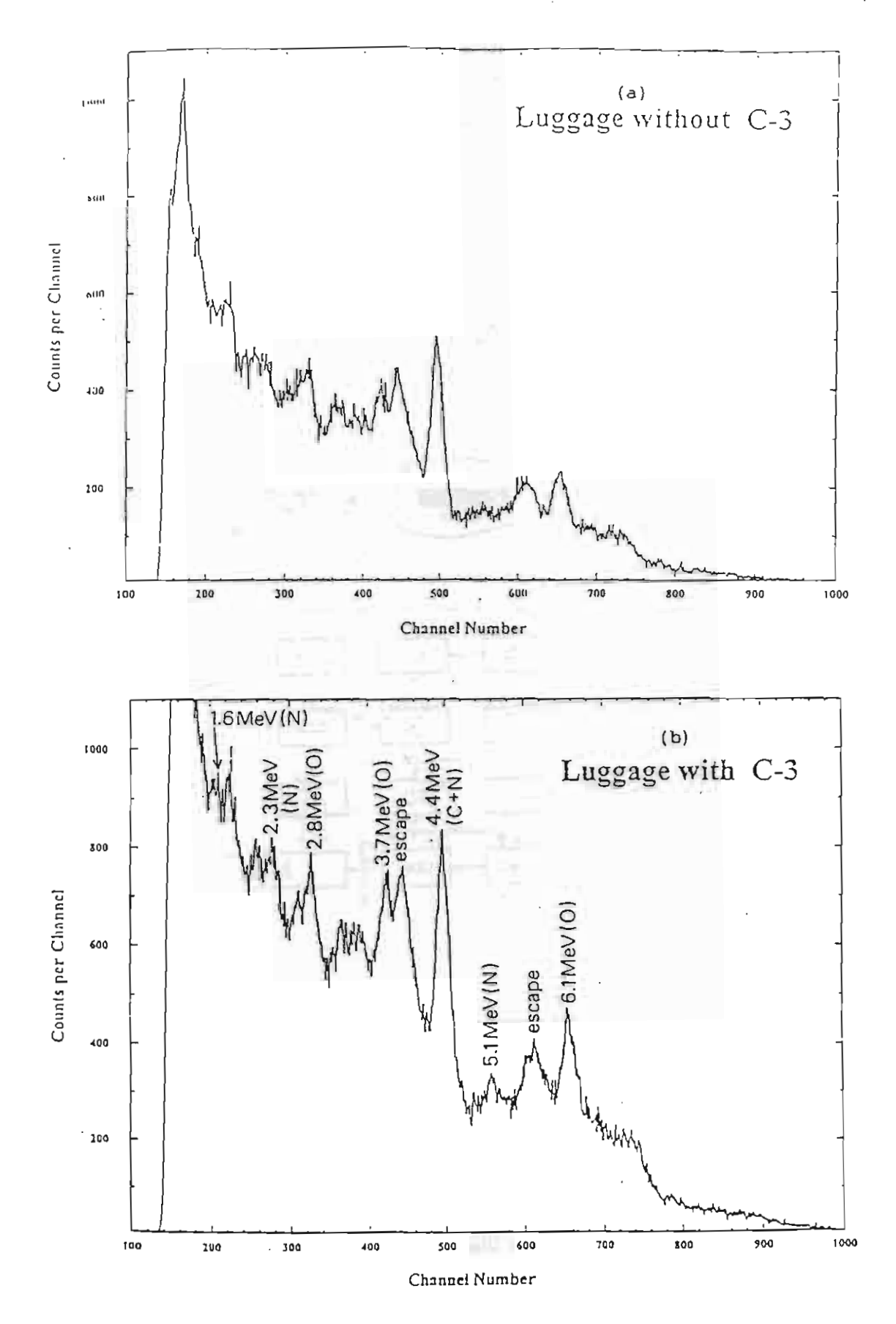


Fig. 7 Time-gated gamma-ray energy spectrum of (a) simulated passenger luggage (b) luggage containing C-3 explosive [14].

V. NEUTRON SOURCE AND DOSIMETRY

The neutron generator is normally used to produce monoenergic 14 MeV neutron from the D-T reaction and 3 MeV neutron from the D-D reaction. We have investigated the properties of neutrons scattered from a circular surface-of revolution paraffin scatterer using the MCNP code and the pulsed neutron TOF measurement [15] Fig. 8 shows the experimental arrangement.

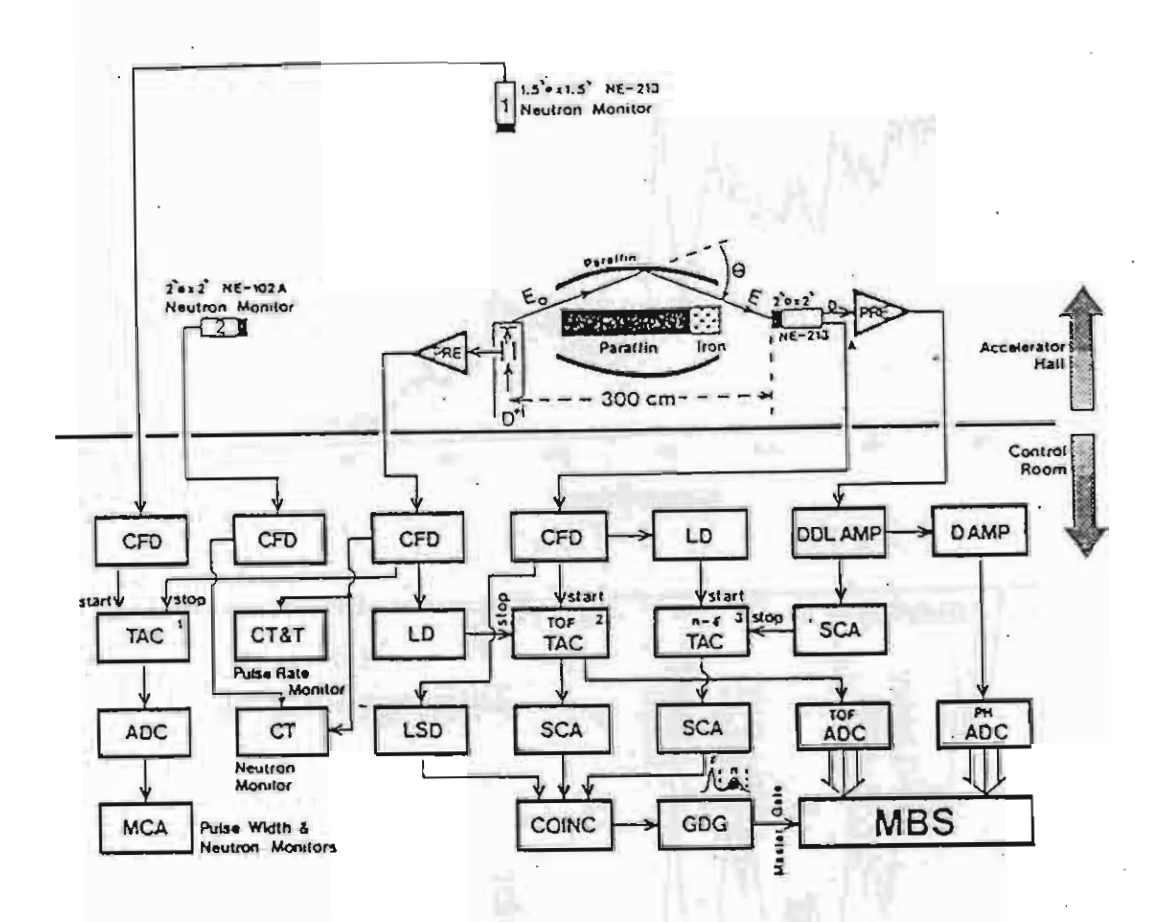


Fig. 8 Experimental set up for elastic scattering of 14 MeV neutron from a circular surface-of revolution paraffin scatterer and the two parameter data acquisition system [15].

The neutron pulse height distributions obtained off-line by gating the pulse height events with appropriate TOF events in a specific time window of interest is shown is Fig. 9. It is noted that the yield of $n + {}^{12}C$ elastic scattering is fairly pronounced which can be used for calibration purpose.

Elastically scattered neutrons from this type of scatterer has been successfully used for measuring the light out put of a small NE-213 detector [15].

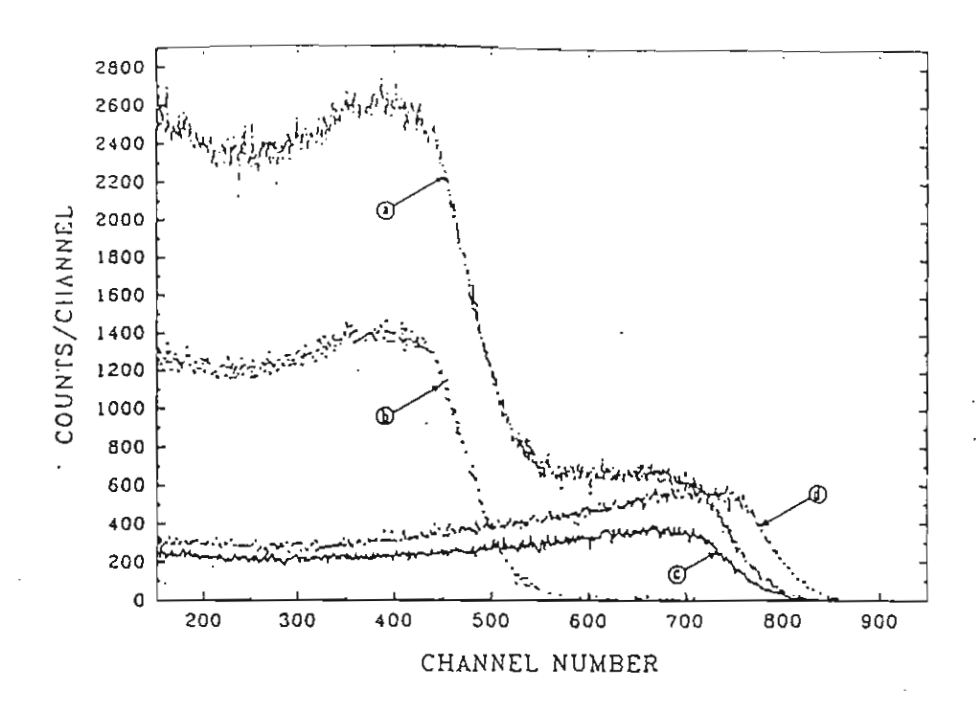


Fig. 9 Measured pulse height spectrum for the 5.08 cm diam x 5.08 cm thick NE-213 liquid scintillation detector. Separate spectra shown are: (a) Scattered-neutrons from full scatterer. (b) Scattered-neutrons from hydrogen elastic scattering in the front half scatterer. (c) Scattered-neutrons from carbon elastic scattering in the front half scatterer. (d) 14.1 MeV neutrons [15].

Neutrons from the 14 MeV neutron generator can also be used to calibrate a neutron dosimeter. The different LET dependences of the low and high temperature glow peaks of of CaF_2 : Tm thermoluminescent material (TLD-300) allow the determination of neutron and gamma dose simultaneously. The method was calibrated for the 14 MeV neutron beam at FNRF [16]. Fig. 10, 11 show glow curves of a TLD-300 dosimeter after 60 Co and 14 MeV neutron irradiations.

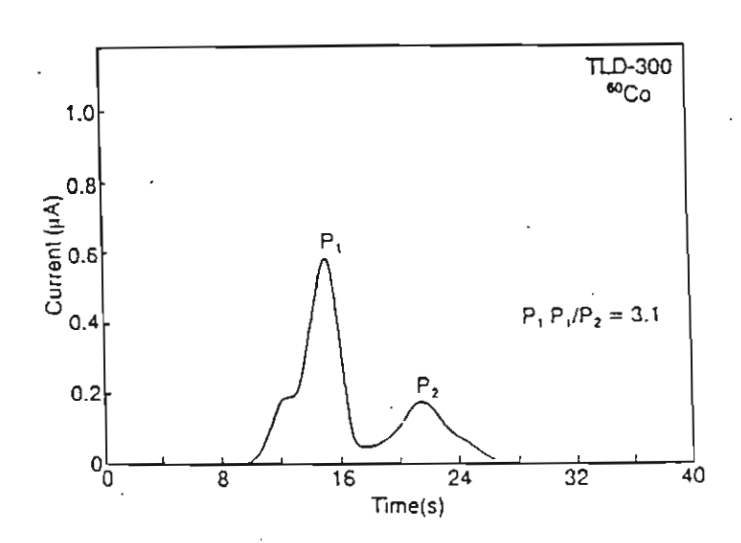


Fig.10 Glow curve of a TLD-300 dosemeter after ⁶⁰Co irradiation [16].

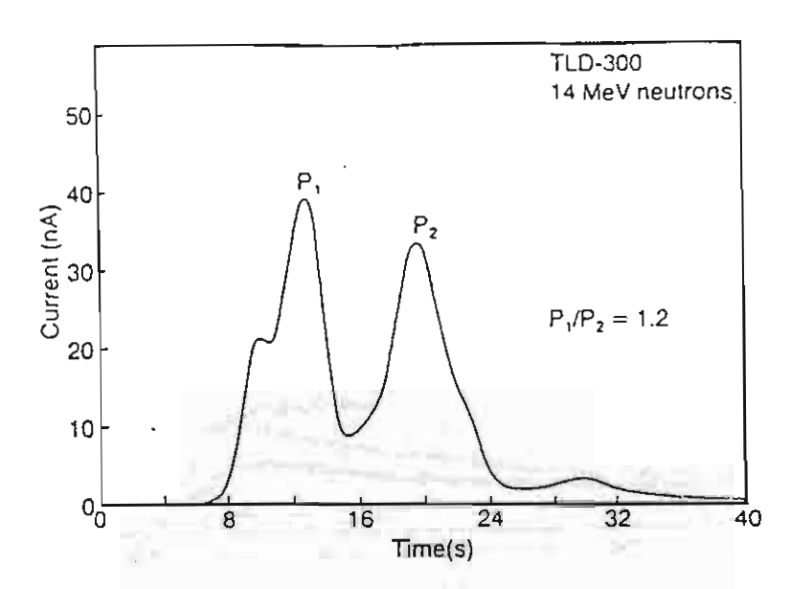


Fig. 11 Glow curve of a TLD-300 dosemeter after irradiation in a 14 MeV neutron beam [16].

The relative neutron responses of both peaks in TLD-300 chips were found to be 0.10 and 0.32. Using this method various dose distributions of neutron and gamma dose in a water phantom were measured and compared with the results of GM counter measurements and the Monte Carlo calculation as shown in Fig. 12.

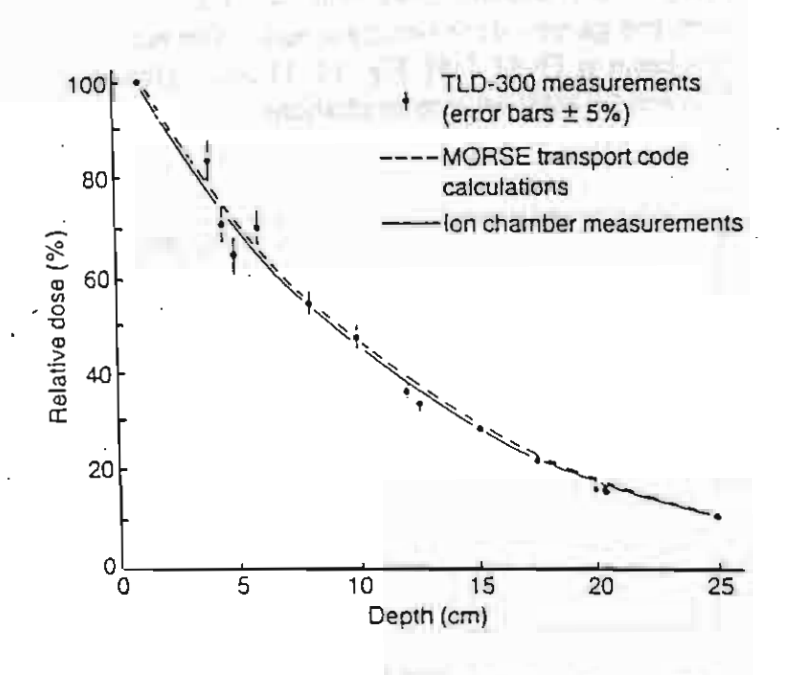


Fig. 12 Comparison of determination of the depth dose $D_{total} = D_n + D_{\gamma}$ of the 14 MeV beam in water by the TLD-300 method, ion chamber measurement, and Monte Carlo transport code calculations [16].

VI. ION IMPLANTATION

<u>:</u> .

Basically, a 14 MeV neutron generator is a 200 kV ion accelerator using palladium tube to leak deuterium gas into the RF-ion source. At FNRF we replaced the palladium tube with a thermomechanical leak valve which enables us to use other gases such as N₂, CO₂, BF₃ etc. Implantation with gaseous ions such as nitrogen, oxygen, boron, argon are possible [17,18]. Surface modification with ion beam based technique has commanded great interest in recent years for improving mechanical, electrical and optical properties of materials [19]. A drift tube neutron generator can be most conveniently modified to be used as an ion implanter concurrently.

VII. CONCLUSION

The 14 MeV neutron generator of Chiang Mai University has been utilized in both continuous and pulsed beam modes. Major applications are nuclear data measurement, elemental analysis with prompt gamma-ray detection technique, calibrations of neutron detector and TLD-300. With minor modification, the accelerator can be converted into a gaseous heavy ion implanter for use in modifying surface properties of materials.

ACKNOWLEDGEMENTS.

We thanks G.G. Hoyes, R. Charoennugul, S. Rattanarin and S. Aumkaew for their technical supports. The applied neutron physics program has been supported by the International Atomic Energy Agency, The International Program in Physical Science (Uppsala University), The National Research Council, The Thailand Toray Science Foundation and The Thai Research Fund.

REFERENCE

- [1] A. Takahashi, E. Ichimura, Y. Sasaki, and H. Sugimoto, J. Nucl. Sci. Technol. 25,215(1988).
- [2] Z. P. Sawa, Nucl. Instr. And Meth. B79,593(1993).
- [3] D. R. Brown, T. Gozani, R. Loveman, J. Bendahan, P. Ryge, J. Stevenson, F. Lin, and M. Sivakuma, Nucl. Instr. And Meth. A353,684(1994).
- [4] J. A. Gran and J. S. Schwetzer, Nucl. Geophys. 1,157(1987).
- [5] J. Csikai, Handbook of Fast Neutron Generator Vol. I, CRC Press, Inc. Boca Raton, Florida(1987).
- [6] S. Singkarat, N. Chirapatpimol, D. Suwannakachorn, W. Pairsuwan, G. Hoyes, and T. Vilaithong, Proc. Int. Conf. on Nuclear Data for Science and Technology, Mito, Japan, Ed. S. Igarasi, pp.367-370(1988).
- [7] T. Vilaithong, S. Singkarat, W. Pairsuwan, J. F. Kral, D. Boonyawan, D. Suwannakachorn, S. Kongklong, P. Kanjanarat, and G. G. Hoyes, Proc. Int. Conf. on Nuclear Data for Science and Technology, Julich, Ed. S. M. Qaim, pp.483-486 (1991).
- [8] T. Vilaithong, D. Boonyawan, S. Konklong, W. Pairsuwan, and S. Singkarat, Nucl. Instr. and Meth. A332,561(1993).
- [9] T. Vilaithong, S. Tippawan, and S. Singkarat, Proc. Int. Conf. on Nuclear Data for Science and Technology, Trieste, Eds. G. Reffo, V. Ventura and C. Grandi, pp574-576(1997).
- [10] A. Takahashi, M. Gotoh, Y. Sasaki, and H. Sugimoto, OKTAVIAN Report A-92-01, Osaka University(1992).
- [11] P. Demetrion, A. Marcinkowski, and P.E. Hodgson, Nucl. Phys. A596,67(1996).
- [12] S. Mitra, J.E. Wolff, R. Garrett, and C.W. Peter, Phys. Med. Biol. 40, 1045 (1995).

[13] L.T. Perkins, A Compact Ion Source for Intense Neutron Generation, Ph.D. Thesis, University of California, Berkeley (1997).

[14] S. Singkarat, U. Tippawan, G.G. Hoyes, N. Chirapatpimol, and T. Vilaithong, presented at the 1998 Symposium on Radiation Measurements and Applications, AnArbor, 12-14 May(1998).

[15] S. Singkarat, T. Vilaithong, R. Charoennugul, and H. Kobus, Nucl. Instr. and Meth. A332,245(1993).

[16] W. Hoffmann and P. Songsiriritthigul, Radiat. Prot. Dosim. 44,301(1992).

[17] L. D. Yu, T. Vilaithong, D. Suwannakachorn, S. Intarasiri, and S. Thongtem, Nucl. Instr. and Meth B127/128,954(1997).

[18] L. D. Yu, T. Vilaithong, B. Yotsombat, S. Thongtem, J.G. Han, and J.S. Lee, Surf. and Coatings Tech. 103-104, 328 (1998).

[19] Proc. of the 9th Int. Conf. on Ion Beam Modification of Materials, Canberra, Eds., J.S. Williams, R.G. Elliman, M.C. Ridgway, Elsevier Science, Amsterdam(1996).

- - And proposed bearing the region have-

I world hill I left dilegest group Maritin the deedless!

ภาคผนวก ก4

C, N, O Investigation Based on a Pulsed 14-MeV Neutron Generator

S. Singkarat, U. Tippawan and T. Vilaithong

Fast Neutron Research Facility, Department of Physics, Faculty of Science,
Chiang Mai University, Chiang Mai 50200, Thailand.

Presented at:

IAEA Technical Committee Meeting on

Application of Accelerator Based Neutron Sources

5-8 October 1999,

Debrecen, Hungary.

C,N,O INVESTIGATION BASED ON A PULSED 14-MeV NEUTRON GENERATOR

by

Somsorn Singkarat, Udomrat Tippawan and Thiraphat Vilaithong
Fast Neutron Research Facility, Department of Physics, Faculty of Science,
Chiang Mai University, Chiang Mai-50200, Thailand

presented at
IAEA Technical Committee Meeting on
Application of Accelerator Based Neutron Sources
Debrecen, Hungary, Oct. 5 – 8, 1999



Fig. 1 Hang Chat Elephant Hospital staff is taking care of the left foreleg of Motala, a 38-year-old elephant that stepped on a landmine in Burma, near Tak province of Thailand, on August 15, 1999[1].



C,N,O INVESTIGATION BASED ON A PULSED 14-MeV NEUTRON GENERATOR

Somsorn Singkarat, Udomrat Tippawan and Thiraphat Vilaithong
Fast Neutron Research Facility, Department of Physics, Faculty of Science,
Chiang Mai University, Chiang Mai-50200, Thailand

ABSTACT

A nano-second pulsed neutron generator has been used to produce 14-MeV neutrons for prompt gamma-ray analysis of light elements such as C, N, and O. In order to reduce the gamma-ray background, a pulsed neutron time-of-flight technique has been adopted. Different neutron pulse widths of 2 ns and 50 ns were used. The narrowest neutron burst was found to give the best signal to noise ratio. Gamma-ray spectroscopy using both NaI(TI) and HPGe detectors are performed on standard military explosives. Technical details and results of the measurements are presented.

1. INTRODUCTION

Fig. 1, on the front cover, tells us that the abandoned landmines are not only a threat to those innocent farmers and children but also endangered animals. A clear need to demining is now being recognized world-wide. But the traditional methods are slow and risky. More advanced techniques that have thus far been proposed include electromagnetic induction, ground probing radar, infrared imager, nuclear quadrupole resonance, nuclear techniques employing either thermal or fast neutrons, etc. To share responsibility in this human created problem, we have decided to use our resources to investigate and find more technical information in the inspection of explosives by using prompt gamma-ray analysis technique (PGA) that is induced by 14 – MeV neutrons.

2. EXPERIMENTAL

2.1 Experimental setup

The measurements were performed using the modified pulsed neutron generator at Chiang Mai University [2] in which the original machine was donated by the IAEA in 1983. A chopper system using X-Y deflector plates on which a D^+ beam is swept across a circular slit producing a chopped beam with ~ 50 ns pulse width. The repetition rate is selectable from 1 kHz to 2 MHz in 10 steps. Afterward the beam is longitudinally bunched to achieve a time focus at the neutron production target on which the narrowest width is ~ 1.5 ns. In this experiment, we generally work at 1 MHz repetition rate with the D^+ beam current at 5 μ A. The first gamma-ray detector to be mentioned here is a 5 in. diameter by 5 in. thick NaI(TI) detector which was well shielded from the direct neutron flux, as shown in Fig.2(A). It is aimed at a side of a sample at a distance of ~ 30 cm while the sample was placed ~ 2.4 m from a 6.3 Ci thick TiT target. The neutron flux at the sample position was estimated to be ~ 300 n. cm⁻².s⁻¹. Three organic scintillation detectors at distances of ~ 4 m from the target

were used as neutron flux monitors during the measurements which were $\sim 45-60$ minutes in duration

Fig. 2(B) shows the system diagram, for the NaI(Tl) detector, which incorporates a two parameter (energy-time) data accumulation and acquisition system. The delay and walk adjustment of CFD2 were carefully tuned to minimize amplitude walk. For a 2-ns neutron pulse width, the FWHM of the resulting time spectra is 15.5 ns. This value is found to be about 2 – 3 times larger than the intrinsic time resolution of the system. We believe that the discrepancy is mainly caused by the time-correlated background.

2.2 Background reduction by time - gated technique

With the two parameter data acquisition technique used, energy or pulse height data of gamma-ray signals that are associated with any interval of the peak of the time spectrum can be selected off-line. This is done by choosing the position and width of the time-window and using them to gate on the associated pulse height data. Figs.3(A) and 3(B) show these pulse height spectra from a liquid nitrogen sample using neutron pulse widths of 50 ns and 2 ns, respectively. In each figure, three ways of time gating, as indicated in the insets, were tried, i.e. full peak window (a and x), right half window (b and y) and left half window (c and z). From the way it was set, the right half of the peak belongs to those signals which come earlier than those belonging to the left half. Fig. 3(A) shows that gating with a time-window from any part of the time spectrum does not change the shape of the energy spectrum, only the yield, which is directly proportional to the width of the time-window. It seems that, for the broad neutron pulse width, signals of prompt gamma-rays are mixed uniformly with background radiation.

The process was repeated with a pulse width of 2 ns (Fig.3(B)) but we get a different result. While maintaining constant neutron monitoring conditions, the fully time-gated energy spectra (a and x) are indistinguishable. In this sense, both cases are similar. But comparing the full and right half time-gated energy spectrum (spectra x and y) with left half timed-gated spectrum (spectrum z), shows that spectrum z mainly comes from background radiation since peaks of prompt gamma-rays do not show up – unlike spectrum c of Fig.3(A). In addition, when comparing spectrum x with spectrum y, we see that when the time-window is correctly set at the right half of the peak the photopeaks of interest from a sample are barely, if at all, disturbed. This is due to the difference in arrival time at the gamma-ray detector between the delayed background radiation and early prompt gamma-rays from the sample. On this basis, it is evident that a narrow pulse is preferred to a broader pulse.

2.3 Gain shift problem

For field applications, a NaI(TI) detector is the most commonly used gamma-ray detector. Unfortunately the detector used in this work has serious gain shifting. The shifting as large as 500 keV can occur at any time during measurement. This effect creates an additional complication to the gamma-ray spectrum. Although this behaviour is not yet clearly understood, we find from separate investigations that, most if not all of the aberration, it depends on the ambient temperature. Shown in fig. 4(B) are the peak positions of 1.332 MeV gamma-rays from a Co-60 source when a photomultiplier base (PMB) of the detector was set to different temperatures, as is shown in Fig.4(A). For this case, we found that between the ORTEC 266 and the Canberra 2007P PMBs neither one are better. Since this is a problem of gain shifting, it can be imagined that at around the region of interest of 4 - 6 MeV the effect will be

more serious. This problem has to be taken into account for field missions in a tropical climate.

3. DEMONSTRATION EXPERIMENT

3.1 Quantitative determination of C, N and O content

The above technique was applied to a quantitative analysis of carbon, nitrogen and oxygen content in a low level explosive which urea was chosen as an example. The analysis is based on the method used in Ref. [3] where only the necessary parts are mentioned here. Data treatment was begun from the gamma-ray energy spectrum of a material to be examined, as shown in Fig.5(A), where only a zone between 4.2 - 7.6 MeV was utilized. It is divided into 3 small regions of interest (ROIs) which are ROI1: 4.2 - 4.8 MeV, ROI2: 4.8 - 7.6 MeV and ROI3: 5.4 - 6.4 MeV. Since the only elemental interferences in this zone are among carbon, nitrogen and oxygen, we set

ROI1 =
$$C'_1 + N'_1 + O'_1$$

ROI2 = $N'_2 + O'_2$
ROI3 = $N'_3 + O'_3$

where C'_i , N'_i , and O'_i are number of counts due to carbon, nitrogen and oxygen, respectively, in each region of interest. These are unknown numbers which can be expressed in terms of the atomic densities of carbon, nitrogen and oxygen as follows:

$$C'_{i} = \begin{pmatrix} C_{i} \\ n_{c} \end{pmatrix} n'_{c}$$

$$N'_{i} = \begin{pmatrix} N_{i} \\ n_{N} \end{pmatrix} n'_{N}$$

$$O'_{i} = \begin{pmatrix} O_{i} \\ n_{O} \end{pmatrix} n'_{O}$$

where n_C' , n_N' and n_O' are unknown atomic densities of carbon, nitrogen and oxygen in the urea. C_i , N_i and O_i are, respectively, number of counts in each region of interest from spectra of standard samples, i.e. liquid paraffin, liquid nitrogen and water, as shown in Fig.5(B). Since the volume and mass of these 4 samples are known parameters, the bulk densities are then easily calculated, i.e. 0.86 g/cc for urea, 0.87 g/cc for liquid paraffin, 0.74 g/cc for liquid nitrogen and 1 g/cc for water. From this, we then find the values of atomic densities $n_C = 3.72 \times 10^{22}$ atoms/cc, $n_N = 3.18 \times 10^{22}$ atoms/cc and $n_O = 3.34 \times 10^{22}$ atoms/cc in each of the standard samples.

By direct substitution, we find an equation for calculating atomic density of oxygen in urea:

$$n'_{O} = \frac{RO12 - \binom{N_2}{N_3}ROI3}{\binom{O_2}{n_0} - \frac{N_2}{N_3} \cdot \frac{O_3}{n_0}}$$

This leads to an equation for atomic density of nitrogen in urea:

$$n'_{N} = \left(\frac{n_{N}}{N_{3}}\right) ROI3 - \left(\frac{n_{N}}{n_{O}} \cdot \frac{O_{3}}{N_{3}}\right) n'_{O}$$

and an equation for calculating atomic density of carbon in urea (n'_c):

ROII =
$$\binom{C_1}{n_C} n'_C + \binom{N_1}{n_N} n'_N + \binom{O_1}{n_O} n'_O$$

From this algorithm, finally, we get

 $n'_{C} = 0.93 \times 10^{22}$ atoms/cc $n'_{N} = 1.21 \times 10^{22}$ atoms/cc

 $n_0' = 0.96 \times 10^{22} \text{ atoms/cc}$

These values appear to be in good agreement with the values determined from a direct calculation of known chemical formula (CH_4N_2O) and bulk density (0.86 g/cc). The result of this study indicates that, under controlled conditions, the quantitative bulk analysis of C, N and O content in chemical compounds or organic materials is feasible.

3.2 File of explosive fingerprints

Since explosives are always found together with other materials, a library of unambiguous gamma-ray spectra of standard explosives are needed in order to ascertain the consistent success of field inspection. We performed this measurement concurrently with both NaI(Tl) and HPGe detectors. The position of the 73.9 cc coaxial HPGe detector is ~30 cm under the sample as can be seen in Fig.6. But this time we used the system configuration shown in Fig. 2(B) for the HPGe detector and switched the NaI(Tl) detector to a single parameter mode which restricted us to set an on line fixed time-window on the pulse height spectrum. The systems of both detectors were trigged by the same pulse produced by a capacitive pick-off that was induced by the D⁺ pulse.

The investigations were performed on 3 different kinds of explosives which are M112, M2 and TNT. They are standard military explosives. With the NaI(Tl) detector, Figs. 7(A) and (B) are the gamma-ray energy spectrum of M112 and M2, respectively. According to military information, M112 is equivalent to C4 and M2 is tetrytol 75/25. In this measurement we used 4 blocks of M112 of which its total volume is 5 X 10 X 28 cm³. This size and shape is approximately equivalent to 2 blocks of M2. The TNT spectrum which is shown in Fig.7(C), has higher yield. This is mainly because TNT is made in a shorter block which, when bundled together (volume = 9.5 X 9.5 X 16 cm³), was better seen by the NaI(Tl) detector. To cope with this spatial problem, we then compare these three explosives spectra with the spectra acquired from NH₄NO₃ powder which was placed in a paper box made to have the same geometry as each explosive. NH₄NO₃ was chosen to be a comparator

because its spectrum above 4.8 MeV is not much different from the explosives. At first glance, the spectrum of M112, M2 and TNT are very much alike but, in detail, we can spot the differences such as TNT contains more carbon than M2 and M112 but contains less oxygen and nitrogen than M112 and M2.

To complete the picture, a dry soil sample enclosed in the same container as NH_4NO_3 , was also taken, as shown in Fig.7(D). We can see from the figure that the shape of the two spectra above 2 MeV are about the same. This implies that for detecting explosives buried in 5-15 cm of soil, it is essential to determine the difference in the carbon peak height at 4.44 MeV, which shows up very clearly for explosives and is negligible for soil.

Gamma-ray spectra in Fig.8 were taken at the same time and from the same samples as in Fig.7; but the gamma-ray detector was the HPGe instead. They play a crucial role in assisting to identify the Nal(Tl) spectra, especially when they were confused by the gain shifting. However, the double-escape pair production peak of 6.13 MeV gamma-rays from oxygen bring difficulty to the identification of nitrogen from the 5.11 MeV peak since they are overlapping. This weakness could be improved only by increasing the detector size. Hence, for this small detector we have to utilize the peaks of 2.31 and 1.63 MeV also. The strong 2.66 MeV line, in Figs.8(A) and (B), is from lead which was used as a shieding around the active volume of the HPGe detector. We did not see this peak from the Nal(Tl) detector because the inner layer of its shielding is iron. This explanation is confirmed in Fig.8(C) which the shielding material was changed from lead to iron.

In addition, it is interesting to note that the FWHM of the 4.44-MeV photopeak is about 3.5 times wider than, for example, the 5.11 MeV peak. From repeat experiments, we have good reason to believe that it is not an experimental error. We have found later that this phenomenon was seen before on which its brief explanations were referred to the Doppler effect [4, 5]. Consequently, its escape peaks at 3.42 and 3.93 MeV are also broad.

4. CONCLUSION

In this work, we have shown both the strengths and weaknesses of the nano-second pulsed fast neutron based PGA technique for explosive detection. We found that a narrow neutron pulse width is more advantageous than a broader one as it permits a diminished neutron – induced gamma – ray background. We can especially see more clearly the low energy region. The system performed quite well, with both NaI(TI) and HPGe detectors, on finding the fingerprints of a variety of real chemical explosives. Proof—of—concept laboratory experience indicates that quantitative analysis of C, N, and O content is feasible. Although the irradiation times in this experiment were ~ 60 minutes, with a judicious choice of the size and / or number of gamma-ray detectors and D⁺ beam current, it would be possible to reduce the counting time and sample mass to the range of interest.

ACKNOWLEDGEMENTS

We are grateful to Dr. R. Garrett of the University of Auckland for providing us with useful informations, Major S. Chaimongkol, ordnance officer of 33rd military circle for loaning us the explosive samples, Prof. W. Hoffmann and M.W. Rhodes for reading the manuscript. We also thank S. Aumkaew, S. Rattanarin and P. Phansuke

for their generous assistance. The research on PGA covered in this paper represents work done over the last few years. It is being currently supported by the National Research Council of Thailand, past support by the Thailand Toray Science Foundation is gratefully acknowledged. Last but not least, we would like to thank the Institute for Science and Technology Research and Development, Chiang Mai University and the Thailand Research Fund for their continuing encouragement and support.

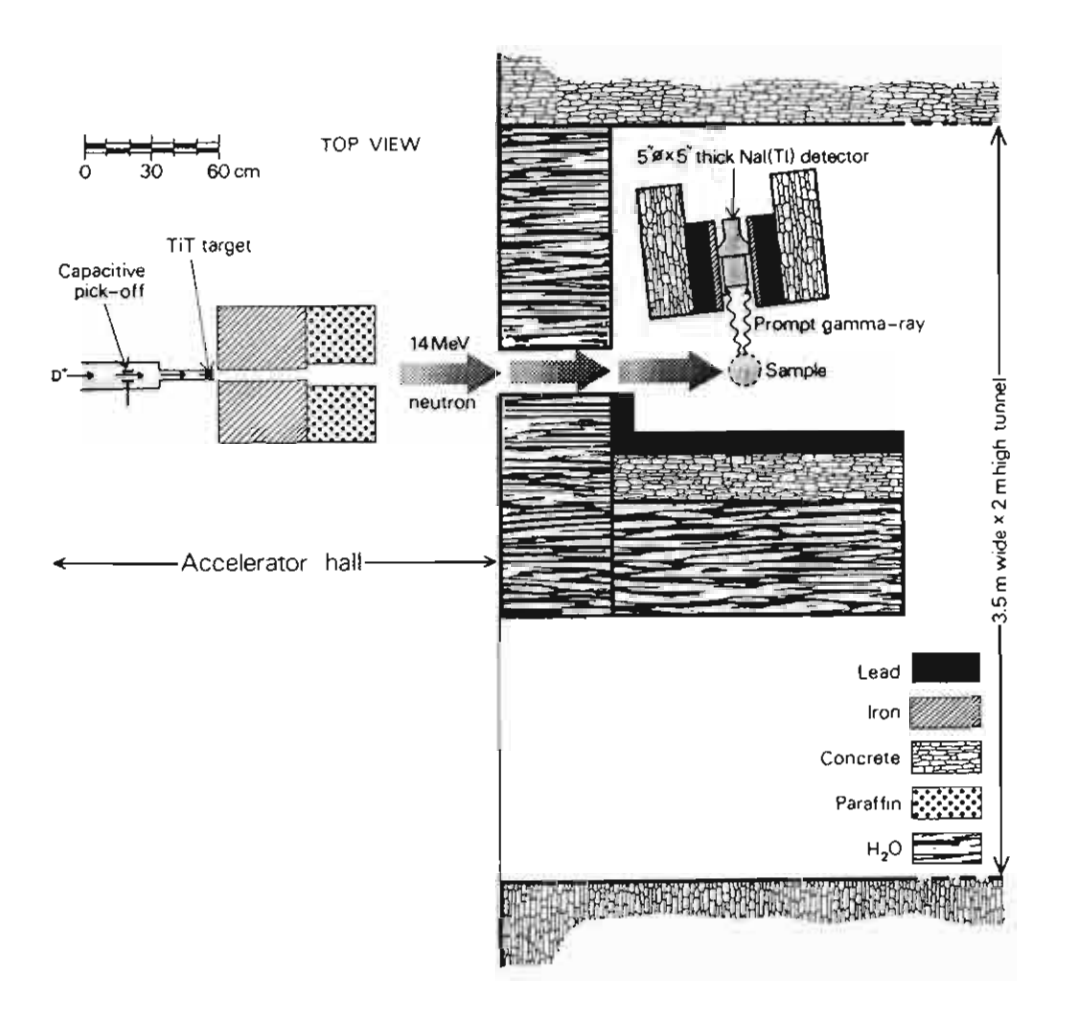
REFERENCES

- [1] Bangkok Post Newspaper, August 23, 1999, p.1.
- [2] T. Vilaithong, S. Singkarat, W. Pairsuwan, J.F. Kral, D. Boonyawan, D. Suwannakachorn, S. Konklong, P. Kanjanarat, and G.G. Hoyes, *Int. Conf. on Nuclear Data for Science and Technology*, May 13 17, 1991, Julich, Germany, pp. 483 486.
- [3] S. Mitra, J.E. Wolff, R. Garrett, and C.W. Peters, Phys. Med. Biol. 40(1995)1050.
- [4] P. Dyer, D. Bodansky, A.G. Seamster, E.B. Norman and D.R. Maxson, *Phys. Rev.*C23(1981)1868.
- [5] Zhou Hongyu, et al., Chinese J. of Nucl. Physics 11(1989)65.

FIGURE CAPTIONS

- Fig. 1 Hang Chat Elephant Hospital staff is taking care of the left foreleg of Motala, a 38-year-old elephant that stepped on a landmine in Burma, near Tak province of Thailand, on August 15, 1999.
- Fig. 2 (A) Experimental arrangement of the NaI(TI) detector for the PGA experiment.
 - (B) Schematic diagram of the electronic setup for data accumulation and acquisition.
- Fig. 3 (A) Gamma-ray pulse height spectrum of 20 kg of liquid nitrogen inside a dewar using a 50 ns neutron pulse width. Inset: selection of time-window on the associated time spectrum (a = 90 ns, b = 50 ns and c = 40 ns).
 - (B) Gamma-ray pulse height spectrum of the same liquid nitrogen but using a neutron pulse width of 2 ns. Inset: selection of time-window on the associated time spectrum (x = 36 ns, y = 16 ns and z = 20 ns).
- Fig. 4 (A) A graph showing the temperature values of the PMB of the NaI(TI) detector.
 - (B) A graph showing positions of a photopeak of 1.332 MeV gamma-rays, from a Co-60 source, in correspondence to the temperature variation in the above graph.
- Fig. 5 (A) Comparision of normalized and time-gated gamma-ray energy spectra acquired from urea and water which the three regions of interest are indicated.
 - (B) Comparison of normalized and time-gated gamma-ray energy spectra of three standard samples which major peaks of irradiated elements have been

- indicated. The unit of all the numbers are MeV. Dimension of the rectangular container was 15 X 18 X 20 cm³ and was made from thin sheet iron. The detector stand used to centered the NaI(Tl) detector is made of wood.
- Fig. 6 Experimental arrangement of the HPGe detector for the PGA experiment.
- Fig. 7 Fingerprints of 3 standard military explosives and dry soil as are seen by NaI (Tl) detector. For clarity, they are compared with a normalized spectrum of ammonium nitrate of the same geometry.
- Fig. 8 Fingerprints of the same samples of Fig. 7 as measured by the HPGe detector (relative efficiency at 1.33 MeV gamma-rays = 15 %). Only major lines are marked.



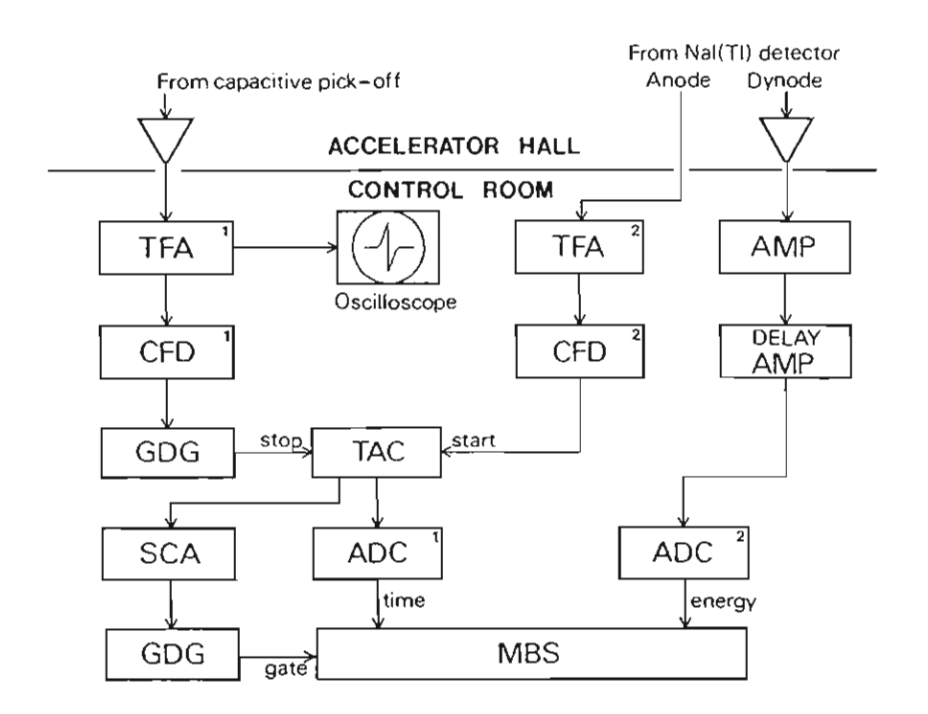


Fig. 2

Α

В

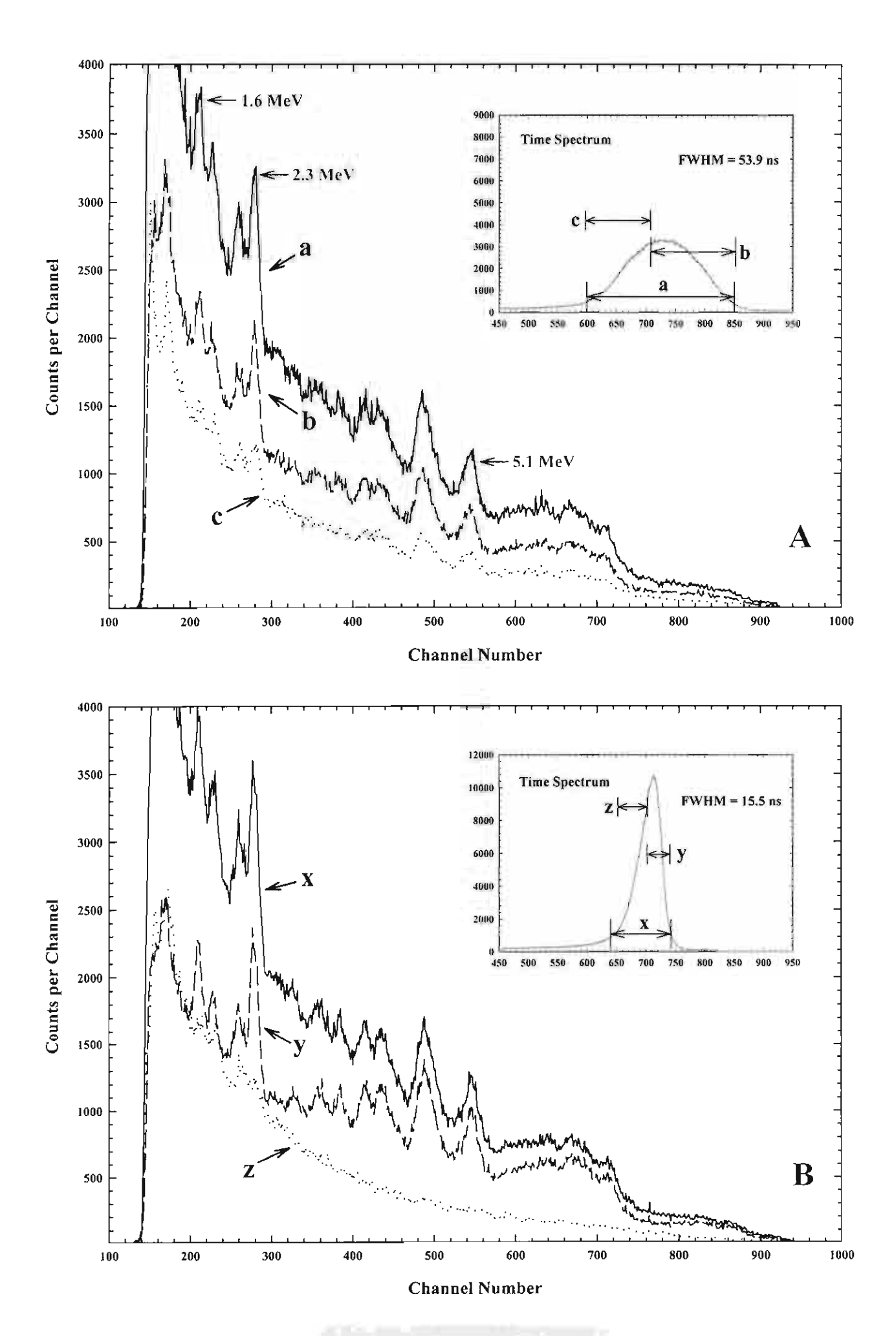


Fig. 3

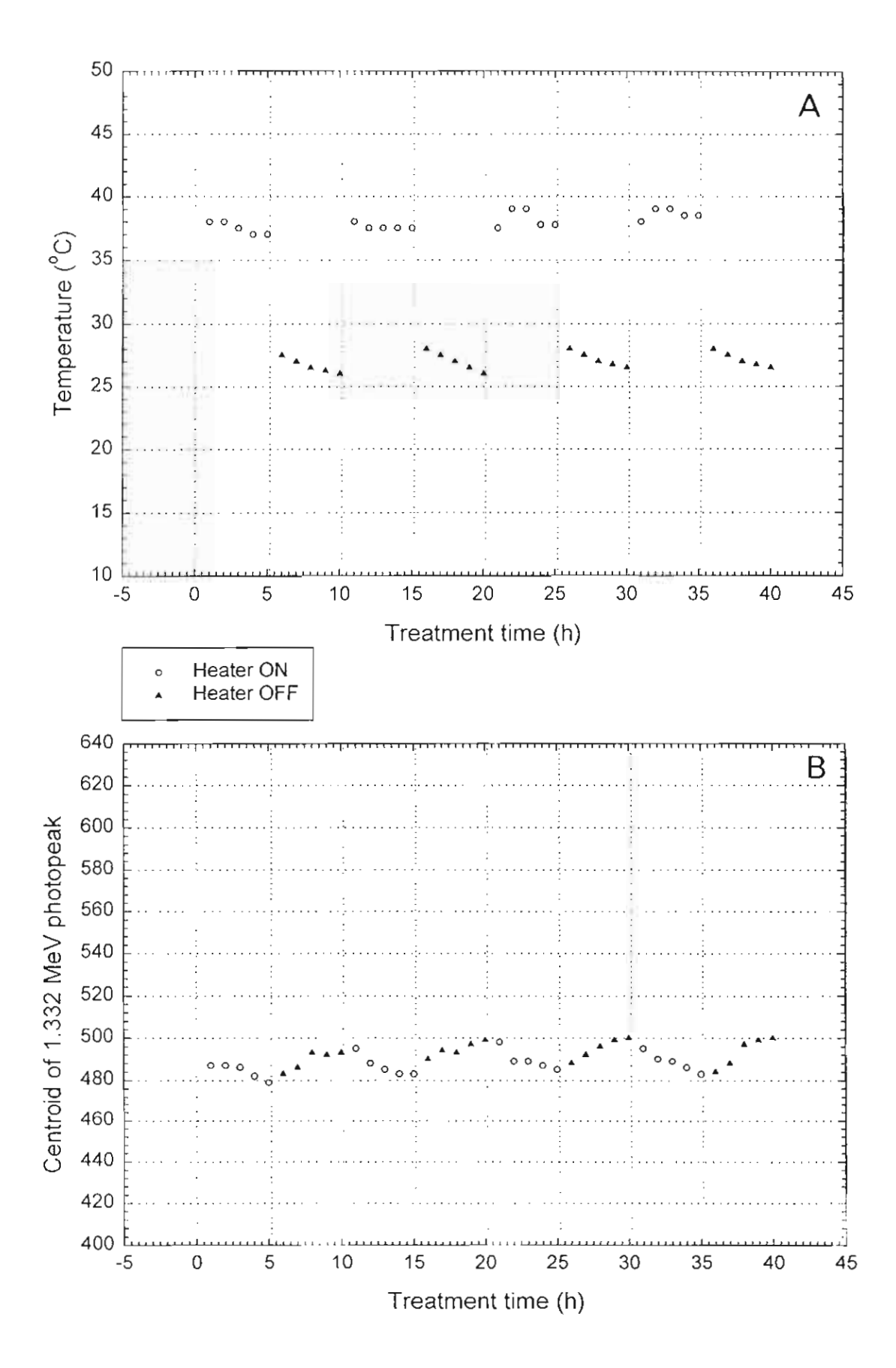
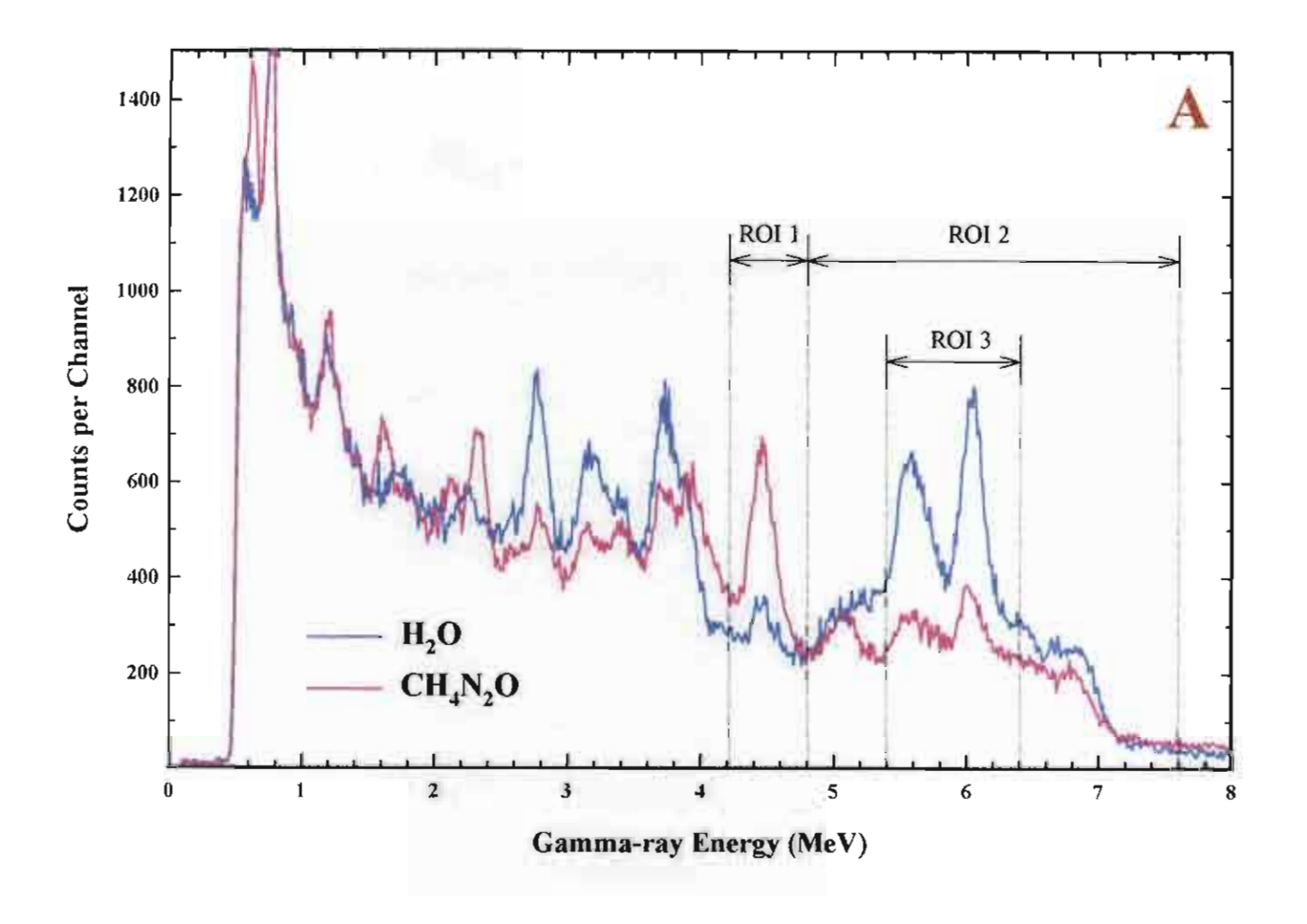


Fig. 4



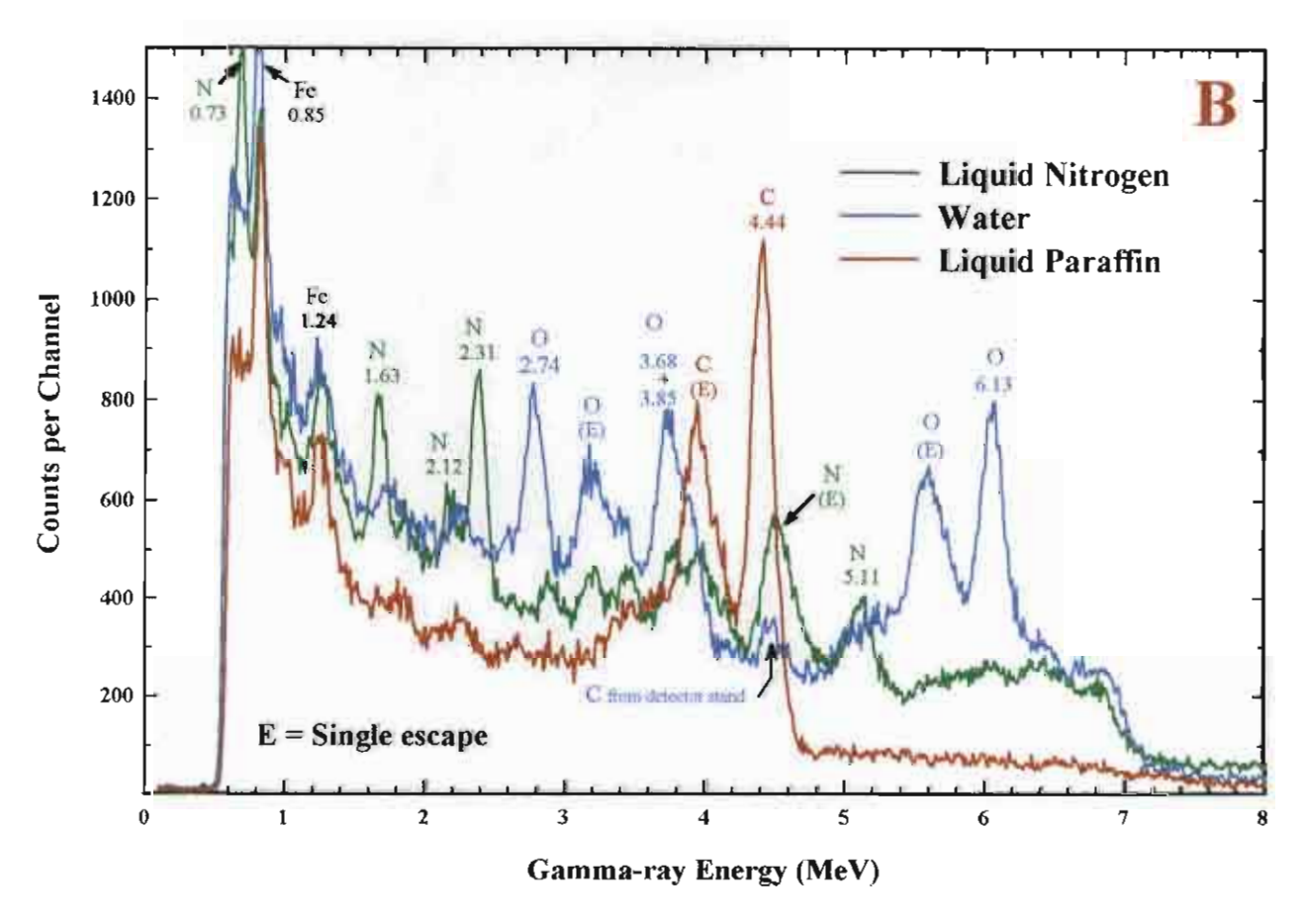


Fig. 5

ภาคผนวก ก8

Hardness, Tribological Behaviour and Corrosion Performance at the Very

Near Surface of Nitrogen Ion-Implanted X5CrNi18.10 Steel

S. Intarasiri¹, L. D. Yu¹, T. Chudoba², H. Reuther², U. Rammelt³ and E. Richter²

¹Institute for Science and Technology Research and Development,
Chiang Mai University, Chiang Mai 50200, Thailand.

²Institute of Ion Beam Physics and Materials Research, D-01314 Dresden, Germany.

³University of Technology Dresden, Institute for Physics Chemistry and
Electrochemical, Mommsen Street 13, D-01062 Dresden, Germany.

Published in:

Surface & Coatings Technology 99 (1998) 305-310.

Reprinted from

SURFACE & COATINGS TECHNOLOGY

Surface and Coatings Technology 99 (1998) 305-310

Hardness, tribological behaviour and corrosion performance at the very near surface of nitrogen ion-implanted X5CrNi18.10 steel

S. Intarasiri ^{a.*}, L.D. Yu ^a, T. Chudoba ^b, H. Reuther ^b, U. Rammelt ^c, E. Richter ^b

Institute for Science and Technology Research and Development, Chiang Mai University, Chiang Mai 50200, Thailand
 Institute of Ion Beam Physics and Materials Research, D-01314 Dresden, Germany
 University of Technology Dresden, Institute for Physical Chemistry and Electrochemistry, Mommsen Street 13,
 D-01062 Dresden, Germany

Received 7 April 1997; accepted 21 October 1997





Surface and Coatings Technology 99 (1998) 305 -310



Hardness, tribological behaviour and corrosion performance at the very near surface of nitrogen ion-implanted X5CrNi18.10 steel

S. Intarasiri a.*, L.D. Yu a, T. Chudoba b, H. Reuther b, U. Rammelt c, E. Richter b

Institute for Science and Technology Research and Development, Chiang Mai University, Chiang Mai 50200, Thailand
 Institute of Ion Beam Physics and Materials Research, D-01314 Dresden, Germany
 University of Technology Dresden, Institute for Physical Chemistry and Electrochemistry, Mommsen Street 13, D-01062 Dresden, Germany

Received 7 April 1997; accepted 21 October 1997

Abstract

The influence of nitrogen ion implantation on the hardness, tribological behaviour and corrosion performance at the very near surface of polished X5CrNi18.10 steel was studied. The specimens were implanted with 120 keV N $^{\circ}$ ions to four different fluences ranging from 10^{16} to 10^{18} ions cm $^{-2}$. It was found that hardness, tribological behaviour in terms of wear and friction, and corrosion resistance of the specimens strongly depend on the implantation conditions. The greatest improvement in the surface properties of the steel was achieved at doses between 1×10^{17} and 5×10^{17} ions cm $^{-2}$. Although hardness, wear resistance and friction behaviour were improved noticeably by the implantation, N ion implantation tended to reduce the corrosion resistance of the specimens in KNO₃. © 1998 Published by Elsevier Science S.A.

Keywords: Nitrogen ion implantation; X5CrNi18.10 steel; Hardness: Tribological behaviour; Corrosion performance

1. Introduction

Stainless steels have been widely used in situations where corrosion resistance is required; however, their hardness, wear and friction properties are not particularly good. Ion implantation is an attractive technique for the improvement of metal surfaces, particularly in the small areas, without altering the bulk properties. Near-surface properties in metal surfaces such as hardness, friction and resistance to wear and corrosion are affected by ion implantation. In addition, the surface composition can be altered, leading to the formation of stable or metastable alloys or compounds which cannot often be formed by conventional methods.

Nitrogen is one of the most promising ion species used in ion implantation to improve the surface mechanical and chemical properties of various steels. With normal energies, e.g. 100 keV, implanted N ions penetrate into steels at a depth of about 100 nm and bring about changes in the relevant properties. However, based on conventional testing techniques, as well as

considering practical applications, most of the previous work investigated the hardness and wear behaviour of the N ion-implanted steels in depth ranges far beyond the ion-implanted layers. This was due to employing either relatively high loads or long testing periods (e.g. [1,2]). The results are certainly useful and beneficial, but lack detail on the behaviour in the implanted-ion layer region. To provide data to fill the gap in the previously obtained results, this experiment attempted to study the hardness, tribological behaviour and corrosion performance of a N ion-implanted stainless steel, X5CrNi18.10, in the depth region within the implanted-ion layer, using newly developed testing methods.

2. Experimental

The samples were mechanically punched out of a X5CrNi18.10 steel sheet (see Table I for composition) into rectangular pieces of dimension $15 \times 10 \times 3$ mm³. Before the implantation, the samples were electrochemically polished to a roughness value (Ra) below 30 nm.

A Danfysik ion implanter version 101 was used for the ion implantation. The samples were implanted with

^{*} Corresponding author. Tel: +66 53 943379; Fax: +66 53 222776; E-mail: sawcat@istrd.emu.ac.th.

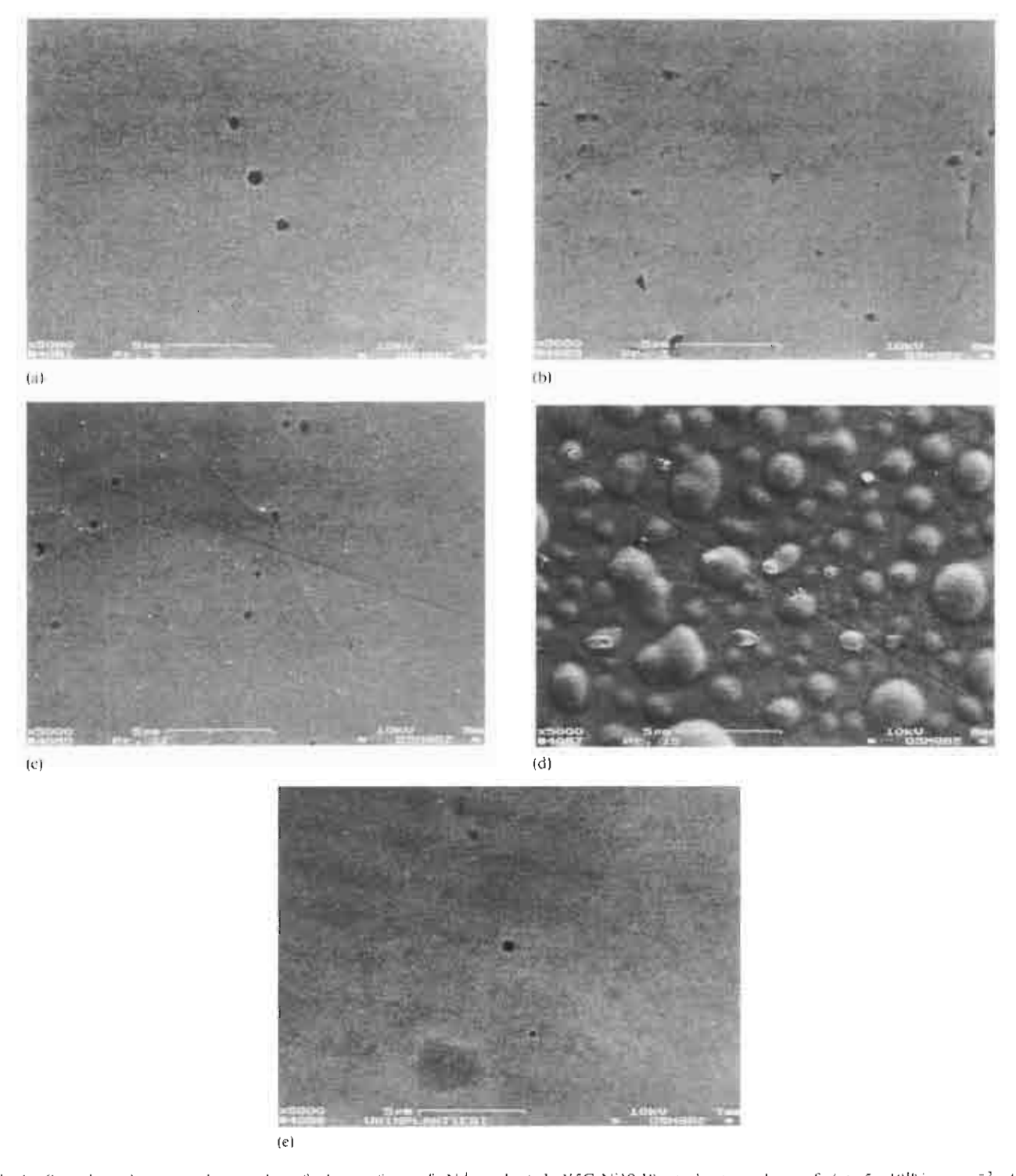
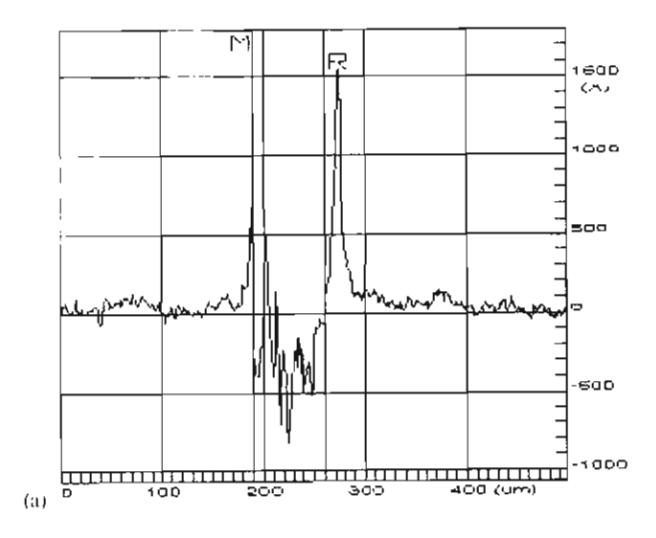


Fig. 1. Scanning electron micrographs of the surface of N 4 -implanted X5CrNi18.10 steel at a dose of (a) 5×10^{16} ions cm $^{-2}$; (b) $1 + 10^4$ ions cm $^{-2}$; (c) $5 + 10^{17}$ ions cm $^{-2}$; and (d) 1×10^{18} ions cm $^{-2}$. For comparison, the scanning electron micrograph of the surface of unimparated X5CrNi18.10 steel is shown in (e).

sliding distance. At the doses of 5×10^{16} ions cm⁻², 1×10^{17} ions cm⁻² and 5×10^{17} ions cm⁻², the nitrogen ion implantation reduced the volume loss of the implanted surface, but at the dose of 1×10^{18} ions cm⁻² at the starting distance, there was an increase

in the volume loss for the implanted surface in comparison with the unimplanted surface, caused by large blisters associated with the formation of nitrogen bubbles.

The effect of the nitrogen ion implantation on the



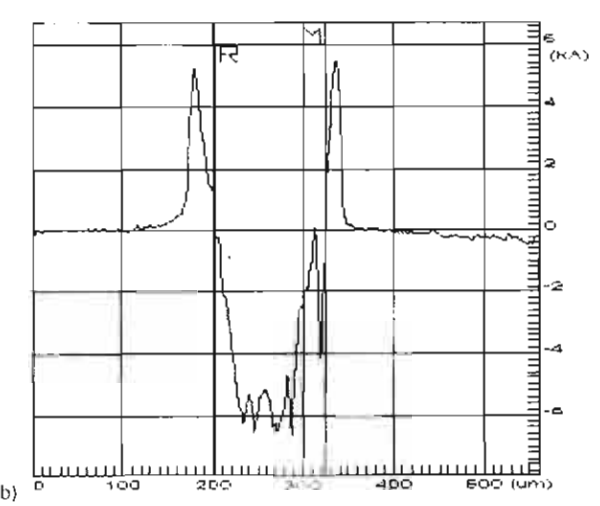


Fig. 5. (a) An example of the profile of a wear trace on the tested sample implanted with a dose of 1×10^{17} N ions cm⁻². The average depth of the trace is less than 60 nm, which is within the implanted N ion layer. For comparison, the wear-trace profile on the unimplanted sample is shown in (b).

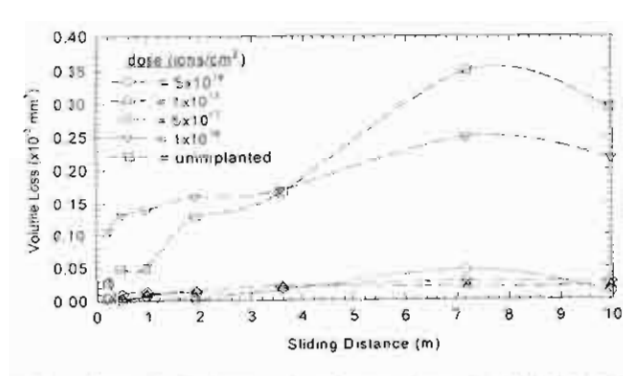


Fig. 6. Dose dependence of volume loss of N*-implanted X5C4Ni18.10 steel.

doses of 5×10^{17} and 1×10^{18} ions cm⁻² the corrosion rate was very high and diffusion processes occurred additionally in the impedance spectra, indicating that

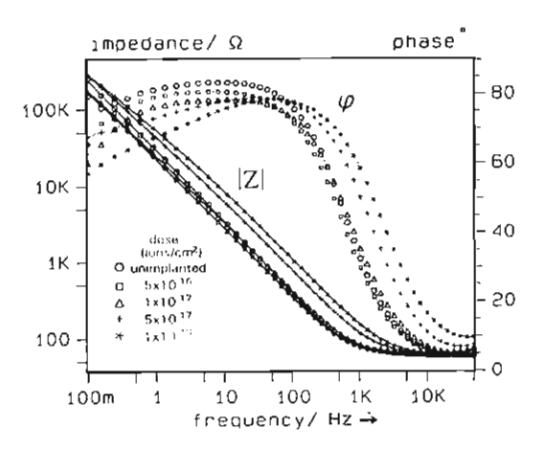


Fig. 7. Bode diagram of N T-implanted X5CrNi18.10 steel.

corrosion products must be transported from the sample surface. The drastic decrease in $R_{\rm pot}$ correlated with the increasing roughness of the surface in the cases of 5×10^{17} and 1×10^{18} ions cm⁻².

4. Discussion

From the experimental results, it can be seen that N ion implantation is certainly beneficial for the improvement of mechanical properties of X5CrNi18.10 steel. even from the very near surface where the implanted N ions remain. The dose dependence of the hardness, wear and friction of the steel indicates that the greatest improvement in the surface properties of the steel could be obtained at doses between 1×1017 and 5×10^{17} ions cm⁻² for normal nitrogen ion implantation. Although there were no differences in the influence on friction and wear properties between the two doses, the dose of 5 × 10¹⁷ ions cm⁻² produced a higher hardness than did the dose of 1×10^{17} ions cm⁻². The surface hardening due to N ion implantation is mainly contributed by the ion-irradiated very-near-surface region, which is slightly shallower than the N ion projectile range, as shown in Fig. 3. It could be supposed that, besides the contribution from the implanted N ions. which form either interstitial decorating dislocations [6] or hard nitride (e.g. [7]), to strengthen the steel, implantation-induced surface oxide (the oxygen distributed in the very-near-surface region is shown in Fig. 2) may also strongly participate in the hardening, as well as decreasing the friction coefficient by weakening the adhesion between two relatively sliding surfaces [8], as demonstrated in Fig. 4. However, as seen in the figures. this effect is not linearly proportional to the ion dose. For the case of the high-dose N ion-implanted sample, it is believed that because of heavy irradiation damage and nitrogen precipitate bubbles on the top surface, mechanical properties including hardness and tribology were not improved as much as for the medium-dose N

Instructions for Authors

Submission of Papers

Manuscripts (original and two clear copies) should be submitted to one of the Editors:

for authors in the Americas

Dr. B. D. Sartwell, Surface Chemistry Branch, Naval Research Laboratory, Code 6170, Washington, DC 20375, USA;

and for authors elsewhere

Professor A. Matthews, Director, The Research Centre in Surface Engineering, The University of Hull, Cottingham Road, North Humberside, HU6 7RX, UK.

Contributions are accepted on the understanding that the authors have obtained the necessary authority for publication. Submission of a manuscript implies that it is not under consideration for publication elsewhere.

Types of contributions

- original papers
- invited or contributed reviews on specific topics
- brief communications on topics of immediate interest
- notices of meetings, symposia and short courses
- technical notes for "Current Industrial Practices" section

Languages

Papers will be published in English. Both English and US spelling are permitted, provided that spelling is consistent within an article.

Authors in Japan please note that information about how to have the English of your paper checked, corrected and improved (before submission) is available from: Elsevier Science Japan, Editorial Service, 1-9-15 Higashi Azabu, Minato-ku, Tokyo 106, Japan; Tel.: +81 3 5561 5032; Fax: +81 3 5561 5045.

Manuscript preparation

Three copies of the manuscript should be submitted, in double-spaced typing on pages of uniform size with a wide margin on the left.

Some flexibility of presentation will be allowed but authors are urged to arrange the subject matter clearly under such headings as Introduction, Experimental details, Results, Discussion etc. Each paper should have an abstract of 100-200 words.

References should be numbered consecutively (numerals in square brackets) throughout the text and collected together in a reference list at the end of the paper. Journal titles should be abbreviated according to the Chemical Abstracts Service Source Index, 1970 edition, and supplements. The abbreviated title should be followed by volume number, year (in parentheses) and page number.

Submission of electronic text

The final text should be submitted on a 3.5 in or 5.25 in diskette (in addition to a hard copy with original figures). Double density (DD) or high density (HD) diskettes formatted for MS-DOS or Apple Macintosh compatibility are acceptable, but must be formatted to their capacity before the files are copied on to them. The files should be saved in the native format of the wordprocessing program used. Most popular wordprocessor file formats are acceptable. It is essential that the name and version of the wordprocessing program, type of computer on which the text was prepared, and format of the text files are clearly indicated.

Illustrations

Line drawings and cyclic or aromatic formulae should be in a form suitable for reproduction. They may be drawn in black ink on drawing paper (letter height, 3-5 mm), but the use of good quality computer-generated figures is encouraged. They should preferably all require the same degree of reduction, and should be submitted on paper of the same size as, or smaller than, the main text to prevent damage in transit. Photographs should be submitted as clear blackand-white prints on glossy paper. Each illustration must be clearly numbered.

Illustrations can be printed in colour when they are judged by the Editor to be essential to the presentation. The publisher and the author will each bear part of the extra costs involved. Further information concerning colour illustrations and the costs to the author can be obtained from the publisher.

Legends to the illustrations must be submitted in a separate list.

All tables and illustrations should be numbered consecutively and separately throughout the paper.

Authors will receive proofs, which they are requested to correct and return as soon as possible. No new material may be inserted in the text at the time of proofreading. All joint communications must indicate the name and full postal address of the author to whom proofs should be sent.

Further information

All questions arising after the acceptance of manuscripts, especially those relating to proofs, should be directed to: Elsevier Science Ireland Ltd. Bay 15K, Shannon Industrial Estate, Shannon, Co. Clare, Ireland; Tel.: +353 61 471944; Fax: +353 61 472144.

The full and complete instructions to authors can be found on the World Wide Web: please visit our website which is accessible via the Elsevier Surfaces and Interfaces HomePage at http://www.elsevier.nl/locate/surfaces

Offprints

Twenty-five offprints will be supplied free of charge to the author(s). Additional offprints can be ordered at prices shown on the offprint order form which accompanies the proofs.

1998 Elsevier Science S.A. All rights reserved.

0257- 8972,08 \$19 00

This journal and the individual contributions contained in it are protected by the copyright of Elsevier Science S.A., and the following terms and

Photocopying

Single photocopies of single articles may be made for personal use as allowed by national copyright laws. Permission of the publisher and payment of a fee is required for all other photocopying, including multiple or systematic copying for advertising or promotional purposes, resale, and all forms of document delivery. Special rates are available for educational institutions that wish to make photocopies for roon profit educational classroom use.

In the USA, use is may clear permissions and make payment through the Copyright Clear nice Center, Inc., 222 Rosewood Drive, Danvers, MA 01923, USA, in the UK, users may clear permissions and make payment through the Copyright Licensing Agency Rapid Clearance Service (CLARCS), 90 Tottenham Court Fload, London W18 DLP, UK, in other countries where a local copyright clearance centre exists, please contact if for information or required compressions and nawness.

on required permissions and payments.

Derivative Works

Subscribers may reproduce tables of contents or prepare lists of articles including abstracts for internal circulation within their institutions. Permission of the publisher is required for resale or distribution outside the institution.

Permission of the publisher is required for all other derivative works, including compilations and translations.

Electronic Storage Permission of the publisher is required to store electronically any material contained in this journal, including any article or part of an article. Contact the publisher at the address indicated.

Except as outlined above, no part of this publication may be reproduced, stored in a retrieval system or transmitted in any form or by any means, electronic, mechanical, photocopying, recording or otherwise, visibnut prior written permission of the publisher.

Disclaimers

Disclaimers

No responsibility is assumed by the publisher for any injury and/or damage to persons or property as a matter of products liability, negligence or otherwise, or from any use or operation of any methods, products, instructions or ideas contained in the material herein.

Although all advertising material is expected to conform to ethical (medical) standards, inclusion in this publication closs not constitute a guarantee or endorsement of the quality or value of such product or of the claims made of it by its manufacturer.

Printed in The Netherlands

- The jumper used in this publication meets the requirements of ANSI, NISO Z39.48-1992 (Permanence of Paper)

ภาคผนวก ก9

Surface Modification of Tool Steels by Combined Cr- and N-lon Implantation

L. D. Yu¹, T. Vilaithong², B. Yotsombat², S. Thongtem², J. G. Han³ and J. S. Lee³

¹Institute for Science and Technology Research and Development,
Chiang Mai University, Chiang Mai 50200, Thailand.

²Department of Physics, Faculty of Science,
Chiang Mai University, Chiang Mai 50200, Thailand.

³Department of Metallurgical Engineering, Sung Kyun Kwan University,
300 Chunchun-dong, Jangan-ku, Suwan, South Korea.

Published in:

Surface & Coatings Technology 103-104 (1998) 328-333.

Experimental determination of the thermal neutron flux around two different types of high intensity ²⁵²Cf sources

R. Schmidta)

Department for Radiation Oucology, University Hospital Eppendorf, University of Hamburg, Martinistasse 52, 20246 Hamburg, Germany

R. L. Maughan, M. Yudelev, and C. Kota

Gershenson Radiation Oncology Center, Karmanos Cancer Institute, Harper Hospital and Wayne State University, 3990 John R., Detroit, Michigan 48230

S. Wanwilairat

Department of Physics, Faculty of Science, Chiang Mai University, Chiang Mai 50200, Thailand

(Received 12 May 1998; accepted for publication 30 October 1998)

The application of neutron emitting radioisotopes in brachytherapy facilitates the use of the higher biological effectiveness of neutrons compared to photons in treating some cancers. Different types of high intensity ²⁵²Cf sources are in use for the treatment of different cancers. To improve the therapy of bulky tumors the dose can be augmented by the additional use of the boron capture reaction of thermal neutrons. This requires information about the thermal neutron dose component around the Cf source. In this work, a Mg/Ar-ionization chamber internally coated with ¹⁰B was used to measure the thermal neutrons. These measurements were performed on two different ²⁵²Cf sources, one in use in the Gershenson Radiation Oncology Center at Harper Hospital in Detroit, MI, and one at the University Hospital of Chiang Mai in Chiang Mai, Thailand. The results of these measurements are compared and indicate that the differences in the construction of the sources influence the thermal dose component. © 1999 American Association of Physicists in Medicine. [S0094-2405(99)01201-8]

Key words: external beam neutron therapy, ²⁵²Cf brachytherapy, boron neutron capture reaction

INTRODUCTION

The greater biological effectiveness of neutrons compared to photons has lead to an interest in using neutron sources in brachytherapy. Because of the achievable neutron intensity and its half-life of 2.65 yr, ²⁵²Cf is very attractive for this type of clinical application. The neutron dose can be enhanced via the boron neutron capture reaction (BNCT) of thermal neutrons in the tumor. ^{1,2} The flux of thermal neutrons around the ²⁵²Cf source has to be evaluated in order to calculate this dose enhancement. For the different types of ²⁵²Cf sources, in use for brachytherapy, the thermal neutron component might be dependent on the constructional details of the sources, such as the encapsulation and overall dimensions.

In this paper the thermal neutron dose distributions around two different ²⁵²Cf sources, one in use at Harper Hospital in Detroit (MI), the other installed at the University Hospital in Chiang Mai (Thailand), are compared. The two ²⁵²Cf sources differ in their construction and in their activity. The same boron-coated magnesium chamber was used at both institutions to evaluate the thermal neutron flux at different positions in a water phantom, where the ²⁵²Cf source was positioned close to the center of the phantom.³

METHODS AND MATERIALS

The parameters of both sources used for this investigation are summarized in Table I. Considerable differences are seen

with respect to the dimensions, activity, and the encapsulation. In Detroit, the dose measurements were performed in a cubic water tank of dimensions $60\,\mathrm{cm}\times30\,\mathrm{cm}\times30\,\mathrm{cm}$ with 1-cm-thick polymethylmethacrylate walls (PMMA). A single $^{252}\mathrm{Cf}$ source was housed in a cylindrical PMMA tube with an outer diameter of 4 mm and the closest distance from center of the source to the center of the chamber was 7 mm. The chamber was positioned manually. In Chiang Mai the measurements were performed in a water tank of dimension $53\,\mathrm{cm}\times56\,\mathrm{cm}\times40\,\mathrm{cm}$ with 1-cm-thick PMMA walls. The $^{252}\mathrm{Cf}$ source was housed in a cylindrical PMMA tube with an outer diameter of 9 mm. The chamber was remotely driven by an isodose recorder (Model FM-0036; Fujitech, Japan) providing a minimum step distance of 1 mm. The closest

TABLE I. Parameters of the 252Cl sources (Refs. 4 and 5).

Institute	Detroit	Chiang Mai	
Manufacturer	Oak Ridge National Laboratory	Frontier Technology Cooperation	
Active length (mm)	15	6	
External length (mm)	23	12 ;	
External diameter (mm)	2.8	6	
Wall thickness (mm)	0.5	1.1	
Wall material	Pt (10%lr)	Zircaloy-2	
Actual weight of 252Cf (μg)	11.4	100.1	

TABLE II. Kerma factors for thermal reactions in tissue and 10B.

Concentration and reaction	Kerma factor (pGy em	
50 ppm ¹⁰ B(n,α)	4.273	
50 ppm ${}^{10}B(n, \gamma)$	0.0278	
Total 50 ppm 10B	4.30	
Muscle tissue	0.231	

distance between source and chamber was 16 mm, defined as the distance between the centers of the source and chamber, respectively.

A thimble ionization chamber with an inner volume of 0.32 cm3 was used for making the measurements (Wellhöfer Dosimetrie, Germany). The magnesium wall of the chamber was internally coated with a 3 µm layer of ¹⁰B of 92% purity, and the chamber was flushed with argon gas of 99,995% purity. The chamber was calibrated in a 60Co beam in terms of absorbed dose to water N_w. The chamber has a gas-flow provision and during the measurements a constant argon gas flow of 17 cm³/min was used. The chamber was connected via a triax cable with a Farmer Electrometer (Model 2570, Nuclear Enterprises, Great Britain), that was operated in the high sensitivity charge mode with a resolution of 0.005 nC and a leakage of ±10 fA. The electrometer applied a high voltage of -250 V to the chamber. The chamber was calibrated in a homogeneous flux of thermal neutrons with a mean energy of 37 meV at the standards laboratory, Physikalisch-Technische Bundesanstalt, in Germany to obtain the calibration factor,

$$R(4\pi,37.0 \text{ meV}) = 1.02 \times 10^{-7} \text{ nC cm}^2/\text{neutron}.$$

The kerma factor for muscle at a neutron energy of 36 meV was taken as 2.31×10^{-13} Gy cm² and used to calculate the dose to muscle tissue.⁶ Kerma factors for calculating the ¹⁰B dose from the neutron fluence were adopted from a paper by Konijnenberg *et al.*⁷ and are shown in Table II.

RESULTS

At each institution, the ionization chamber was checked in a ⁶⁰Co radiation field for stability and proper operation. Table III gives the ratio for the stated to measured dose at the local cobalt unit. In Chaing Mai the MgB/Ar chamber was used to measure the thermal dose distribution at points parallel to the axis of the cylindrical source at distances of 2, 5, and 10 cm axis (longitudinal scans, see Figs. 1 and 2). Transverse scans were made at points along a line perpendicular to the axis at the same distances from the center of the source (see Figs. 1 and 3). From these scans the exact center of the source was determined. Depth scans were performed on the

TABLE III. Calibration of ionization chambers, ratio of stated to measured dose at local cobalt unit.

Chamber	Detroit	Chiang Mai
MgB/Ar	1012	1.006

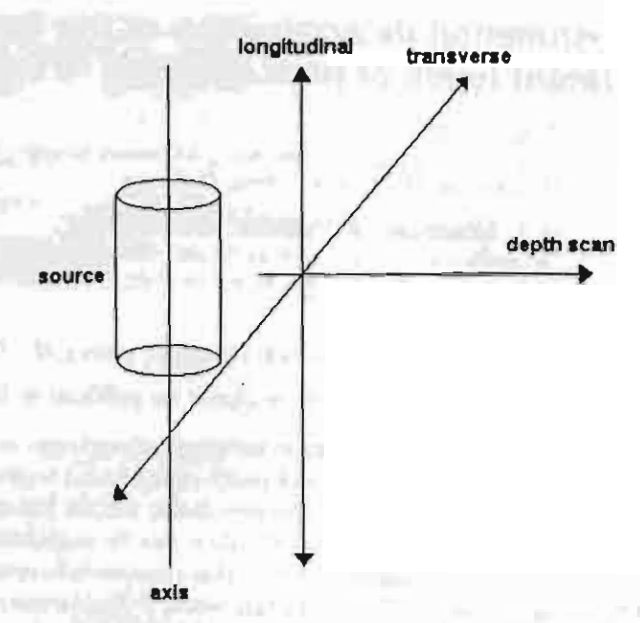


Fig. 1. Sketch of the geometrical situation for longitudinal, transversal, and depth scans.

axis perpendicular to the longitudinal and transverse scans. The distances between source and chamber were defined as the distance from the center of the source to the center of the chamber. In Chiang Mai measurements were made at distances of up to 20 cm from the source. As the source strength

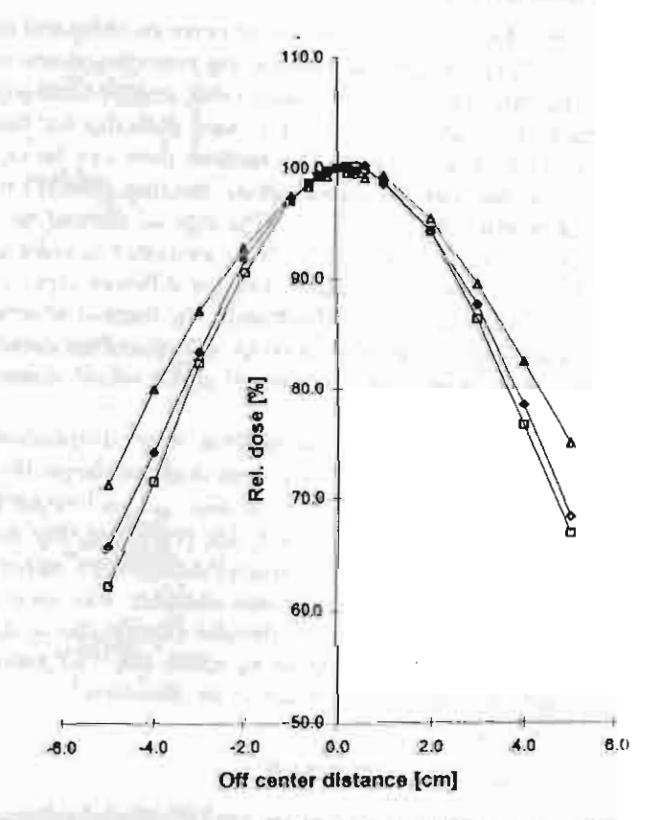


Fig. 2. Longitudinal scans in Chiang Mai at different source-to-chamber distances (d). The scans are normalized to the measured value at the center d = 2 cm (f.1), d = 5 cm (0), and d = 80 cm (0).

Tauti; IV. Doses for muscle tissue and 50 ppm ¹⁰B determined at 3 cm distance.

	Institute	
	Detroit	Chiang Ma
R _u (nC/min)	1.430	11.238
Φ (n/cm ² s)	2.34×10^{7}	0.1836×10^{7}
Dose rate (tissue) (Gy/s)	5.4×10^{-8}	4.24×10^{-7}
Dose rate (tissue) (eGy/µg)	1.704×10^{-3}	1.526×10
Dose rate (50 ppm 10B) (Gy/s)	1.01×10^{-6}	7.90×10^{-6}
Dose rate (50 ppm 10B) (eGy/µg h)	0.032	0.028

was comparably lower in Detroit the greatest distance at which sufficient chamber current was produced to give an accurate measurement was 7 cm.

The measured charges were converted into tissue and boron dose using the factors given in Table II. For comparison the relative thermal neutron dose in water as a function of distance from the source measured in Detroit and Chiang Mai are given in Fig. 4. The dose distributions are normalized to 2 cm source-to-chamber distance. For distance the values of interest are summarized in Table IV.

DISCUSSION

85

Since fast neutrons undergo multiple scattering reactions, mainly with hydrogen until they slow down to thermal energies, the thermal neutron fluence could have a directional

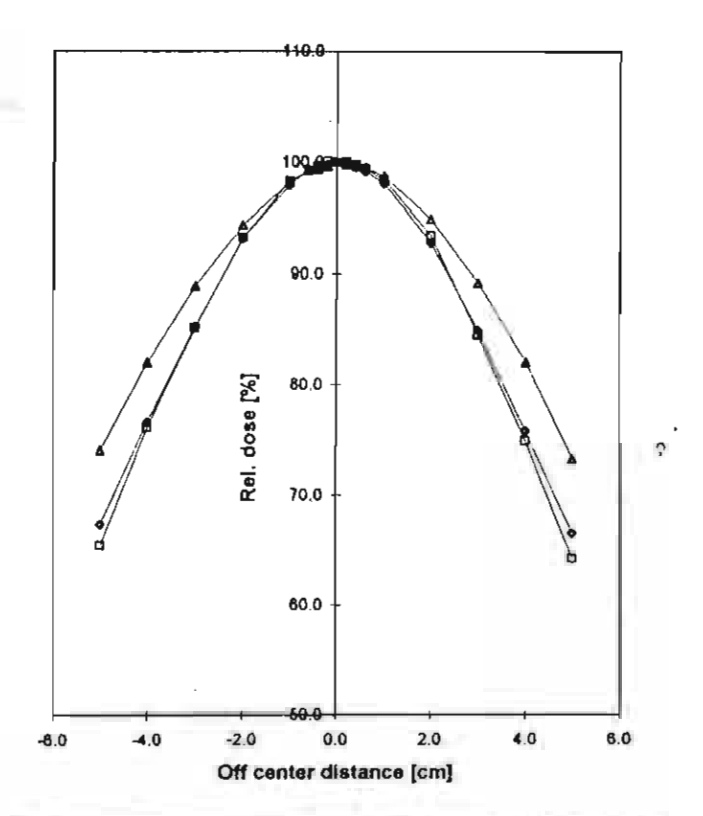


Fig. 3. Transverse scans in Chiang Mai at different source-to-chamber distances (d). The scans are normalized to the measured value at the center d = 2 cm (\square), d = 5 cm (\lozenge), and d = 10 cm (\lozenge)

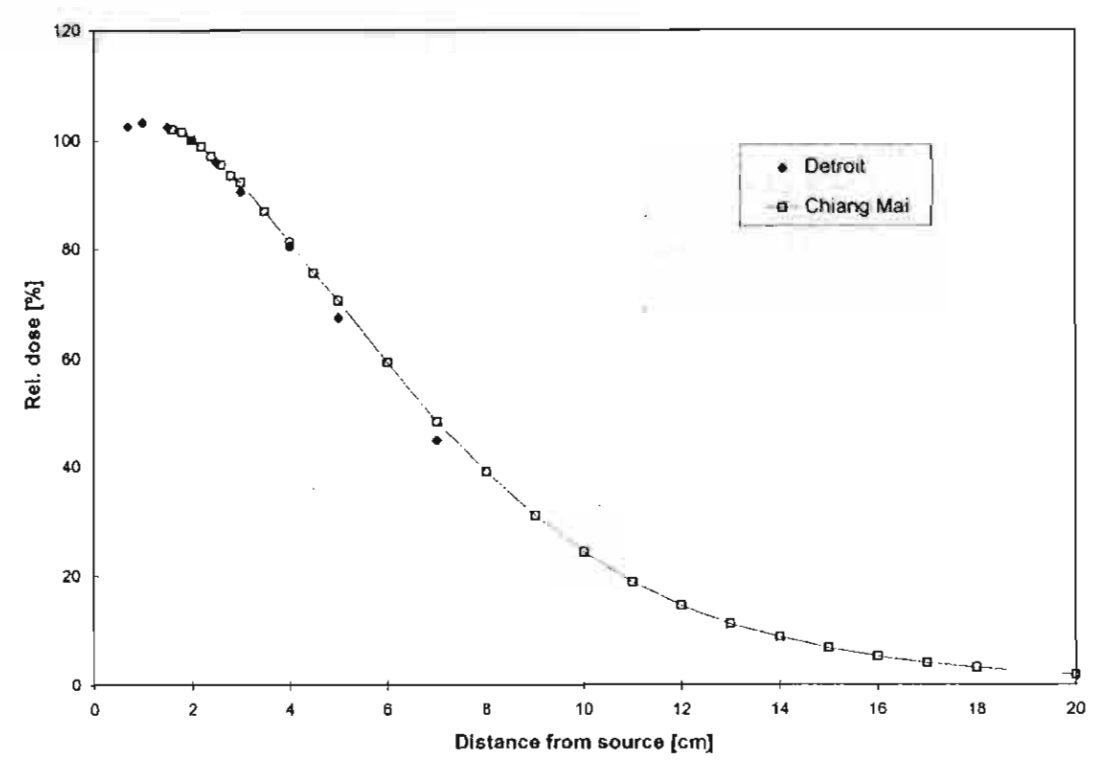


Fig. 4. Relative thermal neutron dose in water as a function of distance from the source in Detroit (♦) and Chiang Mai (□); scans are normalized to the measured value at 3 cm distance.

TABLE V. Estimated uncertainties in dose (%).

ltem	Error
Directional response	4
Neutron calibration	5
Position in phantom	1
Displacement correction	0.5
Temperature, pressure, gas flow	0.5
Electrometer	0.5
Total error	6.5

dependence. The directional response of the MgB/Ar ionization chamber to thermal neutrons was characterized in an earlier work,³ and is given as

$$R(4\pi) = 0.835R(90^{\circ}),$$

where $R(90^{\circ})$ is the response of the chamber to laterally incident thermal neutrons. A comparison with foil activation in a thermal field of a fast neutron beam justified the use of the above calibration relation in a nonhomogeneous thermal neutron beam.³ If the thermal neutron field is not homogeneous the directional response of the chamber could introduce some error that was estimated from the comparison to be <4%.

The MgB/Ar ion chamber used in this work was calibrated for thermal neutron response in a standard field with a mean energy of 37 meV. Any differences between this field and the thermal/epithermal field around the 252Cf sources will introduce some uncertainty into the thermal fluence interpretation and the subsequent 10B dose determination. Since the response of the chamber is due to the ¹⁰B reaction, the chamber response, if calibrated in terms of ¹⁰B dose, can be used to directly infer the ¹⁰B dose without a knowledge of the neutron energy spectrum. In this work, an uncertainty of 5% is assigned to the chamber response due to differences in calibration and ²⁵²Cf thermal/epithermal neutron spectra. At both the facilities; the chambers were positioned with an accuracy of ~1 mm, introducing an uncertainty of ~1% in the calculated dose according to the change of the dose with distance.

The measured charge was several orders of magnitude greater than the leakage current and was corrected for temperature and pressure. The gas flow rate in the chamber was monitored and maintained at a steady level to ensure stability of operation. The inaccuracy of the resulting corrections was taken as 0.5% for temperature, pressure, and gas flow and 0.5% for the electrometer reading. Displacement corrections and stem effects were ignored, thus taken into account as

0.5% introduced inaccuracy. As the measured dose rate is fairly low, saturation effects due to recombination are insignificant. Table V lists the uncertainties discussed above. A total uncertainty of 6.5% is estimated for the present thermal fluence measurements by adding the individual uncertainties in quadrature. For a relative comparison of the dose distribution around the two different sources, uncertainties associated with the directional response and neutron calibrations can be assumed to be identical and, hence, inconsequential. This results in a reduced uncertainty of 5% for this intercomparison. The thermal fluence distributions as a function of distance from the source (Fig. 4) for the two sources are well within this uncertainty, with a maximum difference of 4%.

A difference of 11% in the ¹⁰B dose (for 50 ppm ¹⁰B) at 3 cm distance from the two sources is observed. This is larger than the 5% relative uncertainty and 6.5% total uncertainty. The ¹⁰B dose measurement in Detroit of 0.032 cGy/µg h is in good agreement with a Monte Carlo calculation of Yanch and Zamenhof⁸ which gives a value of 0.031 cGy/µg h for a source of comparable design. This indicates that the observed differences in the absolute thermal fluence around the two sources are real and most likely due to differences in design and construction.

ACKNOWLEDGMENT

Part of this work was supported by the German Academic Exchange Service (DAAD), Germany.

^{a)}Electronic mail: r.schmidt@uke.uni-hamburg.de

¹F. M. Waterman, F. T. Kuchnir, L. S. Skaggs, D. K. Bewley, B. C. Page, and F. H. Attix, "The use of ¹⁰B to enhance the tumor dose in fast neutron therapy," Phys. Med. Biol. 23, 592–602 (1978).

²J. L. Beach, C. B. Schroy, M. Ashtari, M. R. Harris, and Y. Maruyama, "Boron neutron capture enhancement of ²⁵²Cf brachytherapy," Int. J. Radiat. Oncol., Biol., Phys. 18, 1421 a 1427 (1990).

³L. Luedemann, T. Matzen, M. Matzke, R. Schmidt, and W. Scobel, "Determination of the thermal neutron flux in a fast neutron beam by use of a boron-coated ionization chamber," Med. Phys. 22, 1743–1747 (1995).

⁴J. B. Knauer, C. W. Alexander, and J. E. Bigelow, **25°Cf Properties, production, source fabrication and procurement," Nucl. Sci. Appl. (Dhaka) 4, 3–20 (1991)

⁵IAEA Certificate of Competent Authority, Special Form Radiative Materials, Certificate No. USA/0367/S, Revision 3, U.S. Department of Transportation, Washington, DC, 1990.

6International Commission on Radiation Units and Measurements. "Tissue substitutes in radiation dosimetry and measurements," ICRU Report No. 44, Washington, DC, 1989.

⁷M. W. Konijnenberg, L. G. H. Dewit, B. J. Mijnheer, C. P. J. Raaijmakers, and P. R. D. Watkins, "Dose homogeneity in horon neutron capture therapy using an epithermal neutron beam," Radiat. Res. 142, 327–339 (1995).

⁸L. C. Yanch and R. G. Zamenhof, 'Dosimetry of ²⁵²Cf sources for neutron radiotherapy with and without augmentation by boron neutron capture therapy,' Radiat. Res. 131, 249–256 (1992).

ภาคผนวก ก6

Plasma Parameter Characterization of a DC Multicusp Plasma Chamber Operating in He, Ar and Xe Gas

P. Suanpoot¹, T. Vilaithong¹, M. W. Rhodes² and D. Boonyawan¹

¹Fast Neutron Research Facility, Department of Physics, Faculty of Science,
Chiang Mai University, Chiang Mai 50200, Thailand.

²Institute for Science and Technology Research and Development
Chiang Mai University, Chiang Mai 50200, Thailand.

Published in:

J. Plasma Fusion Res. SERIES, Vol.1 (1998) 526-530.

Plasma Parameter Characterization of a DC Multicusp Plasma Chamber Operating in He, Ar and Xe Gas

SUANPOOT Pradoong*, VILAITHONG Thiraphat, RHODES Michael W.¹ and BOONYAWAN Dheerawan

Fast Neutron Research Facility, Department of Physics,
Faculty of Science, Chiang Mai University, Thailand

Institute for Science and Technology Research and Development,
Chiang Mai University, Thailand

(Received: 30 September 1997/Accepted: 12 January 1998)

Abstract

A large dc multicusp plasma chamber has been constructed and installed at Chiang Mai University. The first prototype has a 31.2 cm diameter and a 42.5 cm length and is surrounded by 632 ceramic permanent magnet buttons with a maximum magnetic field of about 2.2 kG for each. The magnetic field at the stainless steel wall with a thickness of 2 mm is about 670 G. A tungsten (W) filament was used as a source of primary electrons. The estimated discharge voltage for helium gas (He), argon gas (Ar), and xenon gas (Xe) was 40 V and the discharge operating current varies from 500 mA to 1 A. Plasmas can be confined within a 20 cm diameter region which are uniformly distributed along the axial path. The plasma density was measured by a single cylindrical Langmuir probe to be between $4.8 \times 10^8 - 4.9 \times 10^9$ cm⁻³ with 650 watts of power applied to the tungsten filament and the gas pressure inside the chamber of 3.8×10^{-4} Torr. Results of the ion density measurements are described. The proportionality constants in the relation between the ion current density arriving at the plasma electrode and the maximum plasma density and the ion sound speed for helium, argon and xenon are found to be 0.42 ± 0.07 , 0.59 ± 0.08 , and 0.46 ± 0.06 , respectively.

Kevwords:

plasma chamber, multicusp field, dc discharge, ion density profile, helium, argon, xenon

1. Introduction

In recent years, multicusp plasma sources have been utilized as ion sources in ion and plasma based processes for materials modification. The plasma chamber is usually surrounded by a certain arrangement of permanent magnets which can produce a large volume of uniform and quiescent plasma with a density exceeding 10^{12} cm⁻³ [1, 2]. These magnetic multicusp devices were shown also to be good candidates for the production of intense uniform ion beams [3].

A large multicusp plasma test chamber, based on the pioneering work of Leung et al. [2-9] was constructed and installed at Chiang Mai University. The first prototype has a diameter of 31.2 cm and is 42.5 cm long as shown in the photograph in Fig. 1. It is primarily intended to be used as a source of atomic and molecular particles for the purpose of studying plasma parameter characterizations.

In this reference, the characteristics of a multicusp plasma generator operating with helium (He), argon (Ar), and xenon (Xe) gases are described. A hot tungsten (W) wire produces electrons, which are emitted and accelerated between the filament cathode and the

*Corresponding author's e-mail: prodoong@istrd.cmu.ac.th Science and Nuclear Fusion Research

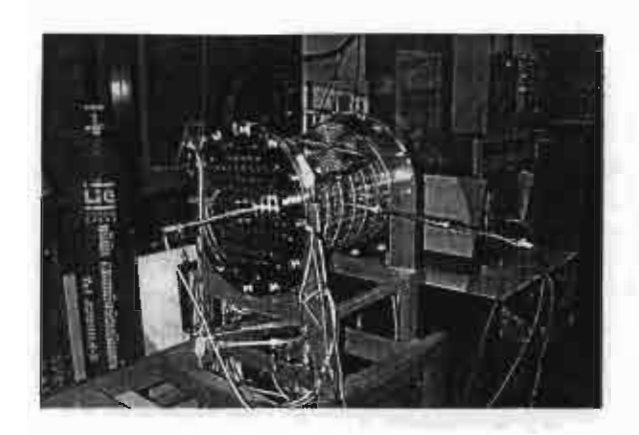


Fig. 1 A dc multicusp plasma source chamber at Chiang Mai University.

anode wall of the chamber. The neutral gas in the chamber is ionized by electron collision and plasmas are generated. However, the mean free path of electrons with 100 eV energy inside the chamber with argon gas pressure of 10^{-4} Torr is about 1 meter. For efficient plasma confinement, permanent magnets are used to produce a large volume of uniform and quiescent plasma. The maximum plasma density in an uniform large volume confined by the multicusp field in this experiment is found to be about 4.9×10^9 cm⁻³.

When the chamber is operated as an ion source, the magnets on one end of the vessel will be removed therefore the plasma density profile in the axial direction will not be uniform. The maximum density is located towards the back plate [3]. Ions generated on the right hand side of this maximum will be pushed toward the plasma electrode. The speed of these ions when they enter the sheath is greater or equal to the ion sound speed $(\sqrt{KT_e/M_i})$ where M_i is the mass of the ion, K is the Boltzmann constant, and T_e is the electron temperature. The relationship between the ion current density J_i arriving at the plasma electrode and the maximum plasma density n and the ion sound speed can be expressed as [14]

$$J_{i} = \alpha n e \sqrt{K} T_{c} / M_{i} \tag{1}$$

Once J_i is determined, the extraction geometry can be designed by using the Child-Langmuir space-charge limited current flow equation. We measured the proportionality constant α for heluim, argon and xenon.

2. Experimental Technique

A schematic diagram of the experimental setup for the positive ion measurement is shown in Fig. 2. The plasma generator is a thin-walled (2 mm) cylindrical stainless steel chamber (31.2 cm diameter by 42.5 cm long). The chamber wall is surrounded externally by 632 of ceramic permanent magnet buttons ($B_{\rm max}\approx 2.2$ kG) in a full-line cusp configuration [2]. The plasma is generated by electrons emitted from a tungsten filament (1 mm diameter by 20 cm long) biased at -40 V with respect to the chamber wall (anode). This filament extends approximately 7 cm into the magnetic field-free region and the input power was about 650 watts. The operating gas (helium, argon, xenon) pressure inside the chamber was 3.8×10^{-4} Torr. Plasma parameters and density profiles were obtained using movable single Langmuir probes 0.15 mm in diameter and 10.0 mm long.

An electrostatic probe control and data acquisition system has been presented elsewhere [11]. They shall briefly be described here. The system consists of 4 subassemblies, excluding power supplies. This includes an IBM/PC printer port to multiport translator, a dual DAC (digital to analog) unit, a multi-channel, programmable gain, 13-bit bipolar ADC, and a dual power amplifier module. The DACs are 12-bit bipolar serial converters (+/- 11 bits) each which drive one power amplifier. The power amp is capable of +/- 30 V and directly drives the plasma probe through an RG-58 coaxial cable. On the power amp board is a current monitoring resistor and a differential amplifier across it. Each of the two channels has one current sense voltage and one load voltage signal sent to channels on the ADC board.

The programming language chosen was Visual Basic for Windows due to its ease of producing a GUI (graphical user interface) for the operator and its flexibility to incorporate libraries from other programs such as assembly language. Data is stored onto disk in three

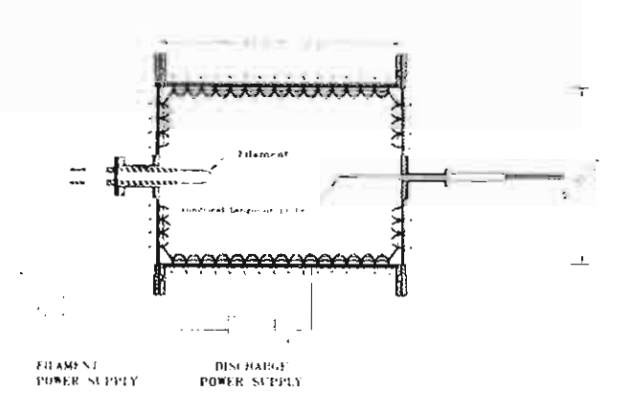


Fig. 2 Schematic diagram of a large muticusp plasma test chamber and experimental set up for positive ion measurement.

formats; native (used for the local plotting program), Sigma Plot and comma delimited format (for exporting into a database or spreadsheet program). This allows more sophisticated analysis of the data off-line. Within the virtual control console is a set of digital meter displays that reflect the conversion voltages and currents of the probes in real time and a graphical plotting display that is updated at the end of the run. The system has the ability to operate in playback mode, that means any data run can be replotted at any time without using an external plotting package. There are also controls for setting full scale of the current axis. The ranges available are, 100 mA f.s, 10 mA f.s, 1 mA f.s, and .1 mA f.s (bipolar). Since the ADC is +/- 12 bits that means a resolution of 1/4096 within the selected full scale for the probe current. The probe voltage conversion is locked at a resolution of 2.4 mV due to the range it operates in normally is high.

The electron density n_e was determined also by using the single Langmuir probe technique. We determined the electron saturation current I_e , and the electron temperature T_e from the slope of a semilog plot of the probe current I_e vs. the probe bias voltage V_p [10]. The electron density of mass m_e was calculated from the following equations.

$$n_{c} = \frac{1}{e} \left(\frac{I_{c}^{*}}{S} \right) \sqrt{\frac{2\pi m_{c}}{KT_{c}}}$$

$$= J_{c} \frac{1}{e} \sqrt{\frac{2\pi m_{c}}{KT_{c}}}$$
(2)

where S is the probe collection area, and J_e is the electron current density. This procedure is easy to use and can give quite reproducible results [11]. We are assuming that at the plasma boundary, the electron density

FILAMENT DISCHARGE HAS 250 OV POWER SUPPLY POWER SUPPLY

Fig. 3 Schematic diagram of an experimental setup for the measurement of the proportionality constant α (see text).

equals the ion or plasma density n [12,13].

The proportionality constant α was determined from equation (1) with an operating discharge voltage V_d set at 50.0 V and a bias voltage V_B at 50.0 V. The experimental set up for determining α is shown in Fig. 3.

3. Experimental Results and Discussion

Fig. 4 shows the axial density profile of helium ion (He⁺), and argon ion (Ar⁺). In this measurement, the discharge current I_d was set at 0.5 A, the discharge voltage V_d was 40 V, and 50 V, and the gas pressure inside the chamber was 3.8×10^{-4} Torr.

Fig. 5 displays the radial density profile of He⁻ and Ar⁺. The operating condition was the same as in the measurement of the axial density profile.

Fig. 6(a) shows the ion density of He⁺, and Ar⁺ as a function of discharge voltage. In this measurement, the discharge current was 0.5 A, and the gas pressure inside the chamber was 3.8×10⁻⁴ Torr. Fig. 6(b) shows the He⁺ and Ar⁺ density as a function of discharge current for a discharge voltage of 50.0 V and the gas

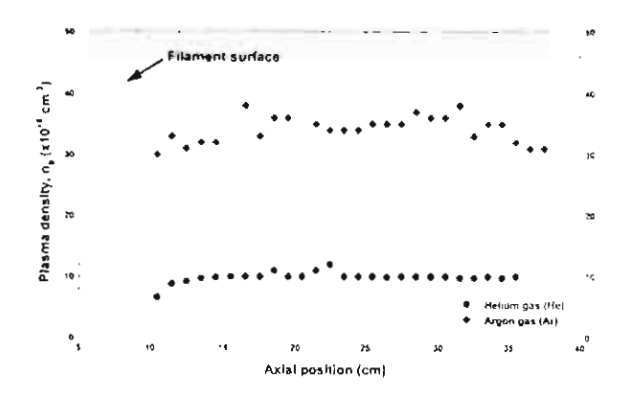


Fig. 4 A typical axial ion density profile of helium and

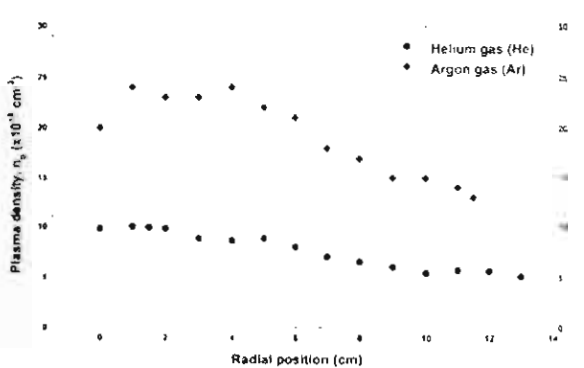


Fig. 5 A typical radial ion density profile of helium and argon.

Suanpoot P. et al., Plasma Parameter Characterization of a DC Multicusp Plasma Chamber Operating in He, Ar and Xe Gas

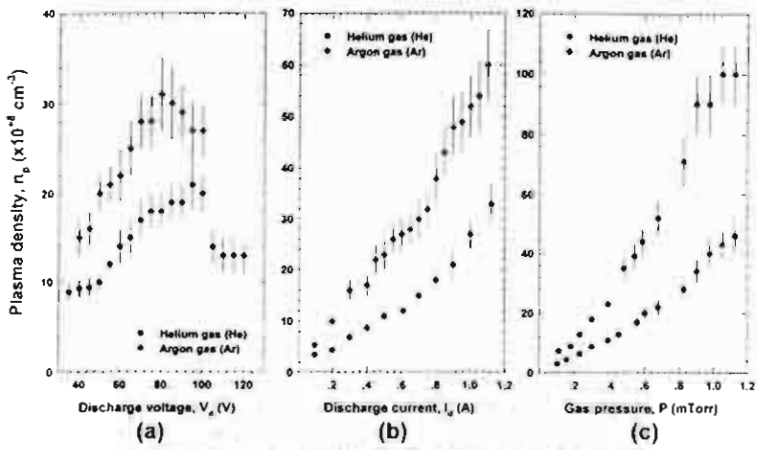


Fig. 6 Plot of ion density of helium and argon versus (a) the discharge voltage, (b) the discharge current, (c) the neutral gas pressure.

pressure inside the chamber of 3.8×10⁻⁴ Torr. The discharge current was kept relatively constant during the measurement by changing the filament current. Fig. 6(b) shows the He⁺ and Ar⁺ density as a function of neutral gas pressure operating with a discharge voltage of 50.0 V and a discharge current of 0.50 A.

Table 1 shows the α factor values determined using helium, argon, and xenon ions, with an operating discharge voltage of 50.0 V and a bias voltage of 50.0 V.

The plasma confinement of the axial density profile for argon and helium ion are fairly uniform. We also found that the plasma potential exhibits a similar uniform profile. These profiles are symmetric because of a symmetric line cusp magnetic confinement around the chamber. This relative uniform ion density profile in the axial direction is to be expected since the vessel is enclosed by magnets at both ends. When the magnets on one end are removed the density profile is not uniform with a maxima located towards the end plate as shown by the work of Leung et al. [3]. The radial density profiles are uniform up to about 6 cm before dropping off to about two-third of the maximum value at a distance of about 12 cm from the axis of the chamber.

Table 1 The proportionality constant a (see text) as determined using helium, argon and xenon gases.

ion	Plasma parameters at $I_d = 0.50$ A, $V_d = 50$ O V, and $V_B = -50$ O V				α	
	<i>T.</i> (cV)	J. (×10 ⁻¹ A/cm ²)	и (×10 ⁻⁴ cm ⁻³)	/ ₈ (mA)	J, (×10 ⁻³ A/cm ²)	factor
He'	1.44	1 55	48 ± .6	0.38	1.92	0.42 ± .07
Ár	1.43	8.37	26. ± 3.	0.90	4.55	0.59 ± .08
Xe'	1.40	15.60	49 ± 6.	0.73	3.69	0.46 ± .06

For a dc discharge plasma confined by the magnetic multicusp field operated under the above conditions, the plasma density in an uniform large volume is found to be between $4 \times 10^8 - 4 \times 10^9$ cm⁻³.

From Fig. 6(a) we can see that the rate of plasma production is maximum when the primary electrons have an initial energy approximately equal to 80 eV for both gases. The same result is also obtained from other gases such as hydrogen and nitrogen [3, 15]. By increasing the discharge current, the plasma production rate and the probability of ionization increases. Fig. 6(b) shows that the rate of plasma production is highest when the discharge current is above about 1 A and the discharge voltage was 60 V. For a large source chamber the plasma production rate increases significantly with the neutral gas pressure.

The measured proportionality constant α for He, Ar, and Xe gases is $0.42\pm.07$, $0.59\pm.08$, and $0.46\pm.06$, respectively. These values are in agreement with the value (0.49) calculated by Forrester [12], if we assume that the electron density equals the ion density. This assumption is reasonable since we use the maximum values of ion density in the determination of the values of α . The available ion current density, ion species and the uniform plasma region are important parameters for proper extracting and accelerating beam of ions.

Acknowledgments

We are grateful to Dr. K.N. Leung of Lawrence Berkeley National Laboratory for his valuable advice and guidance throughout the course of this work. We thank Prof. C. Silawatshananai of Valailux University of Technology for his suggestion on the design of the plasma chamber and his technical assistance on the use of Langmuir probe. This work was supported by the National Institute of Electronic and Computer Technology, the National Research Council, and the Thai Research Fund.

References

- R. Limpaecher and K. R. MacKenzie, Rev. Sci. Instrum. 44, 726(1973).
- [2] K.N. Leung, T.K. Samec and A. Lamm, Phys. Lett. A51, 490 (1975).
- [3] K.N. Leung, R.D. Collier, L.B. Marshall, T.N. Gallaher, W.H. Ingham, R.E. Kribel and G.R. Taylor, Rev. Sci. Instrum. 49, 321(1978).
- [4] K.W. Ehlers, K. N. Leung and M. D. Williams, Rev. Sci. Instrum. 50, 1031(1979).
- [5] K.W. Ehlers and K.N. Leung, Rev. Sci. Instrum. 54, 1296(1983).
- [6] K.N. Leung, K.W. Ehlers, C. A. Hauck, W. B. Kunkel and A.F. Lietzke, Rev. Sci. Instrum. 59, 453(1988).

- [7] S.R. Walther, K.N. Leung, and W.B. Kunkel, J. Appl. Phys. 63, 5678(1988).
- [8] S.R. Walther, K.N. Leung and W.B. Kunkel, Rev. Sci. Instrum. 61, 315(1990).
- [9] K.N. Leung and R. Keller, Rev. Sci. Instrum. 61, 333(1990).
- [10] F.F. Chen, Introduction to Plasma Physics and Controlled Fusion (Plenum, New York, 1984).
- [11] P. Suanpoot et al., Plasma Parameter Characterization of a Multicusp Ion Source Operating in Ar Gas, presented at the Asian Science Seminar on Frontier of Physics in Fusion Relevant Plasma, Hefei, October 1996.
- [12] A.T. Forrester, Large Ion Beams Fundamentals of Generation and Propagation (John Wiley & Sons, Inc., New York, 1988).
- [13] S.A. Self. Phys. Fluids. 6, 1762(1963).
- [14] K.N. Leung, private communication, (1994).
- [15] S.R. Walther, K.N. Leung and W.B. Kunkel, Rev. Sci. Instrum. 61, 315(1990).

ภาคผนวก ก7

A 13.56 MHz Multicusp Ion Souece for Gaseous Ion-Beam Production

D. Boonyawan, P. Suanpoot and T. Vilaithong

Fast Neutron Research Facility, Department of Physics, Faculty of Science,
Chiang Mai University, Chiang Mai 50200, Thailand.

Published in:

Surface & Coatings Technology 112 (1999) 314-317.

Reprinted from

SURFACE & COATINGS TECHNOLOGY

Surface and Coatings Technology 112 (1999) 314-317

A 13.56 MHz multicusp ion source for gaseous ion-beam production

Dheerawan Boonyawan *, Pradoong Suanpoot, Thiraphat Vilaithong

Fast Neutron Research Facility, Department of Physics, Faculty of Science, Chiang Mai University, Chiang Mai 50200, Thailand



SURFACE AND COATINGS TECHNOLOGY

Editors

B. D. Sartwell (Washington, DC, USA) A. Matthews (Hull, UK)

Editorial Board

S. Bull (Newcastle upon Tyne, UK)

R. F. Bunshah (Los Angeles, CA, USA)

G. Dearnaley (San Antonio, TX, USA)

H. Herman (Stony Brook, NY, USA)

H. Hintermann (Ins., Switzerland)

A. Inspektor (Latrobe, PA, USA)

H. Jehn (Schwäbisch Gmünd, Germany)

A. Kinbara (Ishikawa, Japan)

A. S. Korhonen (Espoo, Finland)

P. Martin (Sydney, Australia)

W.-D. Münz (Sheffield, UK)

D. S. Rickerby (Derby, UK)

A. R. Nicoll (Wohlen, Switzerland)

Y. Pauleau (Saint Martin d'Heres, France)

L. Pranevičius (Kaunas, Lithuania)

S. Schiller (Dresden, Germany)

W. D. Sproul (Evanston, IL, USA)

K. N. Strafford (The Levels, S.A., Australia)

J.-E. Sundgren (Linköping, Sweden)

R. C. Tucker (Indianapolis, IN, USA)

J. Vogel (Vaduz, Liechtenstein)

J. von Stebut (Nancy, France)

R. P. Walters (Albany, OR, USA)

Scope

The increasing requirement for high technology materials with specific performance characteristics in various types of environments has dictated that these materials possess nearsurface properties different from their bulk properties. This journal is a principal forum for the interchange of information on the science, technology and applications of thin and thick coatings and modified surfaces which alter the properties of materials. The scope includes all types of coatings and surface modification techniques (including physical vapour deposition, chemical vapour deposition, electroplating and surface modification by directed energy techniques). Of particular emphasis are the emerging advanced processes such as thermal spraying, sputter deposition, activated reactive evaporation, ion plating, molecular beam epitaxy, ion implantation and pulsed laser surface deposition. Contributions range from original scientific articles concerned with applied research or direct applications of coatings to reviews of current technology in specific areas. Papers are solicited on topics which include one or more of the following areas: (1) characterization of coatings and modified surfaces, which includes the determination of composition, structure, adhesion, and internal stresses; (2) the application of coatings and modified surfaces to alter the mechanical, chemical or optical properties of materials. Mechanical properties include friction, wear, erosion, hardness and load bearing capacity. Chemical properties include corrosion and oxidation. Optical and electro-optical properties include reflectivity, selective absorption and electroluminescence. Particular emphasis is also placed on the emerging surface engineering technologies and coatings with a diversity of applications such as diamond, diamond-like carbon, and cubic boron nitride. Other interdisciplinary areas include thermal barrier coatings and coatings for biomedical applications and materials conservation.

Abstracting/Indexing Services

This journal is cited by the following services:
Engineering Index, FIZ Karlsruhe, Metal Finishing Abstracts,
Current Contents — Engineering, Technology and Applied
Sciences, Physikalische Berichte, Cambridge Scientific
Abstracts, Chemical Abstracts, Fluid Abstracts, Metals
Abstracts, Physics Abstracts, PASCAL/Centre National de
Recherche Scientifique, Solid State Abstracts.

Pre-publication abstracts of articles in *Surface and Coatings Technology* and other related journals are now available weekly in electronic form via CoDAS, a new direct alerting service in condensed matter and materials science run jointly by Elsevier Science and Institute of Physics Publishing. For details on a free one-month subscription contact Paul Bancroft on fax +44 1179 294318 or e-mail bancroft@ioppublishing.co.uk.

Publication Information

Surface and Coatings Technology (ISSN 0257-8972). For 1999 volumes 109-121 are scheduled for publication. Subscription

prices are available upon request from the Publisher. Subscriptions are accepted on a prepaid basis only and are entered on a calendar year basis. Issues are sent by surface mail except to the following countries where Air delivery via SAL mail is ensured: Argentina, Australia, Brazil, Canada, Hong Kong, India, Israel, Japan, Malaysia, Mexico, New Zealand, Pakistan, PR China, Singapore, South Africa, South Korea, Taiwan, Thailand, USA. For all other countries airmail rates are available upon request. Claims for missing issues should be made within six months of our publication (mailing) date.

Orders, claims and product enquiries: please contact the Customer Support Department at the Regional Sales Office nearest you:

New York: Elsevier Science, PO Box 945, New York, NY 10159-0945, USA:

phone: (+1) (212) 633 3730 (toll free number for North American customers: 1-888-4ES-INFO (437-4636));

fax: (+1) (212) 633 3680; e-mail: usinfo-f@elsevier.com

Amsterdam: Elsevier Science, PO Box 211, 1000 AE

Amsterdam, The Netherlands;

phone: (+31) 20 4853757; fax: (+31) 20 4853432;

e-mail: nlinfo-f@elsevier.nl

Tokyo: Elsevier Science, 9-15 Higashi-Azabu 1-chome, Minatoku, Tokyo 106-0044, Japan;

phone: (+81) (3) 5561 5033; fax: (+81) (3) 5561 5047;

e-mail: info@elsevier.co.jp

Singapore: Efsevier Science, No. 1 Temasek Avenue, #17-01

Millenia Tower, Singapore 039192;

phone: (+65) 434 3727; fax: (+65) 337 2230;

e-mail: asiainfo@elsevier.com.sg

Rio de Janeiro: Elsevier Science, Rua Sete de Setembro 111/16 Andar, 20050-002 Centro, Rio de Janeiro - RJ, Brazil; phone: (+55) (21) 509 5340; fax: (+55) (21) 507 1991; e-mail: elsevier@campus.com.br [Note (Latin America): for orders, claims and help desk information, please contact the Regional Sales Office in New York as listed above]

US mailing notice—Surface and Coatings Technology (ISSN 0257-8972) is published monthly by Elsevier Science S.A. (PO Box 564, 1001 Lausanne). Annual subscription price in the USA is US\$ 4622.00 (valid in North, Central and South America), including air speed delivery. Second class postage rate is paid at Jamaica, NY 11431.

USA POSTMASTER: Send address changes to Surface and Coatings Technology Publications Expediting, Inc., 200 Meacham Avenue, Elmont, NY 13003.

AIRFREIGHT AND MAILING in the USA by Publications Expediting.



Surface and Coatings Technology 112 (1999) 314-317



A 13.56 MHz multicusp ion source for gaseous ion-beam production

Dheerawan Boonyawan *, Pradoong Suanpoot, Thiraphat Vilaithong

Fast Neutron Research Facility, Department of Physics, Faculty of Science, Chiang Mai University, Chiang Mai 50200, Thailand

Abstract

A 10 cm × 9 cm cylindrical radio-frequency (RF) driven multicusp ion source has been developed for producing high-current ion beams from gases. An inductively coupled 13.56 MHz RF plasma is produced in the presence of 20 rows of Sm-Co₅ magnets which form a longitudinal line-cusp field configuration. The field design was generated using the computer program MAGNUS. By using a 0.35 Tesla magnet, the 100 eV electrons were confined in the source chamber. The RF antenna coil, coated with a thin layer of hard flexible glass to prevent electrical leakage and contamination, has power inlets into the source chamber. A 10:1 turns-ratio matching transformer was used in order to match the 50 Ω output impedance of the RF generator to the impedance of the plasma load. A test run has been performed with 0-500 W of RF power. The source parameters were measured with a Langmuir probe, a mass analyzer and a Faraday cup. For oxygen at 3 mtorr and power set at 500 W, the ion-current density is 36 mA cm⁻², representing an ion density of 1.5 × 10¹¹ cm⁻². The value for nitrogen operating at the same pressure is 34 mA cm⁻² and, for argon and helium at 10 mtorr source pressure, it is 29 and 27 mA cm⁻², respectively. © 1999 Elsevier Science S.A. All rights reserved.

Keywords: RF-driven multicusp ion source

1. Introduction

Compared with a conventional direct-current (DC) discharge ion source, a radio-frequency (RF) discharge source has several advantages [1-3]: (1) it has a simple structure with a longer lifetime; (2) it has a large beamarea capability; (3) it can operate with all gases (even reactive gas); and (4) it gives a uniform plasma density with the presence of a magnetic line-cusp field. A commercial RF generator at 13.56 MHz is quite attractive since it has been widely utilized in all plasma production processes. Development of this ion source is aimed at producing high-current ion beams from N₂ and O2 gases for the CMU ion implanter for materials modification and for future applications in ion lithography. The source developed here is capable of producing an inductively coupled plasma which can generate up to 36 mA cm⁻² ion-current density for oxygen at 500 W RF power.

2. Structure of the ion source

The structure of a multicusp field ion source is shown schematically in Fig. 1. It is similar to the one developed by Leung et al. [1]. This source consists of a cylindrical discharge chamber, permanent magnets, an antenna coil and an ion-extraction system. The RF power is fed to the antenna coil in the ion source via the tunable impedance-matching box. The plasma is produced by an RF discharge in the cusp field and the power is absorbed by the primary electrons which travel, lose their energy and reflect within the discharge chamber. The discharge chamber is made from an anodized aluminum cylinder with a diameter of 10 cm and length of 9 cm. The inner wall is surrounded by 20 columns of Sm-Co₅ magnets. The magnets are enclosed by an outer cylinder with cooling water circulating between the magnets and the inner wall.

The antenna coil, 6 cm in diameter, is placed inside the discharge chamber. It consists of two turns of copper tubing coated with a thin layer of hard flexible glass to prevent electrical leakage and ion contamination as shown in Fig. 2(a). The antenna is also cooled with water circulating inside, so that it is capable of operating

^{*} Corresponding author. Tel: +66-53-943379; Fax: +66-53-222776; e-mail: dherawan@istrd.cmu.ac.th

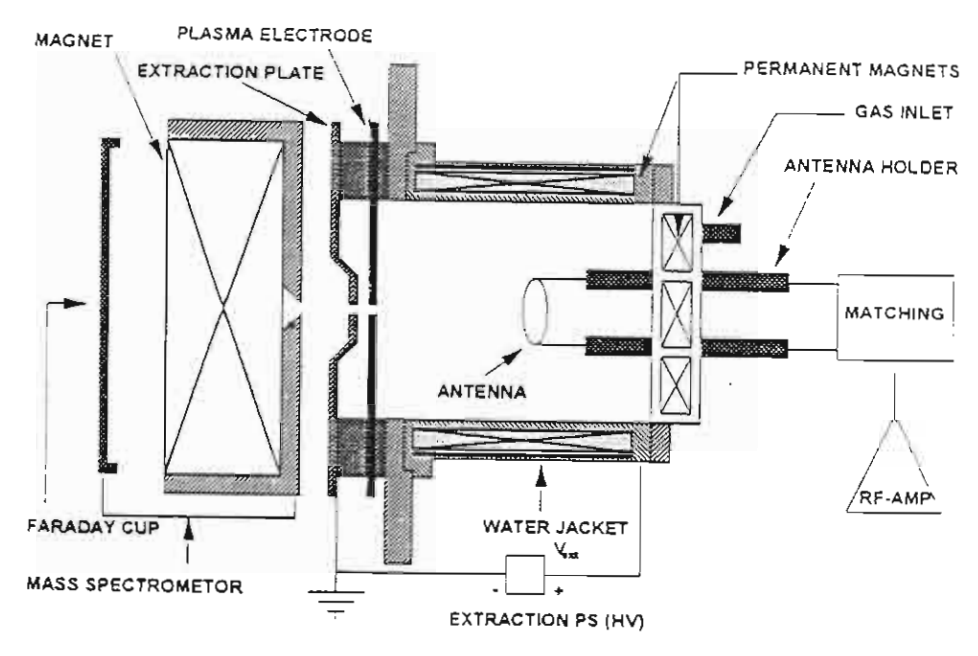


Fig. 1. Schematic diagram of the CMU RF ion source using a magnetic line-cusp field.

at up to $3 \, kW$ of RF power in CW (continuous wave) mode. The RF generator, model HPG 13100 made by Dressler GmbH, supplies the power through a $50 \, \Omega$ coaxial cable to an isolation transformer and matching circuit. The RF-matching circuit (Fig. 3) consists of a variable capacitor and an inductor in series with the antenna coil. The RF power is delivered into the plasma via a 10:1 step-down $30 \, kV$ isolation transformer with a maximum capacity of $3.5 \, kW$.

The 20 columns of Sm-Co₅ magnets form a longitudinal line-cusp field configuration. This type of field plays an important role in both plasma density enhancement and plasma uniformity [4,5]. The magnetic field lines and the field intensity contours in the ion source were simulated by using the computer program MAGNUS [6]. The approximate field-free region was about 6 cm in diameter. The 0.35 Tesla magnets can confine up to 100 eV electrons travelling back along the chamber wall. The magnetron motion and drifts generate a highdensity plasma in the circumferential area of the discharge chamber and the plasma is allowed to diffuse into the zero-field area of the cusp field. In this manner, plasma uniformity can be achieved over the whole region of interest. The confinement region could be observed as shown in Fig. 2(b).

A quasi-Pierce type dual-electrode with a 4 mm diameter beam aperture has been adopted in the extraction system. The first electrode and the discharge chamber are connected to a 0–10 kV power supply while the second electrode is grounded. Both electrodes are separated by a distance of 4 mm, which is equal to the diameter of the beam aperture.

3. Experimental set-up and results

Experiments have been carried out on an ion-source test bench with a 520 l s⁻¹ turbomolecular pump. The extracted ion current was measured at a 3 kV extraction voltage with a Faraday cup, biased at 10–20 V to suppress the emission of secondary electrons. The ratio of atomic to molecular ions of nitrogen and oxygen was measured with a small mass analyzer with a maximum field strength of 3.6 kG [7]. The matching circuit was adjusted to less than 1:1.5 SWR (standing wave ratio) ratio and the reflected power at 500 W forward output power was less than 4 W.

Fig. 4 shows the extracted ion current and current density versus RF power of oxygen and nitrogen gases. For oxygen the ion-current density is up to 36 mA cm⁻², corresponding to an ion density of 1.5×10^{11} cm⁻². The value for nitrogen under the same operating conditions is 34 mA cm⁻². The ratio of atomic to molecular oxygen ions was measured to be about 70:30 at 200 W RF power. For nitrogen gas, the composition of atomic ions was found to be over 50% at the same RF power. Fig. 5 shows the relationship between the atomic current analyzed and the gas pressure at different values of RF power for O2 gas. In all cases, the current density increases significantly with the decrease in source pressure to some limiting value. Our results agree with the recent observation made by Perkin et al. [2].

Inert gas operation was performed with helium and argon. The optimum gas pressure is typically around 10 mtorr. Fig. 6 shows the extractable ion current as a